UNIVERSITÀ DEGLI STUDI DI NAPOLI FEDERICO II

SCHOOL OF MATHEMATICS, PHYSICS AND NATURAL SCIENCES

PHD IN CHEMICAL SCIENCES, CYCLE XXVII

# Molecular Kinetics of Catalytic Olefin Polymerization: an Integrated Quenched-Flow and High-Temperature Cryoprobe NMR Approach

YUE YU

**SUPERVISOR**

PROF. VINCENZO BUSICO

**ASSESSOR**

PROF. GIOVANNI TALARICO

**COORDINATOR**

PROF. LUIGI PADUANO

# Table of Contents

# Chapter 1. General Introduction

Polyolefins belong to a family of polymers that consists of a variety of members— polyethylene, polypropylene, polybutene, polyhexene, polybutadiene, polyisoprene, etc.. Figure 1 gives a few examples of polyolefin structures. With a few exceptions, e.g. low-density polyethylene (LDPE, usually made by radical polymerization under high pressure), polyolefins are mostly produced with transition-metal-based catalytic processes. Olefin polymerization can be mediated by heterogeneous Ziegler-Natta catalysts (ZNCs), metallocenes and post-metallocene molecular ones, etc..

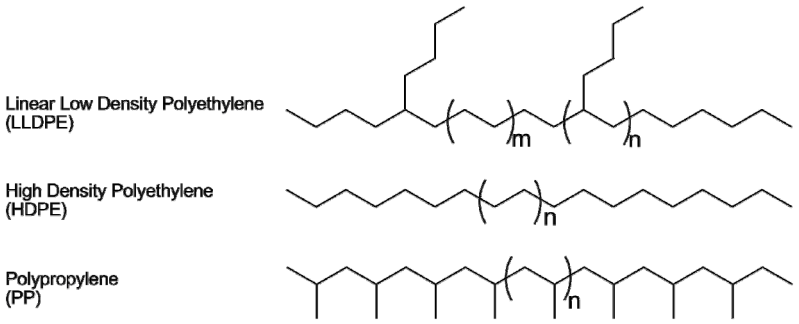


**Figure 1**. Examples of the chemical structures of polyolefins.

This thesis focuses on olefin polymerization kinetics at catalytic species that are supposed to follow the so-called Cossee-Arlman mechanism, which can be described as shown in Figure 2.[1-2] Phillips catalyst, a type of heterogeneous systemt for high-density polyethylene (HDPE), may have a significantly different mechanism and will not be elaborated upon here.

In the present chapter as well as in the introductory parts of the following ones we provide some basic information of use to the readers of this thesis. We had to compress more than 60 years of literature into few pages, and the contributions of several generations of outstanding scientists who devoted their professional life to the

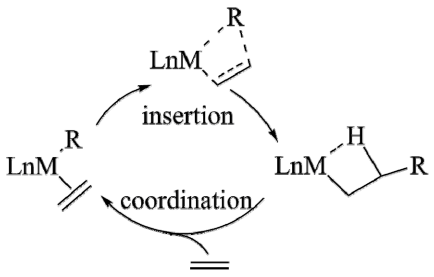


**Figure 2**. Cossee-Arlman mechanism of olefin polymerization.

field which, as is well known, was named after *Karl Ziegler* and *Giulio Natta*, 1963 Nobel laureates in Chemistry and inventors of the first-generation of catalysts. Another major contribution came by *Walter Kaminsky*, who discovered methylaluminoxane (MAO) and opened the door to the industrial use of metallocene catalysts. The impact of polyolefin science on people's life can hardly be

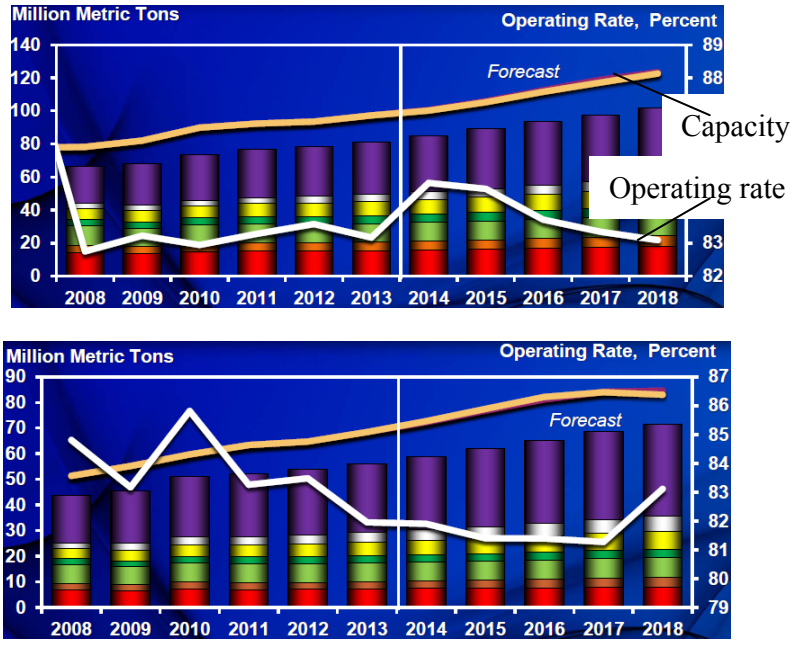


**Figure 3**. The supply and demand of PE (top) and PP (bottom).
Source: *IHS* report 2014

overestimated. Each year above 100 million tons of polyolefins are consumed (Figure 3). For beginners to learn about this field, the comprehensive book by Kissin can be a convenient start, see Ref.[3] Readers who already have some basic background knowledge may want to go through some recent reviews highlighting the state of the art of the field, see Ref. [4-7]. For professionals, the handbook by Vasile is a valuable reference book, see Ref. [8]

## 1.1. A Brief History of Catalytic Systems

The serendipitous finding that traces of colloidal Nickel greatly enhance the rate of ethene insertion into Al-R bonds ("Nickel effect" on the Auf-bau reaction) triggered Ziegler's systematic investigations that led to the discovery of the $TiCl_4/AlEt_3$ "mixed catalyst" for the first practical synthesis of High-Density Poly(Ethylene), HDPE.[9-10] Natta and co-workers, in turn, were the first to realize that the reaction between $TiCl_4$ and $AlEt_3$ in aliphatic hydrocarbon leads to the precipitation of surface-alkylated crystalline $TiCl_3$, and that this is a competent catalyst for the partly stereoselective synthesis of isotactic polypropylene (iPP).[4, 11-12] An inspiring account of history and legend around these facts was recently written by Busico.[4,13]

$TiCl_x$-based heterogeneous catalysts are comprehensively known as Ziegler-Natta catalysts (ZNCs). Sometimes this definition is extended to metallocene catalysts; as a matter of fact, many fundamental aspects of the polymerization process are the same for the two classes.

From here on we will mostly focus on propene polymerization, which is by far the main topic of the present thesis, and also more complex than ethene polymerization due to the aspects related with regio- and stereoselectivity.

$TiCl_3$ is a crystalline substance with four polymorphic phases: α, β, γ and δ. The crystal structures of all four phases were elucidated by

Natta, Corradini and Allegra.[14] Figure 4 shows recent computational models.[15] In all cases, Ti atoms are in octahedral coordination; however, the β-phase contains $(TiCl_3)_n$ fibrils, whereas the other three phases feature a layer structure with the Ti atoms occupying 2/3 of the octahedral cavities between alternate pairs of close-packed Cl atoms. In the α and γ phase the stacking of the Cl layers is regular ($[AB]_n$ and $[ABC]_n$, respectively); in the δ phase, on the other hand, the stacking is statistically disordered. A visual difference between the fibrillar β-phase and the layer phases is that the former is brown in color; the latter instead are violet (and as a matter of fact they are often indicated comprehensively as "violet $TiCl_3$". It should be noted that β-$TiCl_3$ is the kinetic product forming out of Ziegler's mixed catalyst, while reduction of $TiCl_4$ with e.g. $H_2$ or Al leads to violet (primarily α) $TiCl_3$. Importantly, Natta reported that violet-$TiCl_3$-based catalysts are much more stereoselective in propene polymerization than brown-$TiCl_3$-based ones.

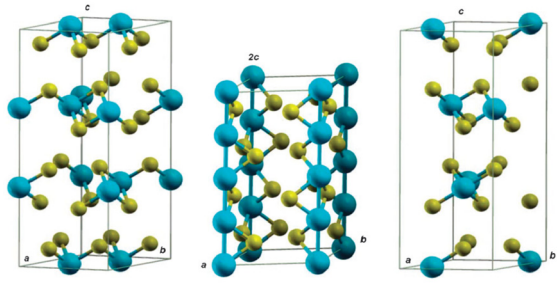


**Figure 4**. Computational models of $TiCl_3$ crystal lattices. α (left), β (center), γ (right). Reproduced from Ref. 15. Larger balls denote Cl atoms and smaller balls denote Ti atoms.

The δ-form of $TiCl_3$ was actually the most widely used for propene polymerization due to a higher activity. It was produced via grinding of α- or γ-$TiCl_3$, and used in combination with $AlR_xCl_{3-x}$ cocatalysts (yielding polymers with a much higher isotacticity than $AlR_3$, Table 1). $AlCl_3$-containing $TiCl_3$ (as resulting from $TiCl_4$ reduction with Al metal or Al-alkyls, or sometimes from the co-grinding of $TiCl_3$ and $AlCl_3$) was a commonly used iPP catalyst. In the late 1950s Stauffer

Chemical Company commercialized an $AlCl_3$-containing $TiCl_3$ with the name "AA-$TiCl_3$" (AA means *aluminum-reduced* and *activated*), often denoted as 1st-generation ZNC.

**Table 1**. Isotacticity of polypropylene produced with Ti-based Ziegler–Natta catalysts. Reproduced from Ref. 4.

| Catalyst | Cocatalyst | Temp./ ℃ | InSolC7/ %[a] | [*mmmm*] |
|---|---|---|---|---|
| δ-$TiCl_3$ | $AlEt_3$ | 60 | 60 | 0.964 |
| δ-$TiCl_3$ | $AlEt_2Cl$ | 60 | 90 | 0.967 |
| δ-$TiCl_3$ | $AlEt_2Br$ | 60 | 88 | 0.965 |
| δ-$TiCl_3$ | $AlEt_2I$ | 60 | 93 | 0.975 |
| $TiCl_4$/δ-$TiCl_3$[b] | $AlEt_3$ | 70 | 59 | 0.958 |
| $TiCl_4$/δ-$TiCl_3$[b] | $AlEt_2Cl$ | 60 | 97 | 0.973 |
| $TiCl_4$/δ-$TiCl_3$[b] | $AlEt_2I$ | 50 | 95 | 0.983 |

[a] Fraction insoluble in boiling *n*-heptane.

[b] Solvay-type catalyst.

In the early 1970s Solvay & Cie S.A. developed a new type of $TiCl_3$-based catalyst with higher stereoselectivity.[16] The preparation started from β-$TiCl_3$, produced in turn by reacting $TiCl_4$ with $AlEtCl_2$ or $Al_2Et_3Cl_3$ at low temperature. This $AlCl_3$-containing $TiCl_3$ was washed with an aliphatic ether, e.g. diisopentyl ether, to remove most of the $AlCl_3$ and bind a small amount of ether onto the $TiCl_3$ matrix. As the last step, the solid was treated with an excess of $TiCl_4$. The final product was called "Solvay catalyst", and is also known as 2nd-generation ZNC.

Due to a relatively low productivity (in terms of kg(polymer)·g(Ti)$^{-1}$), both 1st and 2nd- generation ZNCs left non-neglibible amounts of acidic residues in the propene polymerization products. Therefore, a cumbersome and expensive de-ashing process was a necessary part of the industrial production process (Figure 5).[17]

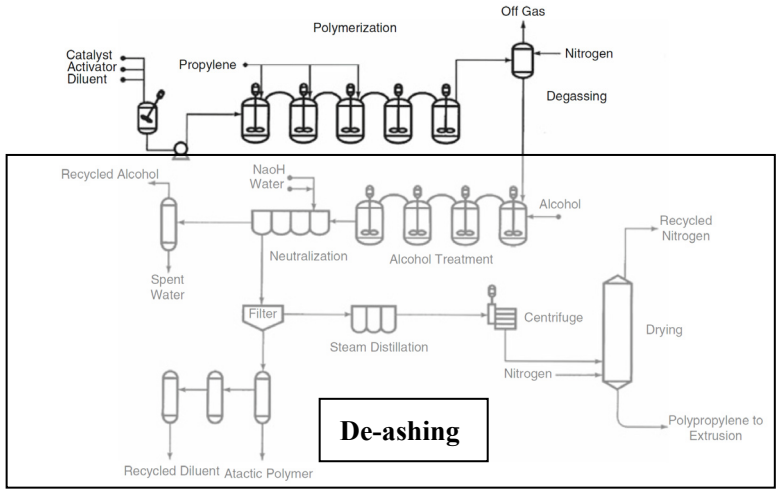


**Figure 5**. Flow-chart of an early iPP production plant based on violet $TiCl_3$ catalysis (Hercules technology; reproduced from Ref. 17). The de-ashing process is highlighted.

In this respect, the breakthrough was the introduction of ZNCs consisting of $TiCl_4$ on a $MgCl_2$ support. The much higher productivity of these catalysts (at least referred to their Ti content) made it possible to skip the demanding polymer de-ashing process (Figure 5).[17] In 1968 Montecatini S.p.A. and Mitsui Chemicals filed patent applications almost at the same time[18]. The new catalysts worked well for ethene polymerization, but in the first formulations yielded a polypropylene with low stereoregularity (Table 2).[18] However, it was soon discovered that the addition of proper Lewis bases, e. g. ethyl benzoate, pushed the index of isotacticity (I.I.) of the polymer from below 40% to above 90%, while keeping the productivity ($kg(PP)\cdot g(Ti)^{-1}$) at a level one order of magnitude higher than for the Solvay-type catalyst. It should be noticed that the Lewis base can be added either during catalyst preparation or just before the polymerization along with the Al-alkyl cocatalyst; in the former case it is often called Internal Donor (ID), in the latter External Donor (ED). The best results in terms of stereoselectivity were usually obtained with proper ID-ED combinations, which actually identify the various generations of ZNCs that were

introduced since then. 3rd-Generation systems feature ethyl benzoate as the ID and a *para*-substituted benzoate as the ED; these systems are discussed in detail in Chapter 3.

**Table 2**. Propene polymerization result with an $TiCl_3$-type catalyst and $MgCl_2$-supported $TiCl_4$ catalyst system. Reproduced from Ref. 18.

| Catalyst | Activity/ g(PP)·mmol(Ti)$^{-1}$·h$^{-1}$·atm$^{-1}$ | | | I.I./ %[a] | [*mm*]/ %[b] |
|---|---|---|---|---|---|
| | Overall | Isotactic PP | Atactic PP | | |
| $TiCl_3/AlEt_3$ | 23 | 17 | 6 | 75.9 | 91 |
| $MgCl_2/TiCl_4/AlEt_3$ | 968 | 328 | 640 | 33.9 | 89 |

[a] Fraction insoluble in boiling *n*-heptane.

[b] Measured with $^{13}$C-NMR of IPP.

In 1977, Mitsui Petrochemical Industries Ltd. and Montedison S.p.A. developed 4th-generation systems making use of an ortho-phthalate ID and an alkoxysilane ED[19-20]; the stereoselectivity of such catalysts was high to the point that for the first time no removal the "atactic" polymer fraction was necessary. Interestingly, the same solid catalyst component in combination with certain types of alkoxybenzene derivatives as the ED can also produce "atactic" (more properly, poorly isotactic) polypropylene (Table 3).[21] Chapter 4 will focus on this type of catalyst.

5th-Generation systems featuring 1,3-diethers IDs and alkoxysilane EDs were patented in the late 1980s.[22] Notably, these catalysts can produce isotactic polypropylene even without an ED (although with the ED the stereoselectivity is appreciably higher). Furthermore, they yield propene polymers with an unusually narrow molecular weight distribution (polydispersity index $M_w/M_n$ ~4, instead of ~6-7 for the previous generations), and respond very promptly to $H_2$ as a chain transfer agent.

**Table 3**. Catalyst systems for synthesis of atactic polypropylene. Reproduced from Ref. 21.

| External donor | Productivity/ $kg \cdot g(Ti)^{-1}$ | I.I./ % [a] |
|---|---|---|
| None | 276 | 57 |
| *o*-Dimethoxybenzene | 352 | 19 |
| 3,4-Dimethoxytoluene | 327 | 17 |
| 1-Allyl-3,4-dimethoxybenzene | 410 | 19 |

[a] Fraction insoluble in boiling *n*-heptane.

Since the late 1990s, the development of novel donors has become faster. Nitrogen-containing alkoxysilanes (1997), malonates (1998), β-substituted glutarates (2000), succinates (2000), maleates (2003) and β-ketoesters (2005) are just some examples.[4] Therefore, it has become difficult to label catalyst generations based on the ID/ED pair. Of special importance are formulations including a 2,3-disubstituted succinate ID, because they yield highly isotactic polypropylene with broad polydispersity index ($M_w/M_n$ >10), which can be valuable for certain applications.

A summary of the previous paragraphs is given in Table 4.[4] The progress in catalyst and polymer properties along successive ZNC generations is amazing, and it can be anticipated that the introduction of High-throughput screening (HTS) tools and methods[23] will result into further improvements, and ultimately approach the catalyst/polymer tailoring typical of molecular catalysis.

**Table 4** Propylene polymerization performance of Ziegler–Natta catalysts of different gneration. Reproduced from Ref. 4.

| Catalyst | External donor | Activity/ g(PP) ·mmol(Ti)$^{-1}$ · h$^{-1}$·atm$^{-1}$ | PDI | I.I./ %[a] |
|---|---|---|---|---|
| AA-$TiCl_3$ | - | ca. 4 | - | 90 |
| Solvay $TiCl_3$ | - | ca. 30 | - | 95 |
| $TiCl_4/MgCl_2$/ benzoate | Benzoate | ca. 1,000 | 5-6 | 92-94 |
| $TiCl_4/MgCl_2$/ phthalate | Alkoxysilane | ca. 1,000-3,000 | 5-7 | > 98 |
| $TiCl_4/MgCl_2$/ 1,3-diether | Alkoxysilane | ca. 3,000-5,000 | 3-4 | > 98 |
| $TiCl_4/MgCl_2$/ dialkylsuccinate | Alkoxysilane | ca. 1,000-3,000 | >7 | >98 |

[a] Insoluble fraction in boiling *n*-heptane.

Molecular catalysts include metallocenes and post-metallocenes. Titanocene dichloride was synthesized and studied independently by Natta and Breslow et al. as early as in 1957[24-25]; however, in combination with $AlR_xCl_{3-x}$ cocatalysts its performance as an olefin polymerization catalyst was poor in all respects. In 1976, Kaminsky and Sinn[26-27] reported a boost of catalyst productivity in ethene polymerization when activated with methylaluminoxane (MAO, a serendipitously discovered and still poorly understood oligomeric reaction product of $AlMe_3$ with $H_2O$ in traces). The Zr(IV) homologue turned out to perform even better, although in propene polymerization it yielded exclusively atactic low-molecular-weight oils. Another breakthrough was Ewen's first iPP synthesis with a chiral *ansa*-titanocene catalyst, namely *rac*-bis(1-indenyl)$TiCl_2$, in combination with MAO. Soon afterwards, Brintzinger and Kaminsky reported impressive results with homologous chiral *ansa*-zirconocenes. Since then, research flourished for over a decade, and thousands of group 4 metallocene structures for application in

stereoselective propene polymerization have been described. A comprehensive review article in a themed issue of *Chemical Reviews*[6] was published in the year 2000 by Resconi et al.[28], highlighting structure/properties relationships in metallocene-based propene polymerization catalysis. Figure 6, reproduced from said article, illustrates the amazing possibility of this family of catalysts, which includes examples of catalysts for the production of highly isotactic, highly syndiotactic, perfectly atactic and hemi-isotactic polypropylene; the latter three cases were unprecedented in ZNC development.

Besides metallocenes, there are other types of remarkable families of molecular catalysts featuring different ancillary ligand frames. Of special importance are cyclopentadienyl-amido complexes of Ti(IV) (known as "Constrained-Geometry Catalysts" (CGC), inspired by homologous Scandium complexes prepared by Bercaw, and elaborated at Dow Chemical and Exxon for the commercial production of Linear-Low-Density PolyEthylene, LLDPE)[29-30], α-diimine complexes of Ni(II) (shown by Brookhart to be applicable for the synthesis of highly branched polyethylenes)[31], and Salen complexes of Ni(II) (by Grubbs)[32-33]. These examples are just the tip of an iceberg, and the flow of novel ligand scaffolds and catalyst classes is not slowing. The results demonstrate that there are almost no limits in what can be achieved in terms of polyolefin microstructures with a proper design of the ancillary ligand frame.

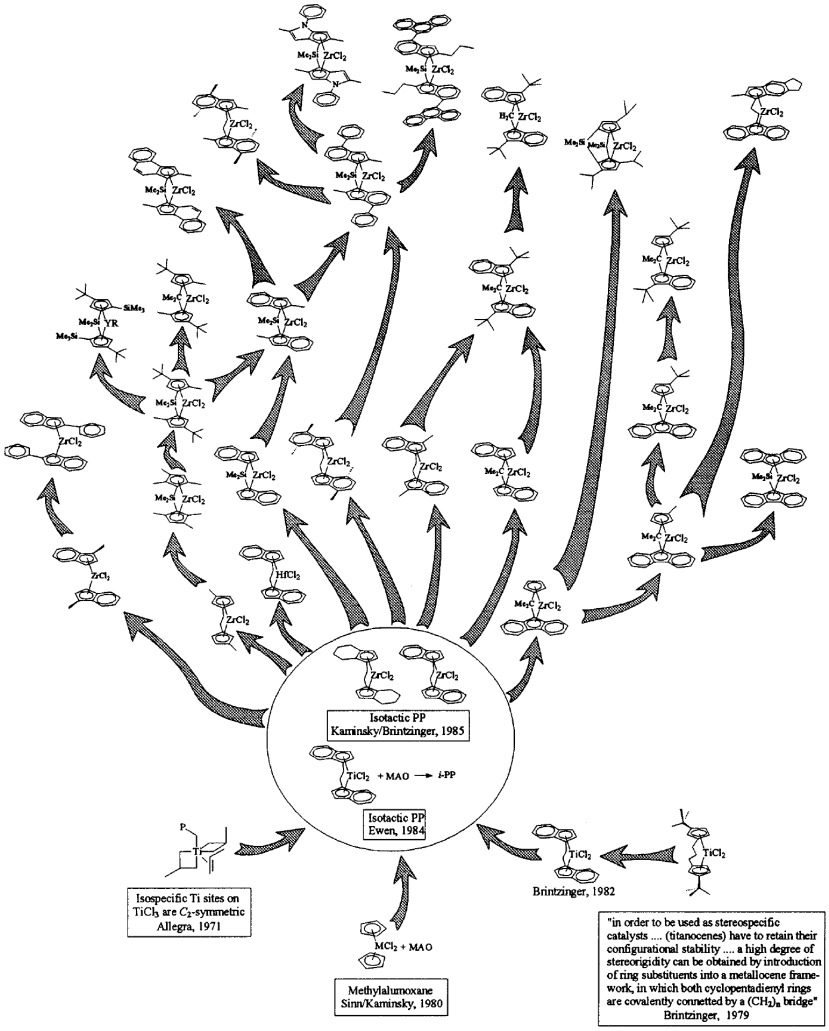


**Figure 6**. The evolution of metallocene catalysts for polypropene. Reproduced from Ref. 28.

An important point to consider is that the active species of metallocene and a vast majority of post-metallocene catalysts is an $L_yMR^+$ cation, formed by the interaction of the $LyMX_2$ precursor with the cocatalyst, e.g. MAO or $B(C_6F_5)_3$. Figure 7 shows briefly how the ion pair is believed to behave during polymerization.[34] The dynamics of the ion pair modulates the accessibility of the metal center, and therefore affects polymerization kinetics.[34] This concept

will be discussed in detail in Chapter 2. Useful literature accounts are, e.g. the reviews by Chen et al.[35] and by Krossing et al.[36]

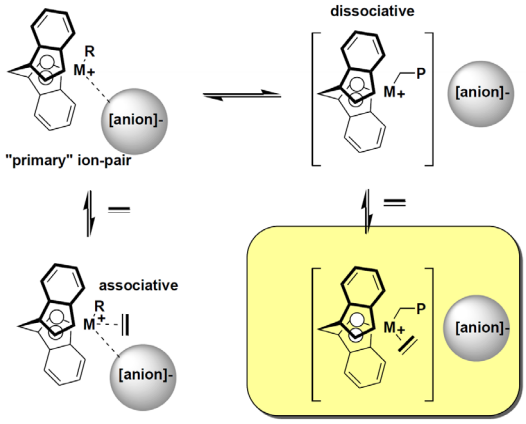


**Figure 7**. The roles of ion pair in molecular catalyst in a case of metallocene. Reproduced from Ref. 34.

## 1.2. Some Important Mechanistic Concepts

### *1.2.1. Precatalyst Activation*

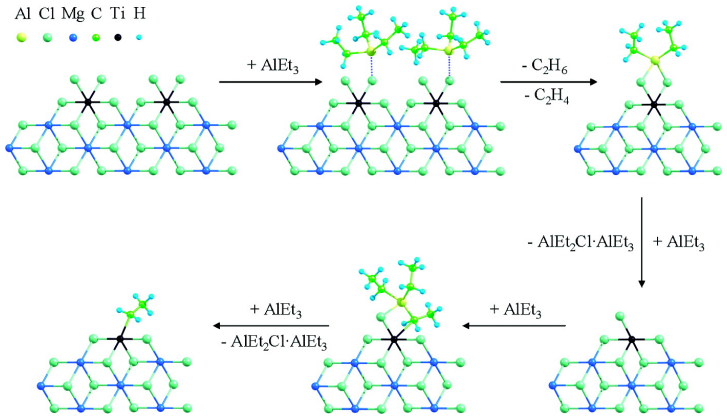


**Figure 8**. Probable mechanism for active site formation (ZNC) schematically illustrated by the example of mononuclear $TiCl_4$ species on the (110) $MgCl_2$ surface. Reproduced from Ref. 37.

In most cases, the so-called catalyst is actually a precatalyst (or catalyst precursor). In the catalytic cycle shown in Figure 2, the key step is monomer insertion into a M-R σ bond, and the precatalyst often does not contain such a bond.

1) Modern ZNCs are usually in the form of $TiCl_4$ supported on $MgCl_2$, as recalled in § 1.1. Alkylaluminum compounds (typically $AlEt_3$) are used as cocatalyst to alkylate the precursor $TiCl_4$ species and reduce them to Ti(III) (assumed to be the active oxidation state, at least for propene polymerization). How this process occurs is not yet fully understood[37-38]; Figure 8 illustrates a possible mechanism.[37]
2) Molecular catalyst precursors can be dichloride ($L_yMCl_2$) or, in some cases, dialkyl ($L_yMR_2$) complexes. Despite the presence of a pre-formed M-R bond in the latter case, both forms are inactive as long as they are coordinatively saturated. Removal of one X (Cl, R) moiety forming a coordinatively unsaturated $L_yMX^+$ cation is a pre-condition for the mechanism of Figure 2; in case X = Cl, another is replacement of Cl for R. Figure 9 illustrates the activation process of a metallocene precatalyst by MAO.[28] Rare examples of neutral coordinatively unsaturated $L_yM$-R active species have only been reported for late transition metal catalysts.[33, 39]

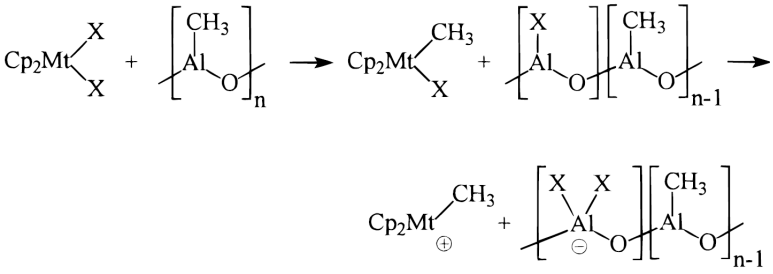


**Figure 9**. Scheme illustrating the activation of a metallocene catalyst by MAO. Mt denotes a transition metal atom. Reproduced from Ref. 28.

### *1.2.2. Stereoselectivity and Regioselectivity of Chain Propagation*

The mechanism of Figure 2, trivial when the monomer is ethene, becomes much more complex with substituted olefins, because regiochemistry and stereochemistry come into play. In the case of propene or higher 1-alkenes (Figure 10), the insertion can occur with different regiochemistry (1,2 or 2,1), giving rise to a β-branched or α-branched polymeryl respectively; moreover, in either case the *cis*-opening of the double bond can take place with opposite enantiofaces of the prochiral monomer, ending up with opposite stereochemistry of the new monomeric unit. Depending on whether the configurations of the newly formed stereogenic center is the same or the opposite with respect to the previous one, a *meso* (*m*) or *racemo* (*r*) diad is obtained. As is well-known, a polymer with a large predominance of *m* diads is named "isotactic", one with a large predominance of *r* diads is named "syndiotactic".

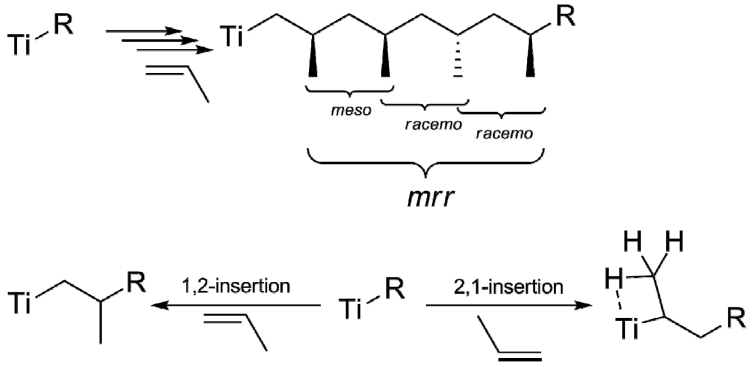


**Figure 10**. Scheme illustrating the stereoselectivity (above) and regioselectivity (bottom) of α-olefin polymerization. For clarification, irrelevant substituents are omitted.

Most olefin polymerization catalysts are highly regioselective, for electronic and steric factors that usually favor synergically 1,2 insertion. Occasional 2,1 insertions give rise to sterically crowded α-branched M-Polymeryl bonds, often referred to as "dormant" sites due to a much lower reactivity towards further insertion than β-branched ones. In rare cases (e.g. bis(phenoxyimine)Ti(IV)

catalysts) 2,1 insertion prevails.[40] It has long been suspected that the fraction of "dormant" sites is very high in $MgCl_2$-supported ZNCs[41-42]; Chapter 4 of this thesis will provide original experimental evidence that this is indeed the case. For a detailed insight into the regiochemistry and stereochemistry of polyolefins, the readers are referred to a recent review by Busico and Cipullo.[43]

### *1.2.3. Chain Transfer and Chain Termination*

The growth of a polymer chain can be interrupted by a chain transfer or termination event; the former leaves behind an active transition metal species at which a new chain can be started, whereas the latter results into an inactive species (catalyst deactivation). The use of these definitions is not univocal, probably due to the different semantic interpretation of the word *"chain"* (which can be referred in statistical sense to the polymerization reaction, or in chemical sense to the polymer; in the latter case, the alternative definition of "*chain release*" has been proposed for chain transfer). A number of chain transfer and termination processes (Figure 11) are well-documented.[44] A specially important case is that of Figure 11e when A-A' is $H_2$; at odds with M-X bonds with X = O, N, S or halogen, M-H bonds can undergo olefin insertion, and therefore are active sites like M-C ones. As a matter of fact, molecular hydrogen is used routinely in industrial processes to modulate polyolefin molecular weight; the competition of $H_2$ with the monomer for reaction with M-Polymeryl bonds is considered as the reason of "hydrogen response" of a given catalyst.[45]

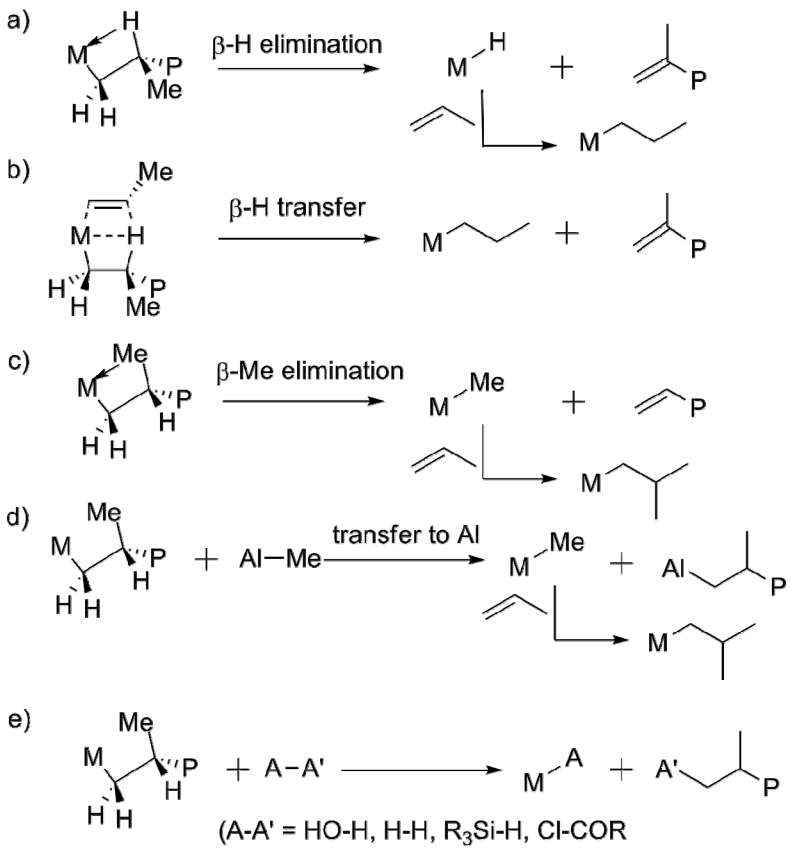


**Figure 11**. Important examples of chain transfer and termination processes in propene polymerization. M denotes a transition metal atom. Reproduced from Ref. 44.

## 1.3. The objectives of this thesis

Despite almost 60 years have passed since the birth of Ziegler-Natta catalysis, a number of fundamental mechanistic questions are still pending. In particular, the heterogeneous nature has hampered a real understanding of the structure of the active species in ZNCs. Moreover, how much of the transition metal is active is usually unknown even with molecular catalysts.[34, 46-55] The present thesis addressed both issues, with a combination of molecular kinetic and spectroscopic studies, as will be discussed in the following Chapters.

Prior to that, though, it is worthy to give a brief account of the previous literature.

One strategy to face the complicated problem of active site counts in catalytic olefin polymerization, as reviewed by Mejzlík et al.,[49] entails the incorporation of a suitable tag into the polymer chains. This approach can be traced back to Natta et al.,[46-47] who used radioactive $^{14}C$-labeled alkyl-aluminum compounds to form tagged initial M-C bonds; unfortunately, these compounds can also act as chain transfer agents (Figure 11-d), and therefore the number of radioactive atoms incorporated in the polymer does not necessarily coincide with that of active sites, but is rather the number of growing (transition-metal-bound) and 'dead' (Al-bound) chains. A later version featuring a tritiated alcohol quencher was developed by Feldman et al.[56] Other suggested quenchers include $^{14}CO$, $^{131}I_2$ and $^{35}SO_2$.[49] In all such cases, apart from flaws possibly arising from the isotope effect and/or the lack of selectivity (reaction with transition and main group metal polymeryls, or multiple insertion in the case of CO[51, 53-55, 57-59]), a most obvious drawback is the need to prepare and handle radioactive substances.

A much more simple and safe strategy, implemented by Keii et al., is based on quenched-flow (QF) polymerization techniques (described by the Authors as "stopped-flow" techniques).[60-62] The idea is to operate at the very early stages of the polymerization process when chain growth is still within the 'controlled' kinetic regime (that is, before chain transfer becomes appreciable); under this regime it is easy to measure active site concentration as well as the specific rates of chain propagation and transfer from the time dependence of polymer molecular weight, according to Eqs1,2 below (originally developed by Natta et al.[47]).

$$R_p = k_p x^* [M][C_n H_{2n}] \tag{1}$$

$$\frac{1}{P_n} = \frac{1}{k_p [C_n H_{2n}]} \cdot \frac{1}{t} + \frac{f_{tr}}{k_p [C_n H_{2n}]} \tag{2}$$

where $R_p$ is polymerization rate; $k_p$ is rate coefficient of polymerization reaction; $x^*$ is the active sites content (ratio); [$M$] is the concentration of the catalyst metal; [$C_nH_{2n}$] is concentration of monomer; $t$ is polymerization time; $P_n$ is number-average degree of polymerization; $f_{tr}$ is average frequency of chain transfer.

In our work, we used Keii's QF approach in a later elaboration due to Terano.[61] Full details on the experimental setup and operation protocols will be provided in the following Chapters.
As we shall see, the QF approach is at the same time relatively simple and very robust, and yields reliable active site counts for both molecular and heterogeneous olefin polymerization catalysts. On the other hand, in the original applications by Keii and Terano the only technique used to characterize the polymers produced was Gel Permeation Chromatography (GPC), to determine molecular weight. An important innovation of this thesis was integration with NMR studies of polymer chain microstructure. In particular, the $^{13}C$ NMR identification of the chain ends in propene polymerization provides important insight into the mechanisms of chain intiation and transfer, as well as the generation and accumulation of 'dormant' sites.

It is worthy to note that even at the short reaction times typical of QF polymerizations number average polymerization degree is typically in the range of $10^2$ to $10^3$. Therefore, quantitative determinations of chain ends require the acquisition of spectra with very high Signal-to-Noise (S/N) ratio. In this respect, the recent implementation of NMR spctrometers with high-temperature cryoprobes, with a S/N higher by over one order of magnitude compared with conventional ones, represented a major step forward. One such spectrometer was used for the present work.

The thesis layout is quite simple. In Chapter 2 we introduce the experimental setup, and illustrate application to the supposedly simple case of ethene homopolymerization at molecular (homogeneous) catalytic centers. Despite the single-center catalyst nature and the well-defined structure of the precursors, we found that

polymerization kinetics can be highly deceptive, due to the interactions of the active sites with a variety of Lewis bases inherently present in the reaction pool. Not surprisingly, the kinetic study was even more complex for propene homopolymerization and copolymerization in the presence of heterogeneous ZNCs; Chapters 3 and 4 present the cases of 3$^{rd}$-generation (ethyl benzoate ID) and 4$^{th}$-generation (phthalate ID) systems, for which the information provided by $^{13}$C NMR chain end analysis was essential to unveil molecular kinetics. A brief summary and outlook is given in a final Chapter 5.

## References

1. Arlman, E. J.; Cossee, P., Ziegler-Natta Catalysis .3. Stereospecific Polymerization of Propene with the Catalyst System $TiCl_3$-$AlEt_3$. *J Catal* **1964,** *3* (1), 99-104.

2. Cossee, P., Ziegler-Natta Catalysis .1. Mechanism of Polymerization of Alpha-Olefins with Ziegler-Natta Catalysts. *J Catal* **1964,** *3* (1), 80-88.

3. Alkene polymerization reactions with transition metal catalysts. In *Studies in Surface Science and Catalysis*, Kissin, Y. V., Ed. Elsevier Science BV: Amsterdam, 2007; Vol. 173, pp 1-592.

4. Polyolefins: 50 years after Ziegler and Natta. I. Polyethylene and polypropylene. In *Adv Polym Sci*, Kaminsky, W., Ed. Springer-Verlag Berlin: Berlin, 2013; Vol. 257, pp 1-257.

5. Polyolefins: 50 years after Ziegler and Natta. II. Polyolefins by metallocenes and other single-site catalysts. In *Adv Polym Sci*, Kaminsky, W., Ed. Springer-Verlag Berlin: Berlin, 2013; Vol. 258, pp 1-362.

6. The themed issue. *Chem Rev* **2000,** *100* (4).

7. Metal catalysts in olefin polymerization. In *Topics in Organometallic Chemistry*, Guan, Z. B., Ed. Springer-Verlag: Berlin, 2009; Vol. 26, pp 1-255.

8. Handbook of polyolefins. Second edition, revised and expanded. Vasile, C., Ed. CRC Press: New York, 2000; pp 1-1032.

9. Haenel MW (2008) Historische Stätten der Chemie: Karl Ziegler. Max-Planck-Institut für Kohlenforschung, Mülheim An der Ruhr. English version available at www.kofo.mpg.de/media/2/D1105213/0478051227/Festschrift_e.pdf

(Accessed 22 March 2015).

10. Ziegler, K.; Holzkamp, E.; Breil, H.; Martin, H., Das Mülheimer Normaldruck-Polyäthylen-Verfahren. *Angew Chem* **1955,** *67* (19-2), 541-547.

11. Natta, G.; Pino, P.; Corradini, P.; Danusso, F.; Mantica, E.; Mazzanti, G.; Moraglio, G., Crystalline High Polymers of α-Olefins. *J Am Chem Soc* **1955,** *77* (6), 1708-1710.

12. Natta, G., Stereospezifische Katalysen und isotaktische Polymere. *Angew Chem* **1956,** *68* (12), 393-403.

13. Busico, V., Giulio Natta and the development of stereoselective propene polymerization. In *Adv Polym Sci*, Kaminsky, W., Ed. Springer-Verlag Berlin: Berlin, 2013; Vol. 257, pp 37-58.

14. Natta, G.; Corradini, P.; Allegra, G., The different crystalline modifications of $TiCl_3$, a catalyst component for the polymerization of α-olefins. I. α-, β-, γ-$TiCl_3$. II: δ-$TiCl_3$. *J Polym Sci* **1961,** *51* (156), 399–410.

15. Sementa, L.; D'Amore, M.; Barone, V.; Busico, V.; Causa, M., A quantum mechanical study of $TiCl_3$ α, β and γ crystal phases: geometry, electronic structure and magnetism. *Phys Chem Chem Phys* **2009,** *11* (47), 11264-11275.

16. Hermans, J. P.; Henrioulle, P. Catalytic complexes. US4210738 A.

17. Polypropylene handbook: polymerization, characterization, properties, applications. Moore, E. P., Ed. Hanser Publishers: Munich, 1996; pp 1-419.

18. Kashiwa, N., The discovery and progress of $MgCl_2$-Supported $TiCl_4$ catalysts. *J Polym Sci A- Polym Chem* **2004,** *42* (1), 1-8.

19. Luciani, L.; Kashiwa, N.; Barbe, P.; Toyota, A. α-Olefin Polymerization Catalyst. JPS52151691 (A) 1977.

20. Parodi, S.; Nocci, R.; Giannini, U.; Barbe, P.; Scata, U. Components and Catalysts for the Polymerization of Olefins. EP0045977 (A2), 1982.

21. Ohnishi, R.; Tsuruoka, M.; Funabashi, H.; Tanaka, A., Effect of 1-Allyl-3,4-Dimethoxybenzene on Propene Polymerization with the TiCl4/DBP(Dibutylphthalate)/$MgCl_2$ Catalyst. *Polym Bull* **1992,** *29* (1-2), 199-203.

22. Albizzati, E.; Barbe, P. C.; Noristi, L.; Scordamaglia, L. R.; Barino, L.; Giannini, U.; Morini, G. Components and catalysts for the polymerization of olefins. EP0361494 (A2)

23. Busico, V.; Pellecchia, R.; Cutillo, F.; Cipullo, R., High-throughput screening in olefin-polymerization catalysis: From serendipitous discovery towards rational understanding. *Macromol Rapid Commun* **2009,** *30* (20),

1697-1708.

24. Natta, G.; Pino, P.; Mazzanti, G.; Giannini, U., Bis-(cyclopentadienyl)-titanium dichloride —alkylaluminum complexes as catalysts for the polymerization of ethylene. *J Am Chem Soc* **1957,** *79* (11), 2975–2976.

25. Breslow, D. S.; Newburg, N. R., Bis-(cyclopentadienyl)-titanium dichloride —alkylaluminum complexes as catalysts for the polymerization of ethylene. *J Am Chem Soc* **1957,** *79* (18), 5072–5073.

26. Sinn, H.; Kaminsky, W., Ziegler-Natta Catalysis. *Adv Organomet Chem* **1980,** *18*, 99–149.

27. Kaminsky, W.; Kulper, K.; Brintzinger, H. H.; Wild, F. R. W. P., Polymerization of Propene and Butene with a Chiral Zirconocene and Methylalumoxane as Cocatalyst. *Angew Chem Int Edit* **1985,** *24* (6), 507-508.

28. Resconi, L.; Cavallo, L.; Fait, A.; Piemontesi, F., Selectivity in propene polymerization with metallocene catalysts. *Chem Rev* **2000,** *100* (4), 1253-1345.

29. Shapiro, P. J.; Bunel, E.; Schaefer, W. P.; Bercaw, J. E., $[((\eta^5\text{-}C_5Me_4)Me_2Si(\eta^1\text{-}NCMe_3))(PMe_3)ScH]_2$ - A Unique Example of a Single-Component α-Olefin Polymerization Catalyst. *Organometallics* **1990,** *9* (3), 867-869.

30. Hughes, A. K.; Kingsley, A. J., Novel syntheses of linked cyclopentadienyl-amide complexes. *J Chem Soc Dalton* **1997,** (22), 4139-4141.

31. Johnson, L. K.; Killian, C. M.; Brookhart, M., New Pd(II)- and Ni(II)-based catalysts for polymerization of ethylene and α-olefins. *J Am Chem Soc* **1995,** *117* (23), 6414-6415.

32. Wang, C. M.; Friedrich, S.; Younkin, T. R.; Li, R. T.; Grubbs, R. H.; Bansleben, D. A.; Day, M. W., Neutral nickel(II)-based catalysts for ethylene polymerization. *Organometallics* **1998,** *17* (15), 3149-3151.

33. Younkin, T. R.; Conner, E. F.; Henderson, J. I.; Friedrich, S. K.; Grubbs, R. H.; Bansleben, D. A., Neutral, single-component nickel (II) polyolefin catalysts that tolerate heteroatoms. *Science* **2000,** *287* (5452), 460-462.

34. Bochmann, M., Kinetic and mechanistic aspects of metallocene polymerisation catalysts. *J Organomet Chem* **2004,** *689* (24), 3982-3998.

35. Chen, E. Y. X.; Marks, T. J., Cocatalysts for metal-catalyzed olefin polymerization: Activators, activation processes, and structure-activity

relationships. *Chem Rev* **2000,** *100* (4), 1391-1434.

36. Krossing, I.; Raabe, I., Noncoordinating anions - Fact or fiction? A survey of likely candidates. *Angew Chem Int Edit* **2004,** *43* (16), 2066-2090.

37. Stukalov, D. V.; Zakharov, V. A., Active site formation in $MgCl_2$-supported Ziegler-Natta catalysts. A density functional theory study. *J Phys Chem C* **2009,** *113* (51), 21376-21382.

38. Bahri-Laleh, N.; Correa, A.; Mehdipour-Ataei, S.; Arabi, H.; Haghighi, M. N.; Zohuri, G.; Cavallo, L., Moving up and down the titanium oxidation state in Ziegler-Natta catalysis. *Macromolecules* **2011,** *44* (4), 778-783.

39. Hicks, F. A.; Brookhart, M., A highly active anilinotropone-based neutral nickel(II) catalyst for ethylene polymerization. *Organometallics* **2001,** *20* (15), 3217-3219.

40. Makio, H.; Terao, H.; Iwashita, A.; Fujita, T., FI catalysts for olefin polymerization-A comprehensive treatment. *Chem Rev* **2011,** *111* (3), 2363-2449.

41. Busico, V.; Cipullo, R.; Ronca, S., Propene/ethene-[1-C-13] copolymerization as a tool for investigating catalyst regioselectivity. 1. Theory and calibration. *Macromolecules* **2002,** *35* (5), 1537-1542.

42. Busico, V.; Cipullo, R.; Polzone, C.; Talarico, G.; Chadwick, J. C., Propene/ethene-[1-C-13] copolymerization as a tool for investigating catalyst regioselectivity. 2. The $MgCl_2/TiCl_4$-$AlR_3$ system. *Macromolecules* **2003,** *36* (8), 2616-2622.

43. Busico, V.; Cipullo, R., Microstructure of polypropylene. *Prog Polym Sci* **2001,** *26* (3), 443-533.

44. Resconi, L.; Camurati, I.; Sudmeijer, O., Chain transfer reactions in propylene polymerization with zirconocene catalysts. *Top Catal* **1999,** *7* (1-4), 145-163.

45. Ali, M. A. H.; Betlem, B.; Roffel, B.; Weickert, G., Hydrogen response in liquid propylene polymerization: Towards a generalized model. *AIChE J* **2006,** *52* (5), 1866-1876.

46. Natta, G., Kinetic studies of α-olefin polymerization. *J Polym Sci* **1959,** *34* (127), 21-48.

47. Natta, G.; Pasquon, I., The Kinetics of the Stereospecific Polymerization of α-Olefins. *Adv Catal* **1959,** *11*, 1-66.

48. Bier, G., Active-centers of $TiCl_3$ catalysts for propene polymerization. *Polym Bull* **1982,** *7* (4), 177-184.

49. Mejzlik, J.; Lesna, M.; Kratochvila, J., Determination of the number of active-centers in Ziegler-Natta polymerizations of olefins. *Adv Polym Sci* **1986,** *81*, 83-120.

50. Marques, M. M.; Tait, P. J. T.; Mejzlik, J.; Dias, A. R., Polymerization of ethylene using high-activity Ziegler-type catalysts: Active center determination. *J Polym Sci A- Polym Chem* **1998,** *36* (4), 573-585.

51. Busico, V.; Guardasole, M.; Margonelli, A.; Segre, A. L., Insertion of carbon monoxide into Zr-polymeryl bonds: "Snapshots" of a running catalyst. *J Am Chem Soc* **2000,** *122* (21), 5226-5227.

52. Liu, Z. X.; Somsook, E.; Landis, C. R., A $^{2}$H-labeling scheme for active-site counts in metallocene-catalyzed alkene polymerization. *J Am Chem Soc* **2001,** *123* (12), 2915-2916.

53. Fukui, Y.; Murata, M., Reaction of carbon monoxide with living PP prepared with a $Cp_2ZrMe_2/B(C_6F_5)_3$ catalyst system. *Macromol Chem Physic* **2001,** *202* (8), 1430-1434.

54. Budzelaar, P. H. M., CO/ethene copolymerization at zirconocene centers? *Organometallics* **2004,** *23* (4), 855-860.

55. Shiono, T.; Ohgizawa, M.; Soga, K., Reaction between carbon monoxide and a Ti-polyethylene bond with a $MgC1_2$-supported $TiCl_4$ catalyst system. *Makromol Chem* **1993,** *194* (7), 2075-2085.

56. Feldman, C. F.; Perry, E., Active Centers in the Polymerization of Ethylene Using Titanium Tetrachloride-Alkylaluminum Catalysts. *J Polym Sci* **1960,** *46* (147), 217-231.

57. Bukatov, G. D.; Goncharov, V. S.; Zakharov, V. A., Number of active-centers and propagation rate constants in the propene polymerization on supported Ti-Mg catalysts in the presence of hydrogen. *Macromol Chem Physic* **1995,** *196* (5), 1751-1759.

58. Zakharov, V. A.; Bukatov, G. D.; Barabanov, A. A., Recent data on the number of active centers and propagation rate constants in olefin polymerization with supported ZN catalysts. *Macromol Symp* **2004,** *213*, 19-28.

59. Mason, M. R.; Song, B. X.; Kirschbaum, K., Remarkable room-temperature insertion of carbon monoxide into an aluminum-carbon bond of tri-tert-butylaluminum. *J Am Chem Soc* **2004,** *126* (38), 11812-11813.

60. Keii, T.; Terano, M.; Kimura, K.; Ishii, K., A kinetic argument for a quasi-living polymerization of propene with a $MgCl_2$-supported catalyst.

*Makromol Chem-Rapid Commun* **1987,** *8* (11), 583-587.

61. Taniike, T.; Sano, S.; Ikeya, M.; Thang, V. Q.; Terano, M., Development of a large-scale stopped-flow system for heterogeneous olefin polymerization kinetics. *Macromol React Eng* **2012,** *6* (6-7), 275-279.

# Chapter 2. The Efforts with Homogeneous Catalytic Systems

## 2.1. Introduction

It is undeniable that 'well-defined' molecular systems of catalytic olefin polymerization, for example metallocenes or post-metallocenes, have been studied intensively. They are believed to be simpler than Ziegler-Natta catalysts (ZNCs) and easier to study. And it is also the fact that much of the knowledge on ZNCs was transplanted from molecular systems. In 2000, there was a themed issue of *Chemical Reviews* (volume 100, issue 4, ACS Publications) on the state of the art which is still highly valid. Among those authors Resconi et al. elaborated on the history and mechanisms of the propene polymerization with metallocene catalysts.[1] It provided a systematic reasoning with the mechanistic insight.

As discussed in Chapter 1 (also Figure 1 in this chapter), the catalytic cycle of olefin polymerization is apparently simple: according to the generally accepted mechanism[2-3], the monomer bonds to a coordinatively unsaturated transition metal-alkyl species, and inserts into the active M-C σ-bond with a chain migratory path passing through a trivial four-centre transition state. β-H elimination, which is the most important competing process, can be effectively modulated with a proper choice of metal and ancillary ligand(s),[4-9] down to the limit of 'living' (more properly 'controlled'[10]) polymerization.

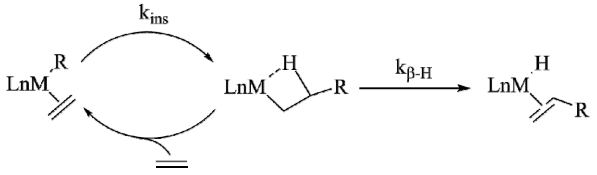


**Figure 1**. Catalytic cycle of olefin polymerization.

Back to the review of Resconi et al.,[1] it actually mostly relied on computational results to address the issues of kinetics. It was four years later when Bochmann summarized the progress in kinetics of metallocene system, including experimental and computational work.[12] This review stressed on hexene polymerization that is slow enough for NMR study[13-16]. It was found the first insertion of hexene was two orders of magnitude slower than the following ones for (EBI)ZrMe(μ-Me)B($C_6F_5$)$_3$ catalyst [EBI= rac-$C_2H_4$(Ind)$_2$]. According to the deuterium labeling that was carried out by Landis et al., the active sites content (ratio of active Zr to total Zr) was almost 100%.[13] For propene or ethene polymerization that is too fast to study with NMR approaches, only a few cases like (SBI)$ZrMe_2$/Al(*i*Bu)$_3$/[$Ph_3C$][CN(B($C_6F_5$)$_3$)$_2$] [SBI = *rac*-$Me_2$-Si(Ind)$_2$],[17] $Cp_2TiCl_2$/MAO[18] and *rac*-$Me_2$Si(2-Me-4-Ph-1-Ind)$_2Zr Cl_2$/MAO[11] were studied with quenched-flow technique. The surprising lack of efforts on kinetics study does not indicate a thorough understanding about the process has been achieved. To the contrary, ironically, predicting the activity of a new catalyst is still practically impossible, and experimental testing remains the best way to find out. This persisting 'black box' is largely due to the ambiguity of what governs the monomer coordination-insertion loop (Figure 1). And the fine structure of the catalytic species is a critical point.

Olefin polymerization catalysts, particularly those based on early transition metals, are highly electrophilic complexes. Thoroughly scavenging heteroatom-containing molecules (ubiquitous impurities like water and dioxygen, but also less obvious poisons) is mandatory for proper functioning of the catalysts.[19-20] Even with the use of scavengers, though, electron donors are all around, some of which unavoidable, like the counterion in case of cationic active species,[21] and the reaction products of precatalyst activation and system scavenging. The latter may include a variety of bridged heterodinuclear adducts, particularly when the activator and/or the scavenger is a main group metal-alkyl[22]; hundreds of papers and several books and reviews deal with the concept of 'non-interactive'

anions and scavengers[21], which unfortunately remains to a large extent wishful thinking.[19, 23] The subtle balance between the opposite requirements of a Lewis acidic character and a controllable crave for electrons is what makes the game difficult and hardly predictable as well.

In the most common scenario for homogeneous systems, methylaluminoxane (MAO) has the dual function of activator and scavenger.[21] Importantly, a significant amount of 'free' $AlMe_3$ is always in equilibrium with MAO, and can be detrimental to catalytic activity by forming heterodinuclear adducts with the active species;[12, 24] in such a case, addition of a sterically demanding $Me_3Al$ trap such as 2,6-*t*$Bu_2$-4-Me-phenol (BHT) is often beneficial.[25]

In this study kinetic parameters of chain propagation were collected with experiments at varying temperatures under controlled polymerization conditions (that is with negligible chain transfer and termination in the time scale of the experiments).[10] In particular, a simple Quenched-Flow (QF) setup was firstly validated with a 'living' non-metallocene catalyst, and then used to assess a much faster *ansa*-zirconocene one.

## 2.2. Experimental Part

### *2.2.1. Chemicals*


**C1** **C2**

**Figure 2**. Catalyst precursors **C1** (R = $C_6F_5$) and **C2.**

Catalyst precursors **C1** and **C2** were purchased from MCAT GmbH.

MAO (10% w/w solution in toluene) was obtained from Chemtura GmbH; according to $^{1}$H NMR analysis, 'free' $Me_3Al$ amounted to ~30% by mol of total Al. Toluene (Romil, HPLC grade) was purified by passing through a column filled up with BASF R 3-11/G catalyst and molecular sieve 3A in an MBraun SPS-5 compact to remove oxygen and moisture. BHT (Aldrich, >99.0%) was used as received.

### *2.2.2. Polymerization*

The quenched-flow polymerization was carried out using the setup shown in Figure 3, adapted from Ref. [26]. The system consists of two 3-necked jacketed 2 L Pyrex glass vessels (A and B). A contains catalyst whereas B contains monomer. The exact formula depends on the experiment as being required. Please see the following chapters for details. Necks 1a and 1b are connected through Rotaflo™ pin valves to a Schlenk line operating under vacuum or argon; neck 1b is also connected to the monomer supply line. Necks 2, with SVL15 pierced caps, are used with an O-ring seal to enter the Viton™ dip tubes. Necks 3 and 4, finally, have SVL15 and SVL30 screw caps respectively and are used for the loading of chemicals. The vessels are connected by Viton™ tubes to a dual channel Masterflex® (mod.7200-60) peristaltic pump capable of dispensing the liquid phases out of vessels A and B in a highly controlled and reproducible way. Downstream to the pump, the dip tubes converge to a Teflon®-made T-junction where the two liquid phases at a Reynolds number of $\sim 1.0\times10^4$ undergo 'instantaneous' mix and start the polymerization reaction, and are then pushed into a polymerization tubing. The reaction phase flowing out of the latter is quenched with >1 L of a methanol/HCl (aq,conc) solution (5% v/v), maintained under vigorous mechanical stirring by a homogeniser ($\sim 1.0\times10^4$ rpm) to assure practically immediate quenching.

The rate of each upstream flow is kept at 10.0 mL $s^{-1}$. The relationship between polymerization time $t$, polymerization line length $l$ and liquid flow $Q$ is given by Equation 1:

$$t = \frac{(l \times \pi r^2 + k)}{Q} \tag{1}$$

with $r$ the inner radius of the line and $k$ a correcting term taking into account the additional volume of the mixing chamber inside the T-junction. The range of t for this study was 0.06 – 4 s.

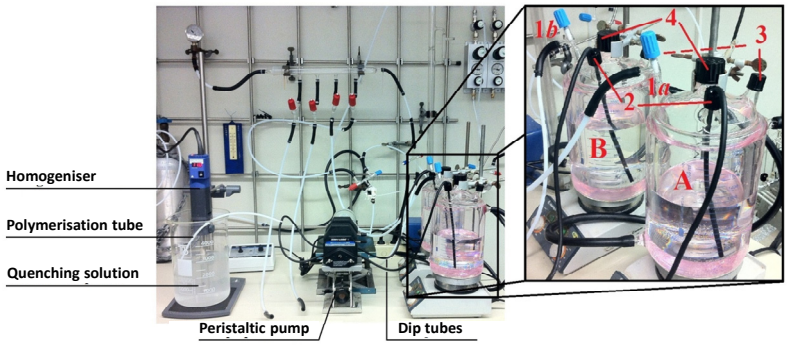


**Figure 3**. The photo of quenched-flow setup.

Vessels A and B are charged under argon with the desired amount of MAO or MAO/BHT in toluene. The solution in vessel B is saturated with the monomer at the desired partial pressure (concentration). Both solutions, under magnetic stirring (~1000 rpm), are brought to the desired temperature by circulating denatured alcohol from a thermostat in the vessel jackets. Finally, the appropriate amount of precatalyst in toluene solution is added into vessel A, and a 5-20 min contact time between precatalyst and activator is allowed. Once the experiment is over, the polymer is left to coagulate overnight in the quenching medium, and then filtered and dried under vacuum.

In the case of batch polymerization with catalyst system **C1**/MAO/BHT, the ethene polymerization experiments were run in a 500 mL jacketed Pyrex glass reactor connected to a Schlenk line operating under argon. 250 mL of a toluene solution of MAO/BHT were saturated under magnetic stirring (800 rpm) at 283 K with ethene at a 70 mM concentration. In a separate vial, a proper amount

of precatalyst was dissolved in a 2 mL aliquot of the MAO/BHT toluene solution, and after an activation time of 5 min injected into the reactor through a silicon rubber septum. After a desired time (10-20 s), the reaction was quenched by injecting through the same septum 5 mL of methanol/HCl. The polymers were collected in the same way as described for the QF experiments.

### *2.2.3. Characterization*

All polymer samples were characterized by Gel Permeation Chromatography (GPC). A Freeslate Rapid-GPC equipment was used under the following conditions: temperature, 145°C; eluent, 1,2-dichlorobenzene (added with BHT, 0.4 mg $mL^{-1}$); 2 Agilent Technologies columns (PLgel 10 μm MIXED-B, 300x7.5 mm); sample concentration, 1.0 mg $mL^{-1}$; flow, 1.0 mL $min^{-1}$. The universal calibration method was adopted, with 12 monodisperse polystyrene standards ($M_n$ between 1.3 and 3700 kDa).

## 2.3. Results and Discussion

Two sets of QF ethene polymerization experiments in toluene solution were carried out at 298 and 313 K in the presence of **C1**/MAO/BHT, and polymer yield and molecular mass distribution were measured at each temperature (the latter by high temperature Gel Permeation Chromatography) as a function of time (Table 1). The very low polydispersity index (PDI) of the polymers, typical of a controlled kinetic regime,[10] is a first indication of consistent setup behavior. Plots of $Y$ *vs* $t$ and $1/P_n$ *vs* $1/t$ feature the linear correlations expected from Equation 2,3 (Figure 4).

$$R_p = k_p x^* [M][C_n H_{2n}] \tag{2}$$

$$\frac{1}{P_n} = \frac{1}{k_p [C_n H_{2n}]} \cdot \frac{1}{t} + \frac{f_{tr}}{k_p [C_n H_{2n}]} \tag{3}$$

where $R_p$ is polymerization rate; $k_p$ is rate coefficient of polymerization reaction; $x^*$ is the active sites content (ratio); [$M$] is

the concentration of the catalyst metal; $[C_nH_{2n}]$ is concentration of monomer; $t$ is polymerization time; $P_n$ is number-average degree of polymerization; $f_{tr}$ is average frequency of chain transfer.

The best-fit straight lines through the data points in the latter plot hit the origin, which confirms that $f_t$ for this catalyst is extremely low.[8-9] As a matter of fact, a direct plot of $P_n$ *vs* $t$ might have been used to measure $k_p$; the implication is that an accurate quantification of $f_t$ with this approach is not feasible.

The values of $x^*$ and $k_p$ in Table 2, obtained by linear regression, are in nice agreement with corresponding ones calculated from previous literature data.[8]

**Table 1**. Results of ethene polymerization experiments in toluene in the presence of **C1**/MAO/BHT.

| *T*/ K | *t*/ s | *n*(Ti)/ μmol | Yield/ mg | $10^{-2}$ $Y^{(a)}$ | $10^{-3}$ $P_n$ | *Mw/Mn* |
|---|---|---|---|---|---|---|
| 283(b) | 10 | 1.09 | 75 | 25 | 2.5 | 1.4 |
| | 15 | 0.75 | 90 | 43 | 4.2 | 1.4 |
| | 20 | 0.44 | 77 | 63 | 6.7 | 1.4 |
| 298(c) | 0.25 | 16.0 | 37 | 0.83 | 0.10 | 1.1 |
| | 0.51 | 7.43 | 38 | 1.8 | 0.23 | 1.1 |
| | 0.94 | 3.17 | 31 | 3.5 | 0.53 | 1.1 |
| 313(c) | 0.51 | 7.43 | 43 | 2.1 | 0.24 | 1.0 |
| | 0.72 | 7.30 | 57 | 2.8 | 0.38 | 1.0 |
| | 1.02 | 5.24 | 58 | 4.0 | 0.56 | 1.1 |

(a) mol($C_2H_4$)/mol(Ti). (b) Conventional polymerization setup. (c) QF polymerization setup. Other experimental conditions: [MAO] = 13.5 mM; [BHT] = 10.0 mM; [Ti] = 4 – 8 μM; precatalyst activation time = 5 min.

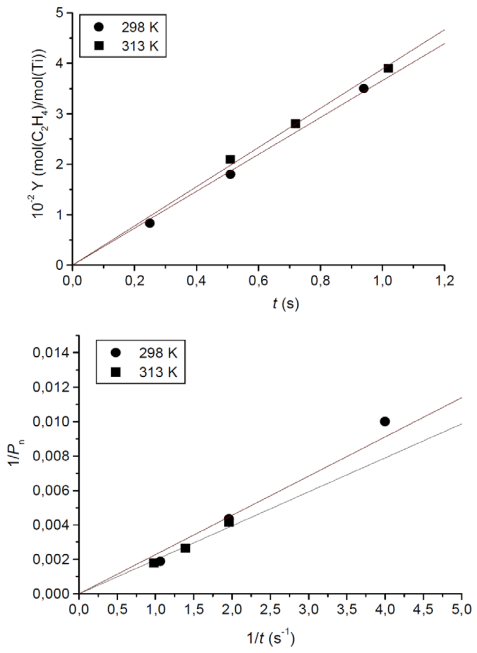


**Figure 4**. Plots of Y *vs* t and 1/Pn vs 1/t for ethene polymerization in the presence of C1/MAO/BHT (based on the data in Table 1).

**Table 2**. Temperature dependence of $k_p$ and $x^*$ for ethene polymerization in the presence of C1/MAO/BHT (based on the data in Table 1).

| *T*/ K | $k_p$/ ($10^3$ L $mol^{-1}$ $s^{-1}$) | $x^*$/ % |
|---|---|---|
| 283 | 3.8±0.4 | 96 |
| 298 | 4.8±0.2 | 75 |
| 313 | 6.7±0.5 | 78 |

A third set of experiments at 283 K was carried out in a conventional glass reactor with longer polymerization times ($t$ = 10-20 s, followed by injection of methanol/HCl). Here $Y$ and $P_n$ increased linearly with $t$ (Table 1) as well; the corresponding values of $k_p$ and $x^*$ are listed in Table 2. The higher polydispersity values are likely due to the effects of polymer precipitation at higher $P_n$.[8]

The Eyring plot of $k_p$ (Figure 5), featuring a very good correlation, yields $\Delta^{\ddagger}H^{o}$ = 2.7±0.4 kcal·mol$^{-1}$, $\Delta^{\ddagger}S^{o}$ = -32±1 cal·K$^{-1}$·mol$^{-1}$. These activation parameters fit paradigmatically with the mechanism of Scheme 1; in particular, $\Delta^{\ddagger}S^{o}$ is in the range expected for an associative process involving monomer capture.

In view of $\Delta^{\ddagger}H^{o}$ that is very low and $x^{*}$ that is close to 1 (Table 2), it is hard to imagine the activity (i.e. the $k_p$ $x^{*}$ product) of C1/MAO/BHT is actually at least one order of magnitude lower than that of the champions in the field.

For one of these, namely *rac*-bis(2-Me-4-Ph-1-Ind)$ZrCl_2$ (**C2** of Figure 2) in combination with MAO, some years ago we carried out a similar QF study with the setup of Ref. 27.[11] Quite surprisingly, from the Eyring plot of kp (Table 3 and Figure 6) we estimated $\Delta^{\ddagger}H^{o}$ = 10±1 kcal·mol$^{-1}$, $\Delta^{\ddagger}S^{o}$ = 3.7±0.3 cal·K$^{-1}$ mol$^{-1}$; therefore, one can conclude that ethene polymerization with C2/MAO is much faster than with C1/MAO/BHT due to a negligible $\Delta^{\ddagger}S^{o}$, which offsets the effects of a high $\Delta^{\ddagger}H^{o}$ and lower $x^{*}$.

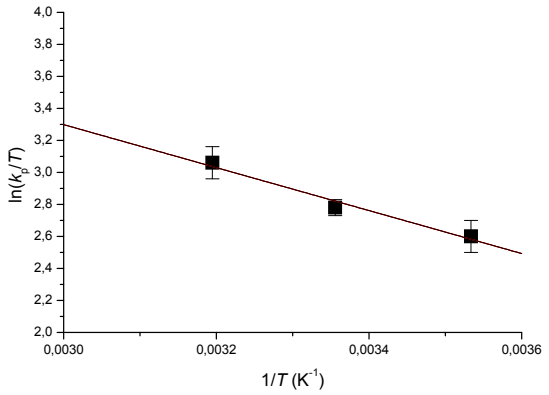


**Figure 5**. Eyring plot of kp for ethene polymerization in the presence of **C1**/MAO/BHT (based on the data in Table 2).

Before endorsing such a conclusion, we considered it worthwhile to

double-check it using the improved QF setup[26] which was just validated with **C1**/MAO/BHT. A first set of experiments at $T$ = 293 K gave the results of Table 4; Figure 7 compares said results with previously published ones.[11] A slight induction observed in the $Y$ *vs* $t$ plot made it necessary to use Equation 4,5 ($f_i$ = average frequency of chain initiation) in the place of Equation 2,3[11]

$$Y = k_p x^* [M][C_n H_{2n}][t + \frac{1}{f_i}(e^{-f_i t} - 1)] \qquad (4)$$

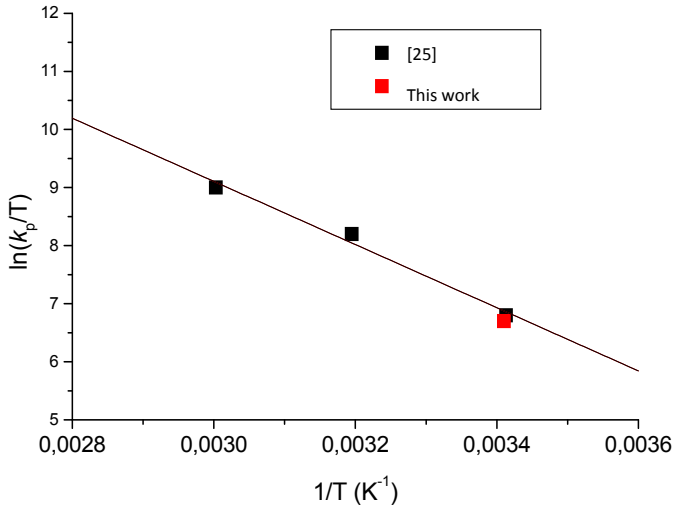


**Figure 6**. Eyring plot of $k_p$ for ethene polymerization in the presence of **C2**/MAO.

$$\frac{1}{P_n} = \frac{1 - e^{-f_i t}}{k_p [C_n H_{2n}][t + \frac{1}{f_i}(e^{-f_i t} - 1)]} + \frac{f_{tr}}{k_p [C_n H_{2n}]} \qquad (5)$$

Practically no difference in $k_p$ was observed although a different curve of $1/P_n$ *vs* $1/t$ was obtained (Figures 6, 7 and Table 3). This demonstrates that the kinetic approach is robust and reliable, even in

the case of extremely active homogeneous catalysts like the one being investigated here.

The next question evidently is how it can be that $\Delta^{\ddagger}S^{o}$ is negligible in a catalytic olefin polymerization process. Looking at Figure 1, a strong $\Delta^{\ddagger}S^{o}$ penalty seems inherent in the mechanism, unless one postulates that (i) the catalytic species is not a 'naked' cation but rather an adduct of said cation with an electron donating species, and (ii) the entropy loss upon monomer capture is compensated by a temporary splitting of the aforementioned adduct.[28] Compared with [**C1**-R]$^{+}$, one should note that the [**C2**-R]$^{+}$ cation features a more sterically open ancillary ligand frame; our working hypothesis is that 'free' $AlMe_3$ in equilibrium with MAO is the most likely interacting moiety.[12, 25]

Determining the kinetic behaviors of **C2**/MAO/BHT for ethene polymerization is critical to test the hypothesis. The data of QF study of propene polymerization listed in Table 5, on the other hand, highlighted a totally different temperature-activity profile for **C2**/MAO and **C2**/MAO/BHT under QF conditions, suggesting indeed a much lower $\Delta^{\ddagger}H^{o}$ for the latter system.

**Table 3**. Temperature dependence of $k_p$ and $x^{*}$ for ethene polymerization in the presence of **C2**/MAO

| $T$/ K | $k_p$/ $10^5$ L·mol$^{-1}$·s$^{-1}$ | $f_{tr}$/ s$^{-1}$ | $f_i$/ s$^{-1}$ | $x^{*}$/ % |
|---|---|---|---|---|
| 293 (this work) | 2.3±0.1 | 3.6±0.7 | 10±2 | 10±1 |
| 293 [25] | 2.6±0.3 | 7±2 | n.d | 4.6±0.7 |
| 313 [25] | 11±1 | 17±3 | n.d | 10±1 |
| 333 [25] | 28±5 | 35±10 | n.d. | 23±4 |

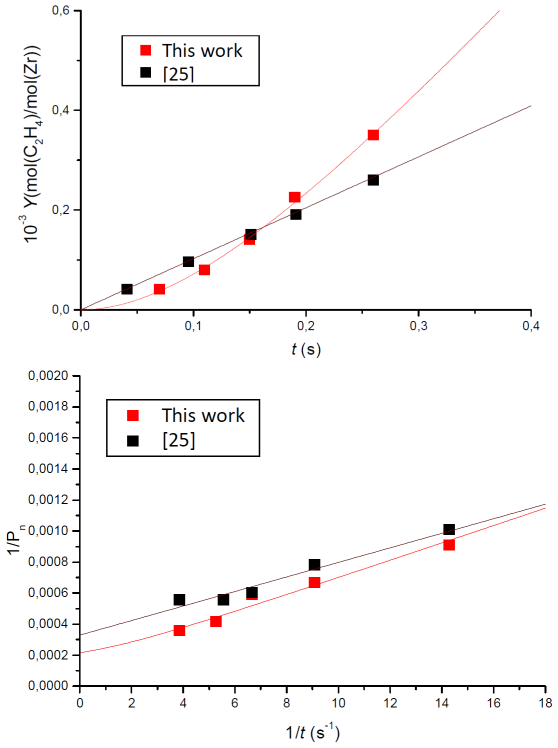


**Figure 7**. Plots of $Y$ *vs* $t$ and $1/P_n$ *vs* $1/t$ for ethene polymerization with **C2**/MAO at $T = 293$ K (based on the data of Table 4 and Ref. [11]).

**Table 4**. Results of QF ethene polymerization experiments in toluene with **C2**/MAO at 293 K.

| $t$/ s | $n$(Zr)/μmol | Yield/ mg | $Y^{(a)}$ | $10^{-3}P_n$ | $M_w/M_n$ |
|---|---|---|---|---|---|
| 0.07 | 45.3 | 51.8 | 40.8 | 1.1 | 1.7 |
| 0.11 | 46.4 | 104.0 | 79.9 | 1.5 | 1.7 |
| 0.15 | 28.6 | 112.6 | 140 | 1.7 | 1.7 |
| 0.19 | 28.9 | 187.3 | 226 | 2.4 | 1.7 |

[(a)] mol($C_2H_4$)/mol(Zr). Other experimental conditions: [MAO] = 65 mM; [Zr] = 30 μM; precatalyst activation time = 20 min.

**Table 5**. Results of QF propene polymerization experiments in toluene in the presence of **C2**/MAO and **C2**/MAO/BHT.

| Catalyst system | *T*/ K | *t*/ s | $10^{-2}Y^{(a)}$ |
|---|---|---|---|
| MAO/BHT | 283 | 0.48 | 5.6 |
| | 298 | 0.44 | 7.4 |
| | 313 | 0.45 | 7.4 |
| MAO | 288 | 0.55 | 0.69 |
| | 298 | 0.47 | 1.6 |
| | 313 | 0.47 | 4.9 |

[(a)] mol($C_3H_6$)/mol(Zr). Other experimental conditions: [MAO] = 0.12 M; [BHT] = 0.09 M; [Zr] = 30 μM; precatalyst activation time = 20 min.

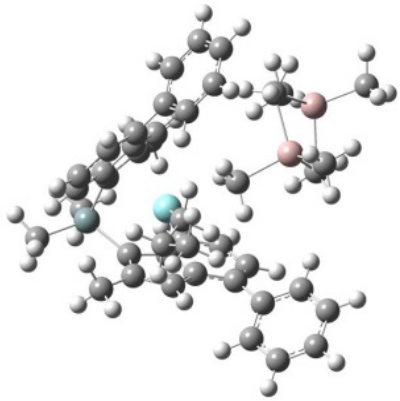

Figure 8. Possible interaction of [**C2**-Propyl]$^+$ with a terminal methyl of $Al_2Me_6$ .

Heterodinuclear ($L_yM$)-(μR)(μ-Me)-($AlMe_2$) adducts are well-documented in metallocene catalysis,[12] but there is evidence that they are catalytically inactive.[12, 24] According to DFT calculations, the energy cost to split typical zirconocenium-(μ-Me)$_2$-($AlMe_2$) cations is >15 kcal·mol$^{-1}$,[24] which may well justify the observed induction in the *Y vs t* plot of Figure 7. A weaker interaction, on the other hand, might involve a terminal methyl of $AlMe_3$ or $Al_2Me_6$ (see e.g. Figure 8).

## 2.4. Conclusions

In principle, catalytic reactions can be tuned by lowering the activation free energy of a desired reaction, thus providing a more convenient path. However, it can happen that the '*free'* qualification is overlooked; as a matter of fact, in typical cases the catalyst acts on the *internal* activation energy, and in all cases entropy is a more difficult concept to grasp and to design for.

In stereoselective catalysis, in particular, some degree of steric hindrance at the catalytic species is a must, and its consequences on the entropy balance of a given reaction can be subtle and non-obvious. The case discussed here is, in our opinion, a nice example to understand why designing a good olefin polymerization catalyst remains a very complicated exercise, with serendipity still playing an important role. On the other hand, it also demonstrates that with a proper kinetic analysis the relevant mechanistic features can be sorted out, and the true features governing catalyst behaviors can be properly highlighted ex-post and ultimately foreseen, at least in fine-tuning elaborations.

## References

1. Resconi, L.; Cavallo, L.; Fait, A.; Piemontesi, F., Selectivity in propene polymerization with metallocene catalysts. *Chem Rev* **2000,** *100* (4), 1253-1345.

2. Cossee, P., Ziegler-Natta catalysis .1. Mechanism of polymerization of α-olefins with Ziegler-Natta catalysts. *J Catal* **1964,** *3* (1), 80-88.

3. Arlman, E. J.; Cossee, P., Ziegler-Natta catalysis .3. Stereospecific polymerization of propene with the catalyst system $TiCl_3$-$AlEt_3$. *J Catal* **1964,** *3* (1), 99-104.

4. Stehling, U.; Diebold, J.; Kirsten, R.; Roll, W.; Brintzinger, H. H.; Jungling, S.; Mulhaupt, R.; Langhauser, F., Ansa-zirconocene polymerization catalysts with annelated ring ligands. Effects on catalytic activity and polymer-chain length. *Organometallics* **1994,** *13* (3), 964-970.

5. Ittel, S. D.; Johnson, L. K.; Brookhart, M., Late-metal catalysts for

ethylene homo- and copolymerization. *Chem Rev* **2000,** *100* (4), 1169-1203.

6. Talarico, G.; Busico, V.; Cavallo, L., "Living" propene polymerization with bis(phenoxyimine) group 4 metal catalysts: New strategies and old concepts. *Organometallics* **2004,** *23* (25), 5989-5993.

7. Mitani, M.; Furuyama, R.; Mohri, J.; Saito, J.; Ishii, S.; Terao, H.; Kashiwa, N.; Fujita, T., Fluorine- and trimethylsilyl-containing phenoxy-imine Ti complex for highly syndiotactic living polypropylenes with extremely high melting temperatures. *J Am Chem Soc* **2002,** *124* (27), 7888-7889.

8. Mitani, M.; Mohri, J.; Yoshida, Y.; Saito, J.; Ishii, S.; Tsuru, K.; Matsui, S.; Furuyama, R.; Nakano, T.; Tanaka, H.; Kojoh, S.; Matsugi, T.; Kashiwa, N.; Fujita, T., Living polymerization of ethylene catalyzed by titanium complexes having fluorine-containing phenoxy-imine chelate ligands. *J Am Chem Soc* **2002,** *124* (13), 3327-3336.

9. Coates, G. W.; Hustad, P. D.; Reinartz, S., Catalysts for the living insertion polymerization of alkenes. Access to new polyolefin architectures using Ziegler-Natta chemistry. *Angew Chem Int Edit* **2002,** *41* (13), 2236-2257.

10. Busico, V.; Talarico, G.; Cipullo, R., Living Ziegler-Natta polymerizations. True or false? *Macromol Symp* **2005,** *226*, 1-16.

11. Busico, V.; Cipullo, R.; Esposito, V., Stopped-flow polymerizations of ethene and propene in the presence of the catalyst system *rac*-$Me_2Si$(2-methyl-4-phenyl-1-indenyl)$_2ZrCl_2$/methylaluminoxane. *Macromol Rapid Commun* **1999,** *20* (3), 116-121.

12. Bochmann, M., Kinetic and mechanistic aspects of metallocene polymerisation catalysts. *J Organomet Chem* **2004,** *689* (24), 3982-3998.

13. Liu, Z. X.; Somsook, E.; White, C. B.; Rosaaen, K. A.; Landis, C. R., Kinetics of initiation, propagation, and termination for the [*rac*-($C_2H_4$(1-indenyl)$_2$)ZrMe][$MeB(C_6F_5)_3$]-catalyzed polymerization of 1-hexene. *J Am Chem Soc* **2001,** *123* (45), 11193-11207.

14. Landis, C. R.; Rosaaen, K. A.; Uddin, J., Heavy-atom kinetic isotope effects, cocatalysts, and the propagation transition state for polymerization of 1-hexene using the *rac*-($C_2H_4$(1-indenyl)$_2$)$ZrMe_2$ catalyst precursor. *J Am Chem Soc* **2002,** *124* (41), 12062-12063.

15. Sillars, D. R.; Landis, C. R., Catalytic propene polymerization. Determination of propagation, termination, and epimerization kinetics by direct NMR observation of the (EBI)Zr($MeB(C_6F_5)_3$)propenyl catalyst species. *J Am Chem Soc* **2003,** *125* (33), 9894-9895.

16. Landis, C. R.; Rosaaen, K. A.; Sillars, D. R., Direct observation of insertion events at *rac*-($C_2H_4$(1-indenyl)$_2$)Zr(MeB(C6F5)$_3$)-polymeryl intermediates. Distinction between continuous and intermittent propagation modes. *J Am Chem Soc* **2003,** *125* (7), 1710-1711.

17. Song, F. Q.; Cannon, R. D.; Bochmann, M., Zirconocene-catalyzed propene polymerization. A quenched-flow kinetic study. *J Am Chem Soc* **2003,** *125* (25), 7641-7653.

18. Shiono, T.; Ohgizawa, M.; Soga, K., Reaction of the Ti-polyethylene bond with carbon-monoxide over the bis(cyclopentadienyl)titanium dichloride methylaluminoxane catalyst system. *Polymer* **1994,** *35* (1), 187-192.

19. Stapleton, R. A.; Galan, B. R.; Collins, S.; Simons, R. S.; Garrison, J. C.; Youngs, W. J., Bulky aluminum alkyl scavengers in olefin polymerization with group 4 catalysts. *J Am Chem Soc* **2003,** *125* (31), 9246-9247.

20. Shreve, A. P.; Mulhaupt, R.; Fultz, W.; Calabrese, J.; Robbins, W.; Ittel, S. D., Sterically hindered aryloxide-substituted alkylaluminum compounds. *Organometallics* **1988,** *7* (2), 409-416.

21. Chen, E. Y. X.; Marks, T. J., Cocatalysts for metal-catalyzed olefin polymerization. Activators, activation processes, and structure-activity relationships. *Chem Rev* **2000,** *100* (4), 1391-1434.

22. Rocchigiani, L.; Busico, V.; Pastore, A.; Talarico, G.; Macchioni, A., Unusual hafnium-pyridylamido/ERn heterobimetallic adducts (ERn = $ZnR_2$ or $AlR_3$). *Angew Chem Int Edit* **2014,** *53* (8), 2157-2161.

23. Williams, V. C.; Dai, C. Y.; Li, Z. M.; Collins, S.; Piers, W. E.; Clegg, W.; Elsegood, M. R. J.; Marder, T. B., Activation of [$Cp_2ZrMe_2$] with new perfluoroaryl diboranes. Solution chemistry and ethylene polymerization behavior in the presence of MeAl(BHT)$_2$. *Angew Chem Int Edit* **1999,** *38* (24), 3695-3698.

24. Busico, V.; Cipullo, R.; Pellecchia, R.; Talarico, G.; Razavi, A., Hafnocenes and MAO. Beware of trimethylaluminum! *Macromolecules* **2009,** *42* (6), 1789-1791.

25. Busico, V.; Cipullo, R.; Cutillo, F.; Friederichs, N.; Ronca, S.; Wang, B., Improving the performance of methylalumoxane. A facile and efficient method to trap "free" trimethylaluminum. *J Am Chem Soc* **2003,** *125* (41), 12402-12403.

26. Taniike, T.; Sano, S.; Ikeya, M.; Thang, V. Q.; Terano, M., Development of a large-scale stopped-flow system for heterogeneous olefin polymerization

kinetics. *Macromol React Eng* **2012,** *6* (6-7), 275-279.

27. Keii, T.; Terano, M.; Kimura, K.; Ishii, K., A kinetic argument for a quasi-living polymerization of propene with a $MgCl_2$-supported catalyst. *Makromol Chem-Rapid Commun* **1987,** *8* (11), 583-587.

28. Ciancaleoni, G.; Fraldi, N.; Budzelaar, P. H. M.; Busico, V.; Cipullo, R.; Macchioni, A., Structure-activity relationship in olefin polymerization catalysis. Is entropy the key? *J Am Chem Soc* **2010,** *132* (39), 13651-13653.

# Chapter 3. A Quenched-Flow Pilot Study Using a $MgCl_2/TiCl_4$/EB Catalyst

## 3.1. Introduction

Third-generation Ziegler-Natta catalysts are prepared using ethyl benzoate (EB) as internal donor (ID), usually combined with EB or a *para*-substituted benzoate as external donor (ED). The $MgCl_2$ support is usually activated by ball-milling with the ID. The precatalyst is then activated by adding the ED and the trialkyl aluminum cocatalyst.

Although the ID and ED used for this system are chemically similar, experimental evidence suggests they may play rather different roles. Catalysts with ID have higher activity and higher stereo-specificity[1] than the ones without ID. However, this stereo-specificity deteriorates during polymerization. Addition of an ED effectively stabilizes stereo-specificity, sacrificing part of the activity.[1] A more detailed study has shown that the system with ID produces a higher amount of stereoregular polymer but a similar amount of non-stereoregular product in the presence of an ED.[2]

$AlR_3$ has been shown to interact with electron donors, and in particular to extract the ID from ZN precatalysts.[3-4] Addition of EB as ED apparently reduces or compensates for the loss of ID, and even increases the EB content of the catalyst.[1] Other external donors, such as methyl *para*-toluate (MPT) or phenyltriethoxysilane (PTES), can be used to similar effect.[5] In addition its 'extraction' role, $AlR_3$ also competes with EB for adsorption to the catalyst surface.[4]

Spectroscopic[6-7] and computational[8] studies show EB binds more strongly to $MgCl_2$ than to $TiCl_4$. This binding stabilizes[9] particles of $MgCl_2$ and exposes unsaturated, Lewis acidic lateral cuts during catalyst preparation. EB could potentially bind to a variety of lattice planes of $MgCl_2$ crystallites, including the (110) and (104) faces[1-2, 10] that have been long believed to be responsible for catalytic activity.

One could imagine two binding modes for EB: monodentate and bidentate/bridging. Early solid-state $^{13}C$ NMR studies concluded from a very short relaxation time,[11] that coordination is very rigid, suggesting a bidentate (bridging or chelate) binding mode. It was interesting that D*i*BP/$MgCl_2$ (unactivated) gave shorter relaxation time than D*i*BP/$MgCl_2$ (mechanically activated).[12] If the similar behavior of EB is assumed, EB/$MgCl_2$ (mechanically activated) should have given narrower peaks than EB/$MgCl_2$ (unactivated) which is the opposite to the fact. This likely suggests a diversity of adsorption of EB on $MgCl_2$. Accordingly it also showed EB adsorbed on $MgCl_2$ gave splitting methyl peaks due to the diversity of coordination environments.[12] Computational results depend on the choice of models and calculation levels. Terano et al. claimed that only monodentate coordination is feasible: they did not find any local minima corresponding to bidentate modes.[8] In contrast, Stukalov et al.[13] proposed four possible coordination modes (Figure 1) based on a series of experimental[14] and computational[13] studies.

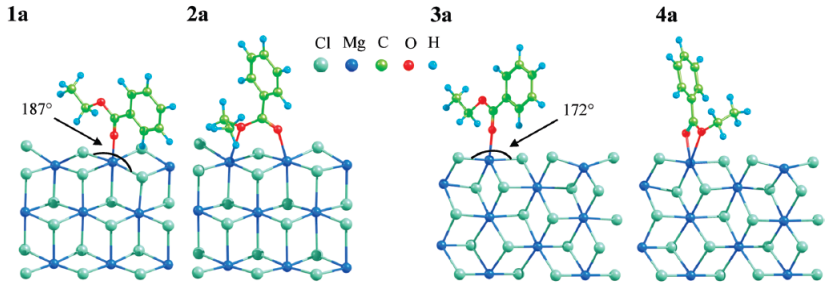


**Figure 1.** EB coordination modes, reproduced from Ref. 13.

The adsorption of Ti species on $MgCl_2$ is another important issue and might be affected by the presence of an electron donor. Computational[15-16] and Raman[17-18] studies indicate that the (110) cut is favored by mononuclear $TiCl_4$ and $TiCl_3$. Such sites have been proposed to be aspecific, but convertible into isospecific sites by coadsorption of EB.[8, 19] In addition to steric effects, Taniike et al.[8, 19] have proposed that this coadsorption results in charge transfer from the electron donor to Ti. These combined effects would enhance

activity, molecular weight and regio- and stereo-selectivity.

There seems to be an equilibrium between adsorption of EB and $TiCl_4$, evidenced by the fact that a change in order of addition of Ti and EB does not affect the composition of the resulting catalyst.[14] The exposure of EB/$MgCl_2$ to $TiCl_4$ causes a decrease of EB content[10]. But it reaches a constant value instead of the depletion. It implies EB and $TiCl_4$ have their own preferential positions on $MgCl_2$.

Early EXAFS[20] results suggest the (104) face is favored by dinuclear $Ti_2Cl_8$ moieties ('Corradini dimers') that have been proposed to produce isospecific sites.[21] However, D'Amore et al.[16] concluded from a periodic hybrid DFT study including dispersion corrections that:

1) mononuclear $TiCl_4$ can bind to 4-coordinate planes such as (110), but not to the 5-coordinate (104) plane
2) binding of dinuclear $Ti_2Cl_8$ units is highly unlikely on *any* surface, including (104)

On the other hand, Terano et al.[22] have suggested the binding of dinuclear species to (110); formation of 'zipped' (bridging between layers) dinuclear $Ti_2Cl_8$[23] is another possibility. It will be clear from this discussion that a consensus on $TiCl_x$ adsorption modes has not been reached. It is generally agreed that Ti species ($TiCl_3$ and $TiCl_4$) preferentially adsorb on (110), but this does not mean that activated sites will be generated at these positons. For example, Lin et al.[24] have suggested that polynuclear Ti species can be generated via an aggregation process during precatalyst activation. This implies the studies on precatalyst surface structure might not yield an accurate picture of the activated system. The $TiCl_3$-pyridine route,[25-26] which can be used to prepare a catalyst with ultra-low Ti content, is a promising tool for the investigation of aggregation of Ti species; a recent but ambiguous EXAFS study supports the assertion of predominance of mononuclear Ti species[27] at Ti contents below 0.1 wt%. For a catalyst type with ultra-low Ti content prepared by a different strategy[28-30], ESR provided support for a large fraction (up

to 70% total Ti) occurring as mononuclear species.

With all of these adsorption models, it should be kept in mind that the active sites constitute probably just a small fraction of the Ti species occurring on the surface, meaning the majority species are not necessarily representative of the actual active sites. At this point, neither EXAFS nor ESR is sufficiently sensitive to provide a full picture of the active sites. Recently a new type of X-ray absorption spectroscopy employing x-ray free electron laser (XFEL) has emerged[31-34] which might improve on sensitivity and resolution of existing methods. However, the low *relative* content of active species (vs total Ti content) will remain a problem.

The $MgCl_2/TiCl_4$/EB-$AlR_3$ system (R = alkyl) has proved to be a useful benchmark for quenched-flow experiments (called 'stopped-flow' by Keii, Terano, et al.[35-36]). Although the system shows rapidly declining kinetics at longer time-scales,[1] it behaves as an excellent example of quasi-living polymerization in the nascent stage (0-0.5 s). It shows a linear t-yield correlation as well as a linear 1/t vs 1/Pn plot, allowing the use Natta analysis to determine kinetic parameters and active site content.[35-36] This chapter presents a study of quenched-flow polymerization with the $MgCl_2/TiCl_4$/EB-Al(*i*Bu)$_3$ catalyst as a benchmark for heterogeneous Ziegler-Natta catalytic systems. Different from the EB system adopted by Terano et al., the one in this study presents a significant induction. However it gave similar kinetic parameters to the former one with a first-order activation model. We confirmed the reliability of the active sites content determined with quenched-flow/GPC by directly measuring the chain number with high temperature cryoprobe NMR which was not carried out before. Based on this seemingly simple system, we will investigate more complicated phthalate-based system in Chapter 4 which involves significant issues of dormancy.

## 3.2. Experimental Part

### *3.2.1. Chemicals*

Pre-catalyst slurry $MgCl_2/TiCl_4$/EB in *iso*-dodecane was kindly donated by SABIC Europe. HPLC grade *n*-heptane (Romil) was purified by passing through a column filled up with copper catalyst (BASF R 3-11/G) and molecular sieve 3Å in an MBraun SPS-5 compact to remove oxygen and moisture. Propene was purified by passing through the same type of column to remove oxygen and moisture. Neat Al(*i*Bu)$_3$ (Sigma-Aldrich), acetone (Sigma-Aldrich), HPLC grade methanol (Romil), 37% HCl (Romil) and 99% xylene (Romil) were used without additional treatment.

### *3.2.2. Polymerization*

Polymerization reactions were carried out at 30 ℃ with the quenched-flow setup described in Chapter 2. Vessel A was loaded with catalyst slurry and *n*-heptane, Ti concentration 0.114 g/L. Vessel B was loaded with the same volume of *n*-heptane solution of Al(*i*Bu)$_3$ and saturated with 1.7 bar propene ([$C_3$]= 1.017 M), Al/Ti mole ratio 60. For each tubing pumping rate is 10mL·s$^{-1}$, the total Reynolds number Re is 15000, indicating the system is turbulent. Polymerization was quenched by acidified methanol under mechanical agitation.

The lower organic layer (mostly methanol and catalyst residual) was siphoned off. Acetone was added to the polymer-heptane suspension (acetone:heptane =1:1 by volume) to induce coagulation. The polymer was recovered by filtration, dissolved and re-coagulated from boiling xylene, washed with methanol and dried *in vacuo* at 60 ℃.

### *3.2.3. Characterization*

Gel permeation chromatography (GPC) was carried out with a Freeslate Rapid-GPC : eluent, 1,2-dichlorobenzene (stabilized with BHT, 0.4 mg·mL$^{-1}$); column, 2×Agilent PLgel 10 μm MIXED-B, 300×7.5 mm, 145 ℃; detector, Polymer Char IR4, 150 ℃; universal calibration, monodispersed polystyrene standards (Mn 1.3 kDa-3700

kDa).

$^{13}C$ NMR spectra were recorded with a Bruker Avance III spectrometer (100 MHz for $^{13}C$) equipped with high-temperature CryoProbe for 5mm tubes, on 2.6% w/w polymer solutions in tetrachloroethane-1,2-$d_2$ (also used as internal standard) at 120 °C. Conditions for $^{13}C$ NMR: zgpg45 pulse; acquisition time, 1.8s; relaxation time, 5s; number of scans, 1000-10000.

## 3.3. Results and discussion

### *3.3.1. Apparent Kinetics*

Polymerization results are shown as Table 1.

The kinetic curve shown in Figure 2 indicates the occurrence of an induction period of ~0.06 s. This is at odds with reports by Terano et al.[35-39] which show straight lines through the origin. A possible reason is that we have used Al(*i*Bu)$_3$ for catalyst activation instead of the $AlEt_3$ used by Terano. Zambelli et al.[40] have reported that in $AlEt_3$ activated PP catalysis some ethene is formed from $AlEt_3$ and is then incorporated in the final PP product. A trial run in our lab has confirmed this for a quenched-flow type experiment (Figure 3), and so we decided to use Al(*i*Bu)$_3$ for most of our QF studies. However, Al(*i*Bu)$_3$ is more hindered than $AlEt_3$ which might result in slower precatalyst activation.[41] Interestingly, according to Terano et al.[42], the isotacticity of polypropylene decreases with increasing steric hindrance of the alkylaluminum cocatalyst, which might be related to the monomer-dimer equilibrium of $AlR_3$: the presence of alkylaluminum dimers near active sites might enhance stereoselectivity.

Table 1. Polymerization results of PP with $MgCl_2/TiCl_4$/EB- Al($i$Bu)$_3$ at 30℃.

| Code | $t_p$ /s | Ti /mg | PP /mg | Yield /mg(PP)·mg(Ti)$^{-1}$ | Mn | PDI |
|---|---|---|---|---|---|---|
| PP4 | 0.10 | 18.45 | 18.4 | 0.997 | 6585 | 5.9 |
| PP3 | 0.12 | 13.53 | 27.5 | 2.032 | 7696 | 3.8 |
| PP7 | 0.16 | 3.70 | 20.3 | 5.486 | 8926 | 3.2 |
| PP1 | 0.20 | 7.30 | 42.0 | 5.753 | 10708 | 3 |
| PP5 | 0.25 | 6.30 | 49.6 | 7.873 | 14848 | 4.4 |
| PP2 | 0.30 | 3.26 | 26.4 | 8.098 | 15263 | 5.2 |
| PP6 | 0.40 | 3.60 | 45.7 | 12.694 | 22024 | 4.7 |

Assuming catalyst activation is a first-order process,[43-44] the relevant kinetic equations are:

$$[C^*] = [C_s^*] \cdot (1 - e^{-<f_i> \cdot t}) \tag{1}$$

$$Y = <f_p> \cdot [C_s^*] \cdot (t + \frac{e^{-<f_i> \cdot t} - 1}{<f_i>}) \tag{2}$$

where [$C$*] is active sites content at time t; [$C_s$*] is the total active sites content when catalyst is fully activated; $<f_i>$ is the average frequency of activation for active sites; $Y$ is yield of polymer; $<f_p> \equiv <k_p> \cdot [M]$ is the average frequency of insertion, $<k_p>$ is the average rate coefficient of insertion and [$M$] is the monomer concentration. These equations assume that there is a specific and constant number of active sites to be activated. One could also imagine, as an alternative, the possibility of continuous further activation and deactivation processes, but kinetic equations based on such complicated models would have too many fitted parameters to be useful.

In any case, based on equations 1 and 2 we obtain by non-linear least-squares fitting (Figure 2): $<f_p> \cdot [C_s^*]$ = (38.6 ± 5.8) mol($C_3$)· mol(Ti)$^{-1}$·s$^{-1}$ and $<f_i>$ = (14.1 ± 7.4) s$^{-1}$.

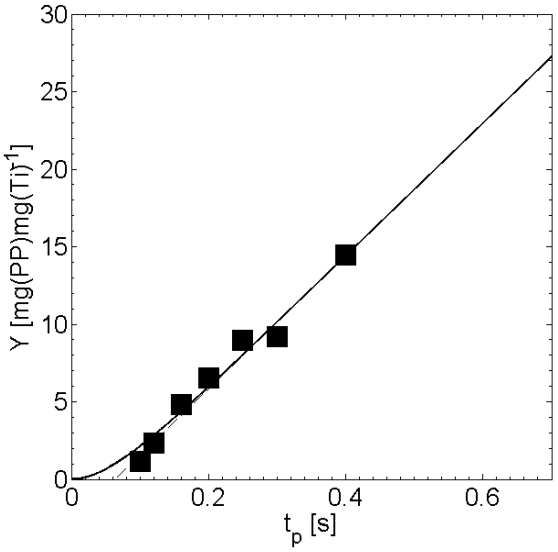


**Figure 2.** Curve of yield (Y) *versus* polymerization time ($t_p$).

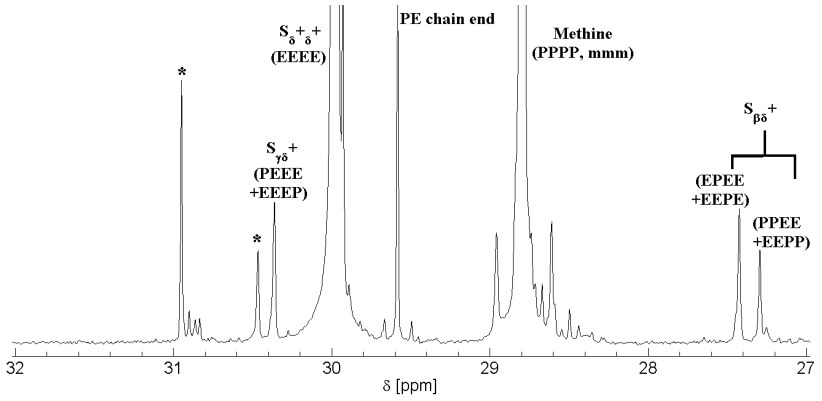


**Figure 3.** $^{13}C$ NMR spectrum of PP prepared by quenched-flow (0.06s) with $MgCl_2/TiCl_4$/di*iso*butyl phthalate-$AlEt_3$, indicating incorporation of ethene units in the PP backbone. * denotes impurities.

The GPC profiles show an evolution of product characteristics with time. The lower-MW part of the GPC profile does not completely 'move' with time, indicating the corresponding polymer components tend be keep constant (i.e. a non-living fraction). The PDI values

decline in the first 0.2 s and seem to increase again. Apparently, the high-MW fraction grows faster in the later stage of the polymerization. One possible interpretation is extraction of EB by TIBA, which would result in a less hindered environment around some active sites, and hence in faster monomer insertion.

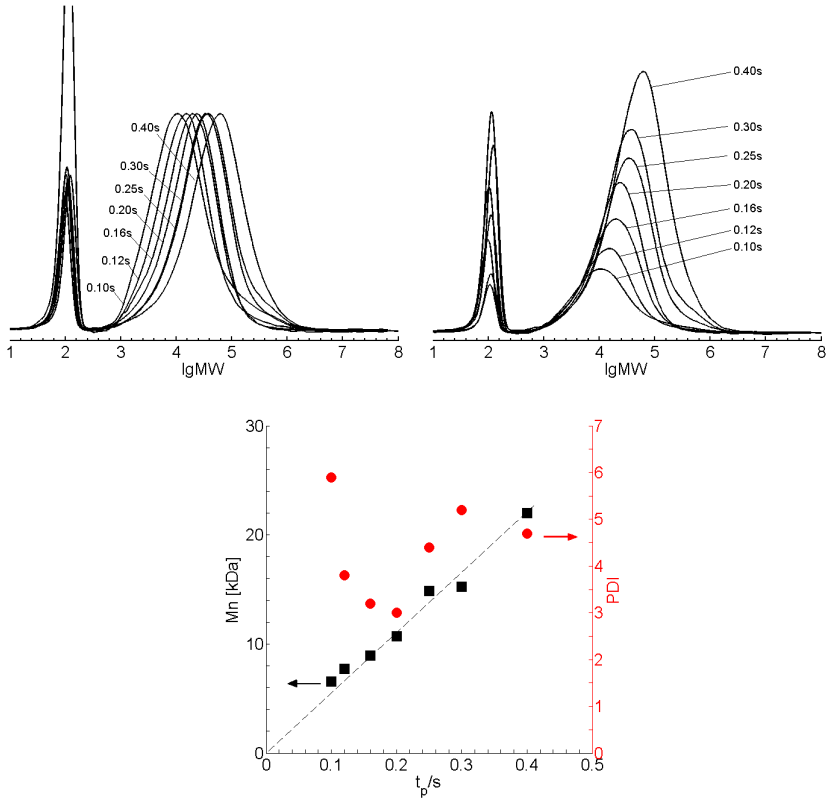


**Figure 4.** Molecular weight (MW) distribution of PP at different polymerization times $t_p$. (top left) GPC profiles normalized to the peak height; (top right) areas normalized to yields; (bottom) MW distribution data.

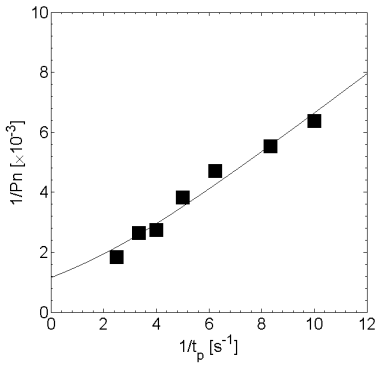


**Figure 5.** Fitting the reciprocal of average degree of polymerization ($P_n$) *versus* the reciprocal of polymerization time ($t_p$) ('Natta plot').

### *3.3.2. Active sites content*

In order to obtain the kinetic parameter $\langle f_p \rangle$ we use a Natta analysis. Including the effect of induction, the equation has the following form:[43-44]

$$\frac{1}{P_n} = \frac{1 - e^{-\langle f_i \rangle \cdot t}}{\langle f_p \rangle \cdot \{t + \frac{e^{-\langle f_i \rangle \cdot t} - 1}{\langle f_i \rangle}\}} + \frac{\langle f_{tr} \rangle}{\langle f_p \rangle} \tag{3}$$

where $P_n$ is the average degree of polymerization and $\langle f_{tr} \rangle$ is the average frequency of chain transfer. From non-linear least-squares fitting (Figure 5) we obtain the kinetic parameters $\langle f_p \rangle$ = (3.01 ± 0.63) × $10^3$ $s^{-1}$ and $\langle f_{tr} \rangle$ = (3.7 ± 1.2) $s^{-1}$. Combined with the t-yield results discussed earlier, this gives $\langle k_p \rangle$ = (5.92 ± 1.24) × $10^3$ $L \cdot mol^{-1} \cdot s^{-1}$ and $[C_s^*]$ = (12.8 ± 1.9) $mmol \cdot mol(Ti)^{-1}$. For comparison, we recall the results reported by Terano et al:[42] $\langle k_p \rangle$ = 2.8 × $10^3$ $L \cdot mol^{-1} \cdot s^{-1}$ and $[C_s^*]$ = 20 $mmol \cdot mol(Ti)^{-1}$. The difference in $\langle k_p \rangle$ of a factor of 2 can be partly ascribed to inclusion of induction in our analysis, but may also reflect different activities for TIBA and TEA activated systems.

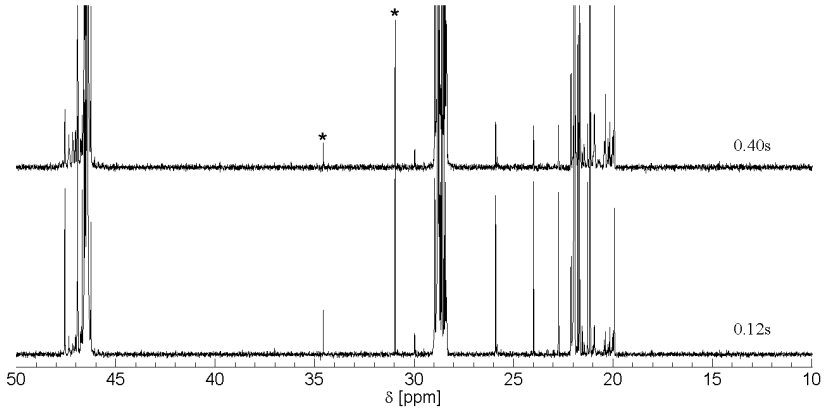


**Figure 6.** $^{13}$C NMR spectrum of PP prepared with an EB-based catalyst at 0.4 (top) and 0.12 (bottom) s reaction time. Methyl peaks (21.94 ppm) are normalized to the same height. * denotes impurities.

### *3.3.3. Microstructures*

Within the time range of this study (≤ 0.4 s), the system can be characterized as quasi-living, and there are no detectable saturated chain ends produced by chain transfer (Figure 6). The only abundant chain end is *i*Bu which can be due to initial active site alkylation by TIBA and/or quenching of a growing chain with a 1,2 last-inserted unit. The *i*Bu content in the PP product keeps declining while the average molecular weight keeps growing with time (Figure 7). The absence of *n*Pr indicates there is no significant chain initiation at Ti-H species or chain transfer to monomer; the absence of *n*Bu implies the insertion of monomer is highly regio-selective.

High-field NMR using a cryoprobe allows quantification of chain ends content with high accuracy and is an important tool for this project. Quantifying chain end amounts can help understanding of the initial kinetics. If we assume all PP chains start and end with *i*Bu, the total number of chains should be equal to a half the number of *i*Bu end groups. This seems to be approximately true from 0.2 s on (Figure 8), but not at the shortest reaction time (0.12 s). It may be that the simple first-order model used to derive equations 1-3 is not

entirely adequate for this system.

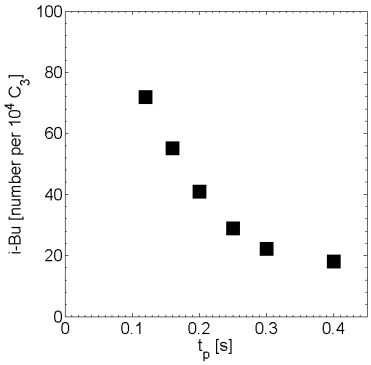


**Figure 7.** PP *i*Bu content *versus* polymerization time.

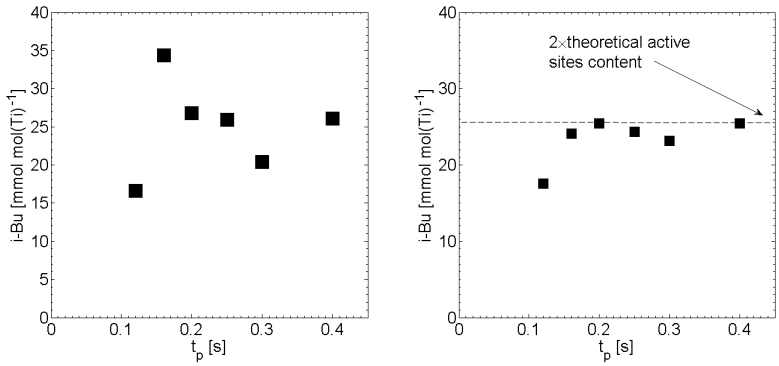


**Figure 8.** *i*Bu amount relative to total Ti: (left) values calculated from original yield data; (right) values calculated from fitted yield data.

The $^{13}C$ NMR results also reveal a fast evolution of stereoregularity. As shown in Figure 9, the isotacticity of PP produced in the first fraction of a second is very high, close to 95%, but then decreases with time. Interestingly the trend in isotacticity is similar to that in the PDI. A possible interpretation is that the quickly activated species yielding constant (and low) MW in the initial stage of the reaction are highly isotactic. The decline in isotacticity after 0.25 s might due to the extraction of EB by alkylaluminum.

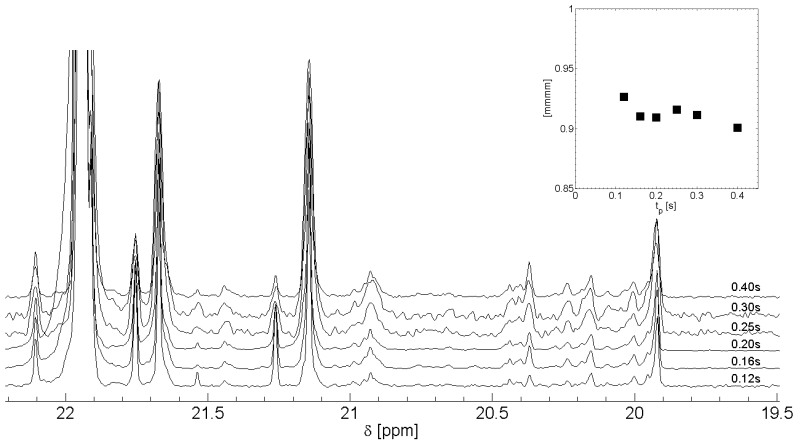


**Figure 9.** Methyl region of $^{13}C$ NMR of PP prepared with an EB-based catalyst, demonstrating the stereo-error evolution. (insert) temporal evolution of PP isotacticity.

## 3.4. Conclusions

By employing a combined quenched-flow and NMR approach, a $MgCl_2/TiCl_4$/EB-Al(*i*Bu)$_3$ catalyst was studied as a benchmark for the polymerization of propylene. A short induction period of about 0.06 s was found. Based on a model involving first-order activation kinetics, parameters were determined from GPC and yield data; the active sites content was in perfect agreement with NMR (chain end) data. The results are compatible with a consistent set of kinetic parameters between the two approaches, and revealed a highly dynamic process in the nascent stage of the reaction.

## References

1. Busico, V.; Corradini, P.; Demartino, L.; Proto, A.; Savino, V.; Albizzati, E., Polymerization of propene in the presence of $MgCl_2$-supported Ziegler-Natta catalysts .1. The role of ethyl benzoate as internal and external base. *Makromol Chem* **1985,** *186* (6), 1279-1288.

2. Busico, V.; Corradini, P.; Demartino, L.; Proto, A.; Albizzati, E., Polymerization of propene in the presence of $MgCl_2$-supported Ziegler-Natta

catalysts .2. Effects of the cocatalyst composition. *Makromol Chem* **1986,** *187* (5), 1115-1124.

3. Noristi, L.; Barbe, P. C.; Baruzzi, G., Effect of the internal external donor pair in high-yield catalysts for propylene polymerization .1. Catalyst-cocatalyst interactions. *Makromol Chem* **1991,** *192* (5), 1115-1127.

4. Potapov, A. G.; Bukatov, G. D.; Zakharov, V. A., DRIFTS study of the interaction of the $AlEt_3$ cocatalyst with the internal donor ethyl benzoate in supported Ziegler-Natta catalysts. *J Mol Catal A-Chem* **2009,** *301* (1-2), 18-23.

5. Sacchi, M. C.; Tritto, I.; Shan, C. J.; Mendichi, R.; Noristi, L., Role of the pair of internal and external donors in $MgCl_2$-supported Ziegler-Natta catalysts. *Macromolecules* **1991,** *24* (26), 6823-6826.

6. Terano, M.; Saito, M.; Kataoka, T., Solid-state $^{13}C$ NNR study on the state of the electron-donor in $MgCl_2$-supported catalysts. *Makromol Chem-Rapid Commun* **1992,** *13* (2), 103-108.

7. Terano, M.; Kataoka, T.; Keii, T., A study on the states of ethyl benzoate and $TiCl_4$ in $MgCl_2$-supported high-yield catalysts. *Makromol Chem* **1987,** *188* (6), 1477-1487.

8. Taniike, T.; Terano, M., Coadsorption and support-mediated interaction of ti species with ethyl benzoate in $MgCl_2$-supported heterogeneous Ziegler-Natta catalysts studied by density functional calculations. *Macromol Rapid Commun* **2007,** *28* (18-19), 1918-1922.

9. Sergeev, S. A.; Bukatov, G. D.; Zakharov, V. A.; Moroz, E. M., Propylene Polymerization on Titanium-Magnesium Catalysts .2. Study of Catalyst Formation. *Makromol Chem* **1983,** *184* (12), 2421-2429.

10. Potapov, A. G.; Bukatov, G. D.; Zakharov, V. A., DRIFT study of internal donors in supported Ziegler-Natta catalysts. *J Mol Catal A-Chem* **2006,** *246* (1-2), 248-254.

11. Chien, J. C. W.; Dickinson, L. C.; Vizzini, J., Magnesium-chloride supported high mileage catalysts for olefin polymerization .20. Solid-state NMR. *J Polym Sci A- Polym Chem* **1990,** *28* (9), 2321-2333.

12. Sormunen, P.; Hjertberg, T.; Iiskola, E., A solid-state $^{13}C$ NMR study on heterogeneous Ziegler-Natta catalyst components. *Makromol Chem* **1990,** *191* (11), 2663-2673.

13. Stukalov, D. V.; Zakharov, V. A.; Zilberberg, I. L., Adsorption species of ethyl benzoate in $MgCl_2$-supported Ziegler-Natta catalysts. A density functional theory study. *J Phys Chem C* **2010,** *114* (1), 429-435.

14. Stukalov, D. V.; Zakharov, V. A.; Potapov, A. G.; Bukatov, G. D., Supported Ziegler-Natta catalysts for propylene polymerization. Study of surface species formed at interaction of electron donors and $TiCl_4$ with activated $MgCl_2$. *J Catal* **2009,** *266* (1), 39-49.

15. Monaco, G.; Toto, M.; Guerra, G.; Corradini, P.; Cavallo, L., Geometry and stability of titanium chloride species adsorbed on the (100) and (110) cuts of the $MgCl_2$ support of the heterogeneous Ziegler-Natta catalysts. *Macromolecules* **2000,** *33* (24), 8953-8962.

16. D'Amore, M.; Credendino, R.; Budzelaar, P. H. M.; Causa, M.; Busico, V., A periodic hybrid DFT approach (including dispersion) to $MgCl_2$-supported Ziegler-Natta catalysts.1. $TiCl_4$ adsorption on $MgCl_2$ crystal surfaces. *J Catal* **2012,** *286*, 103-110.

17. Brambilla, L.; Zerbi, G.; Nascetti, S.; Piemontesi, F.; Morini, G., Experimental and calculated vibrational spectra and structure of Ziegler-Natta catalyst precursor. 50/1 comilled $MgCl_2$-$TiCl_4$. *Macromol Symp* **2004,** *213*, 287-301.

18. Brambilla, L.; Zerbi, G.; Piemontesi, F.; Nascetti, S.; Morini, G., Structure of $MgCl_2$-$TiCl_4$ complex in co-milled Ziegler-Natta catalyst precursors with different $TiCl_4$ content. Experimental and theoretical vibrational spectra. *J Mol Catal A-Chem* **2007,** *263* (1-2), 103-111.

19. Taniike, T.; Terano, M., Coadsorption model for first-principle description of roles of donors in heterogeneous Ziegler-Natta propylene polymerization. *J Catal* **2012,** *293*, 39-50.

20. Potapov, A. G.; Kriventsov, V. V.; Kochubey, D. I.; Bukatov, G. D.; Zakharov, V. A., EXAFS study of supported $TiCl_4/MgCl_2$ catalyst. *Macromol Chem Physic* **1997,** *198* (11), 3477-3484.

21. Corradini, P.; Barone, V.; Fusco, R.; Guerra, G., A possible model of catalytic sites for the stereospecific polymerization of alpha-olefins on 1st-generation and supported Ziegler-Natta catalysts. *Gazz Chim Ital* **1983,** *113* (9-10), 601-607.

22. Taniike, T.; Terano, M., Reductive formation of isospecific Ti dinuclear species on a $MgCl_2$ (110) surface in heterogeneous Ziegler-Natta catalysts. *Macromol Rapid Commun* **2008,** *29* (17), 1472-1476.

23. Stukalov, D. V.; Zilberberg, I. L.; Zakharov, V. A., Surface species of titanium(IV) and titanium(III) in $MgCl_2$-supported Ziegler-Natta catalysts. A periodic density functional theory study. *Macromolecules* **2009,** *42* (21),

8165-8171.

24. Lin, J. S.; Catlow, C. R. A., Computer-modeling studies on $MgCl_2$-supported Ziegler-Natta catalysts. *J Mater Chem* **1993,** *3* (12), 1217-1225.

25. Soga, K.; Park, J. R.; Shiono, T.; Kashiwa, N., A direct evidence for the improvement of isospecificity in Ziegler-Natta catalysts by ethyl benzoate. *Makromol Chem-Rapid Commun* **1990,** *11* (3), 117-121.

26. Wada, T.; Taniike, T.; Kouzai, I.; Takahashi, S.; Terano, M., Propylene polymerization performance of isolated and aggregated Ti species studied using a well-designed $TiCl_3/MgCl_2$ Ziegler-Natta model catalyst. *Macromol Rapid Commun* **2009,** *30* (11), 887-891.

27. Taniike, T.; Takahashi, S.; Wada, T.; Tonosaki, K.; Dwivedi, S.; Terano, M., Model catalysts for clarification of active site-polymer relationship in heterogeneous olefin polymerization. *Macromol Symp* **2012,** *313-314* (1), 1-7.

28. Echevskaya, L. G.; Matsko, M. A.; Mikenas, T. B.; Nikitin, V. E.; Zakharov, V. A., Supported titanium-magnesium catalysts with different titanium content. Kinetic peculiarities at ethylene homopolymerization and copolymerization and molecular weight characteristics of polyethylene. *J Appl Polym Sci* **2006,** *102* (6), 5436-5442.

29. Mikenas, T. B.; Koshevoy, E. I.; Zakharov, V. A.; Nikolaeva, M. I., Formation of isolated titanium(III) ions as active sites of supported titanium-magnesium catalysts for polymerization of olefins. *Macromol Chem Physic* **2014,** *215* (18), 1707-1720.

30. Koshevoy, E. I.; Mikenas, T. B.; Zakharov, V. A.; Volodin, A. M.; Kenzhin, R. M., Formation of isolated titanium(III) ions in superactive titanium-magnesium catalysts with a low titanium content as active sites in ethylene polymerization. *Catal Commun* **2014,** *48*, 38-40.

31. Bordiga, S.; Groppo, E.; Agostini, G.; van Bokhoven, J. A.; Lamberti, C., Reactivity of surface species in heterogeneous catalysts probed by in situ X-ray absorption techniques. *Chem Rev* **2013,** *113* (3), 1736-1850.

32. Sa, J.; Szlachetko, J., Heterogeneous catalysis experiments at XFELs. Are we close to producing a catalysis movie? *Catal Lett* **2014,** *144* (2), 197-203.

33. O'Shea, P. G.; Freund, H. P., Laser technology - Free-electron lasers. Status and applications. *Science* **2001,** *292* (5523), 1853-1858.

34. Gaffney, K. J.; Chapman, H. N., Imaging atomic structure and dynamics with ultrafast X-ray scattering. *Science* **2007,** *316* (5830), 1444-1448.

35. Keii, T.; Terano, M.; Kimura, K.; Ishii, K., A kinetic argument for a quasi-living polymerization of propene with a $MgCl_2$-supported catalyst. *Makromol Chem-Rapid Commun* **1987,** *8* (11), 583-587.

36. Terano, M.; Kataoka, T.; Keii, T., Stopped-flow polymerization of propene with typical $MgCl_2$-supported high-yield catalysts. *J Mol Catal* **1989,** *56* (1-3), 203-210.

37. Liu, B. P.; Matsuoka, H.; Terano, M., Stopped-flow techniques in Ziegler catalysis. *Macromol Rapid Commun* **2001,** *22* (1), 1-24.

38. Liu, B. P.; Matsuoka, H.; Terano, M., Kinetic investigation of propene polymerization with stopped-flow method. *Macromol Symp* **2001,** *165*, 3-10.

39. Terano, M.; Kataoka, T., A kinetic-study of propene polymerization using $MgCl_2$-supported catalysts. *Makromol Chem-Rapid Commun* **1989,** *10* (2), 97-102.

40. Zambelli, A.; Ammendola, P.; Locatelli, P.; Sacchi, M. C., Ethylene Units in Al(CH3)3-Cocatalyzed Polymerization of 3-Methyl-1-Pentene. *Macromolecules* **1984,** *17* (4), 977-978.

41. Trischler, H.; Hochfurtner, T.; Ruff, M.; Paulik, C., Influence of the aluminum alkyl co-catalyst type in Ziegler-Natta ethene polymerization on the formation of active sites, polymerization rate, and molecular weight. *Kinet Catal* **2013,** *54* (5), 559-565.

42. Mori, H.; Iguchi, H.; Hasebe, K.; Terano, M., Kinetic study of isospecific active sites formed by various alkylaluminiums on $MgCl_2$-supported Ziegler catalyst at the initial stage of propene polymerization. *Macromol Chem Physic* **1997,** *198* (4), 1249-1255.

43. Shiono, T.; Ohgizawa, M.; Soga, K., Reaction of the Ti-polyethylene bond with carbon-monoxide over the bis(cyclopentadienyl)titanium dichloride methylaluminoxane catalyst system. *Polymer* **1994,** *35* (1), 187-192.

44. Busico, V.; Cipullo, R.; Esposito, V., Stopped-flow polymerizations of ethene and propene in the presence of the catalyst system *rac*-$Me_2Si$(2-methyl-4-phenyl-1-indenyl)$_2ZrCl_2$/methylaluminoxane. *Macromol Rapid Commun* **1999,** *20* (3), 116-121.

# Chapter 4. Macro- and Microscopic Kinetics of $MgCl_2/TiCl_4$/DiBP System

## 4.1. Introduction

The fourth−generation Ziegler-Natta catalyst formulation was developed by Mitsui Petrochemical Industries Ltd. and Montedison S.p.A.[1-2] in 1977, a few years after the invention of benzoate-based catalysts.[3] Fourth-generation catalysts are prepared using a phthalate internal donor (e.g. diisobutyl phthalate, DIBP) in combination with an external donor which is usually an alkoxysilane, although piperidine derivatives have been employed as well.[4-6]

The pre-catalyst is usually prepared via chemical activation, reacting a $MgCl_2$-alcohol adduct[7-10] or magnesium alkoxide[11-14] with $TiCl_4$ in the presence of the internal donor. Grignard reagents or dialkylmagnesium compounds are sometimes used for ethene homo- or co-polymerization catalysts but rarely for propene polymerization catalysts,[15-17] although there is evidence that addition of a Grignard agent can improve PP performance.[19]

Like benzoate, phthalate can be extracted by alkylaluminum compounds.[14] However, phthalate catalysts appear to have a more robust performance than benzoate systems, maintaining better isotacticity over a range of alkylaluminum[20] concentrations and better activity on catalyst aging with alkylaluminum.[21] Phthalates also perform significantly better than terephthalates in terms of both activity and isotacticity.[22] The alkyl substituent is another critical factor. Empirically, larger substituents give higher activity per g of Ti (methyl < ethyl < *iso*-butyl < 2-ethylhexyl < *iso*-decyl) but similar isotacticity.[22-25] At the same time, larger alkyls also result in lower Ti content of the precatalyst.[22] Apparently, *iso*-butyl is a good compromise balancing catalyst productivity and industrial availability of the ester.

Like benzoate, phthalate has been shown to predominantly interact

with $MgCl_2$ instead of with $TiCl_4$.[26-27] However, underactivation (titanation carried out at too-low temperatures) can produce detectable amounts of phthalate-$TiCl_4$ complexes, while overactivation (titanation at too-high temperatures) may induce a chemical reaction between $TiCl_4$ and phthalate producing phthaloyl chloride.[25, 27] These side reactions, which have not been observed in ethylbenzoate (EB) systems, may result in poorer catalyst performance.

Although phthalates may play a direct role in polymerization catalysis, their most important role is currently believed to be connected to pre-catalyst formation. It is believed phthalates stabilize certain lateral cuts of $MgCl_2$ via complexation during catalyst preparation. A number of computational studies[28-29] suggest phthalate can efficiently bind to (110) and (104) cuts. Assuming coordination of both carbonyl groups, bridged binding is the only possibility for (104) cuts, whereas for (110) cuts a variety of binding modes have been proposed, including chelating, bridging and "zipped" (bridging between different $MgCl_2$ layers); the (110)-bridged mode is believed to be favored. However, monodentate coordination is also possible and might be relevant to the mobility of adsorbed phthalate.[30] Experimental evidence supports a modest preference of phthalates for (110) over (104), similar to benzoates but distinctly different from diethers which strongly prefers (110) cuts.[31-32]

The overall activity of phthalate-based catalysts is not necessarily higher than that of benzoate systems, but activity towards isotactic products is definitely superior as shown in Figure 1. The combination of a phthalate internal donor with an alkoxysilane external donor was the first system that eliminated the need for a separate process step to remove a poorly isotactic PP fraction. The addition of alkoxysilane greatly improves the isotacticity of the produced polymer both by increasing the isotactic productivity and by decreasing the atactic productivity.[18, 33-34] The alkoxysilane does not significantly affect the removal of the internal donor, but the

presence of the internal donor remarkably enhances the adsorption of external donor.[14, 34] Empirically, good alkoxysilane external donor have[35] 1) at least two alkoxy groups not larger than ethoxy

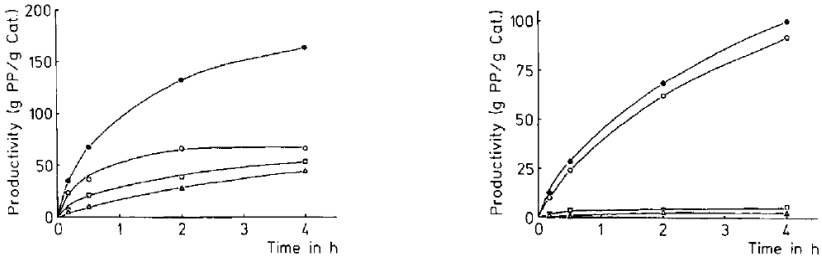


**Figure 1.** Productivities vs. time. Ethyl benzoate/methyl *p*-toluate (left) and diisobutyl phthalate/triethoxy(phenyl)silane (right) systems. ●: total, ○: octane (C8) insoluble fraction, □: C8 soluble fraction, △: heptane (C7) soluble fraction. Reproduced from Ref.[18].

and 2) alkyl groups with sufficient steric hindrance. One rationalization of these requirements is that the alkoxy groups poison atactic sites while the alkyl groups induce stereo-regulation. Based on the discrepancy between the results of diisopropyldimethoxy-silane (DIPDMS) and dicyclohexyldimethoxysilane (DCHDMS), Terano, et al. concluded that not only the bulkiness but also the configuration of the alkyl can greatly affect the performance[36]. The alkoxysilane can interact with both $MgCl_2$ and $TiCl_x$ centres. Its basicity is higher than that of a phthalate and close to that of a diether.[37] Since dialkoxysilanes can be considered analogues of geminal diethers (or acetals), one might expected them to behave similarly to diethers. However, computational work suggests that 1, 3-diethers are highly mobile on (110) cuts of $MgCl_2$[30] whereas alkoxysilanes have been experimentally found to be poorly mobile.[38] It might be that the spacing between the two oxygen atoms critically affects the accessible coordination modes. Interestingly, monomethoxy- and dimethoxy-silanes have the same threshold (Si:Mg ratio) above which they become more mobile. HR-MAS (high-resolution magic-angle spinning) NMR has shown that

monomethoxysilane binds to both 4- and 5-coordinate Mg whereas dimethoxysilane only binds to 4-coordinate sites.[38] Unfortunately it is not clear yet how alkoxysilanes mechanistically affect cataytically active sites.

Quenched-flow (QF) has been demonstrated to be a reliable technique for the study of nascent kinetics. The active site content measured by QF agrees well with NMR results, as shown in the previous chapters. An early QF study of the effects of alkoxysilane on internal-donor-free catalysts provided convincing evidence that the number of methoxy groups only affects the number of active sites but not the isospecificity of particular active sites.[39] In the present study we combine the QF technique with cryoprobe NMR analysis of the resulting polymer, allowing detailed analysis of chain ends and stereoerrors. With this combined strategy, we have revisited important issues including dormancy and donor effects. A comparison between propene and ethene polymerization hints at mechanistic differences between the two systems.

According to preliminary experiments, phthalate-based catalysts have a significant induction period (longer than 0.5 s). Extracting the precatalyst with hot toluene has been reported to eliminate the induction,[40] but it may also alter the nature of the catalyst e.g. through removal of a significant amount of internal donor and Ti. Here, we instead apply a precontact time to eliminate the induction. This procedure is justified by the fact that phthalate-based catalysts show robust performance in the presence of aluminum alkyls,[21, 41] indicating the catalyst is relatively stable in the presence of the cocatalyst.

## 4.2. Experimental Part

### *4.2.1. Chemicals*

Pre-catalyst $MgCl_2/TiCl_4$/diisobutyl phthalate (2.5 wt% Ti) was kindly donated by SABIC Europe. HPLC grade *n*-heptane (Romil)

was purified by passing through a column filled up with copper catalyst (BASF R 3-11/G) and molecular sieve 3Å in an MBraun SPS-5 compact to remove oxygen and moisture. Propene and ethene was purified by passing through a column filled up with the same filler to remove oxygen and moisture. Neat $AlEt_3$ (Sigma-Aldrich), $Al(iBu)_3$ (Sigma-Aldrich), diisobutyldimethoxysilane (SABIC Europe), acetone (Sigma- Aldrich), HPLC grade methanol (Romil) and 37% HCl (Romil) were used without additional treatment.

### *4.2.2. A Typical Quenched-flow Propene Polymerization Procedure*

The polymerization reactions were carried out at various temperatures between 20 ℃ and 70 ℃ with the quenched-flow setup described in Chapter 2. The vessel A was loaded with precatalyst, $Al(iBu)_3$ and *n*-heptane, precatalyst concentration 4 g/L, [Al]=23.8 mM. When alkoxysilane, diisobutyldimethoxysilane (DiBDMS) in this study, was used, Al/Si=28.3 mol/mol. Vessel B was loaded with the same volume of *n*-heptane solution of $Al(iBu)_3$ and saturated with 1.7 bar propene ($[C_3]$= 0.83 M at 40 ℃), [Al]= 39.6 mM. When alkoxysilane was used, it was employed at a ratio Al/Si=28.3 mol/mol. At 40 ℃, the total $[C_3]$=0.42 M, [Ti]=1.0 mM, Al/Ti= 30.4 mol/mol, Al/Si= 28.2 mol/mol. The concentration of $C_3$ depends on the temperature. Before carrying out polymerization, the precatalyst reacted with cocatalyst for 13 min. This is enough to maintain a steady state of the catalyst system according to preliminary PPR tests and the report of Terano et al.[41] For total pumping rate=20mL·s$^{-1}$, Reynolds number Re = 15000, indicating that the system was turbulent. Polymerization was quenched with acidified methanol under mechanical agitation.

The lower organic layer (mostly methanol and catalyst residual) was removed with siphon. Acetone and methanol were added to the polymer-heptane suspension (heptane: acetone: methanol= 2: 2: 1 V/V) to induce coagulation. The polymer was recovered by filtration, washed with methanol and dried *in vacuo* at 60 ℃.

### *4.2.3. Ethene Polymerization*

For ethene polymerization, the monomer was replaced with ethene, which implies a change of monomer concentration: at 40 ℃, $[C_2]$= 0.09 M. No external donor was used. Other conditions were maintained as described before in propene polymerization.

### *4.2.4. Ethene/Propene Copolymerization*

Ethene and propene were mixed in a cylinder. The mixture was stored for at least one night prior to usage in order to ensure the mixture was homogenized. The exact ratio was determined with GC just before polymerization. Calibration curves using neat propene and ethene were made every time when the determination was carried out.

Propene polymerization in the presence of hydrogen was carried out in a similar manner. But since the GC instrument does not detect hydrogen, the propene content was estimated solely with a pressure reading.

### *4.2.5. Slurry Polymerization*

In order to mimic the conditions of quenched-flow polymerization, a precontact time was also used for slurry polymerization experiments. The amount of precatalyst was reduced to 1/25 of the amount used in most QF experiments. All the concentrations were kept the same. The monomer pressure was 1 bar.

### *4.2.6. Characterization*

Gel permeation chromatography (GPC) was carried out with Freeslate Rapid-GPC : eluent, 1,2-dichlorobenzene (stabilized with BHT, 0.4 $mg \cdot mL^{-1}$); column, 2×Agilent PLgel 10 μm MIXED-B, 300×7.5 mm, 145 ℃; detector, Polymer Char IR4, 150 ℃; universal calibration, monodispersed polystyrene standards (Mn 1.3 kDa-3700

kDa).

NMR spectra of the polymer samples were recorded with a Bruker Avance III spectrometer (100MHz for $^{13}C$) equipped with high-temperature CryoProbe for 5mm tubes, on 2.6% w/w polymer solutions in tetrachloroethane-1,2-$d_2$ (also used as internal standard) at 120 °C. Conditions for $^{13}C$-NMR: zgpg45 pulse; acquisition time, 1.8s; relaxation time, 5s; number of scans, 1000-10000. Conditions for $^{1}H$-NMR: zg pulse, acquisition time 2.0s, relaxation time 10s, number of scans 6.

### 4.3. Computational Algorithm

Monte Carlo simulation was carried out to study the effects of dormancy. It was set up according to Gillespie's integral method[42-43]. The procedure and performance were described in Figure 2. The program was coded by the author of this thesis with MATLAB® script language and run on version R2010b.

A typical simulation used $N=10^6$ model sites. It starts with all active sites bearing one *i*Bu chain, denoted with $Pn_{i\ (i=1,\ldots,N)} = 1$. Uniformly distributed random numbers $r_1$ and $r_2$ were generated for time step and reaction selection, respectively. The time step $\tau$ between two reactions is not uniformly distributed, but a logarithmic function of the reciprocal of the random number $r_1$. Each site is assigned a number of $r_2$. For whichever value of $\nu$ that satisfies the inequality involving $r_2$, the corresponding reaction is applied for the active site.

Up to four types of reactions (M=4) were modeled:

1) primary insertion into primary sites (major event);
2) chain transfer of primary chains;
3) secondary insertion into primary sites;
4) primary insertion into secondary sites.

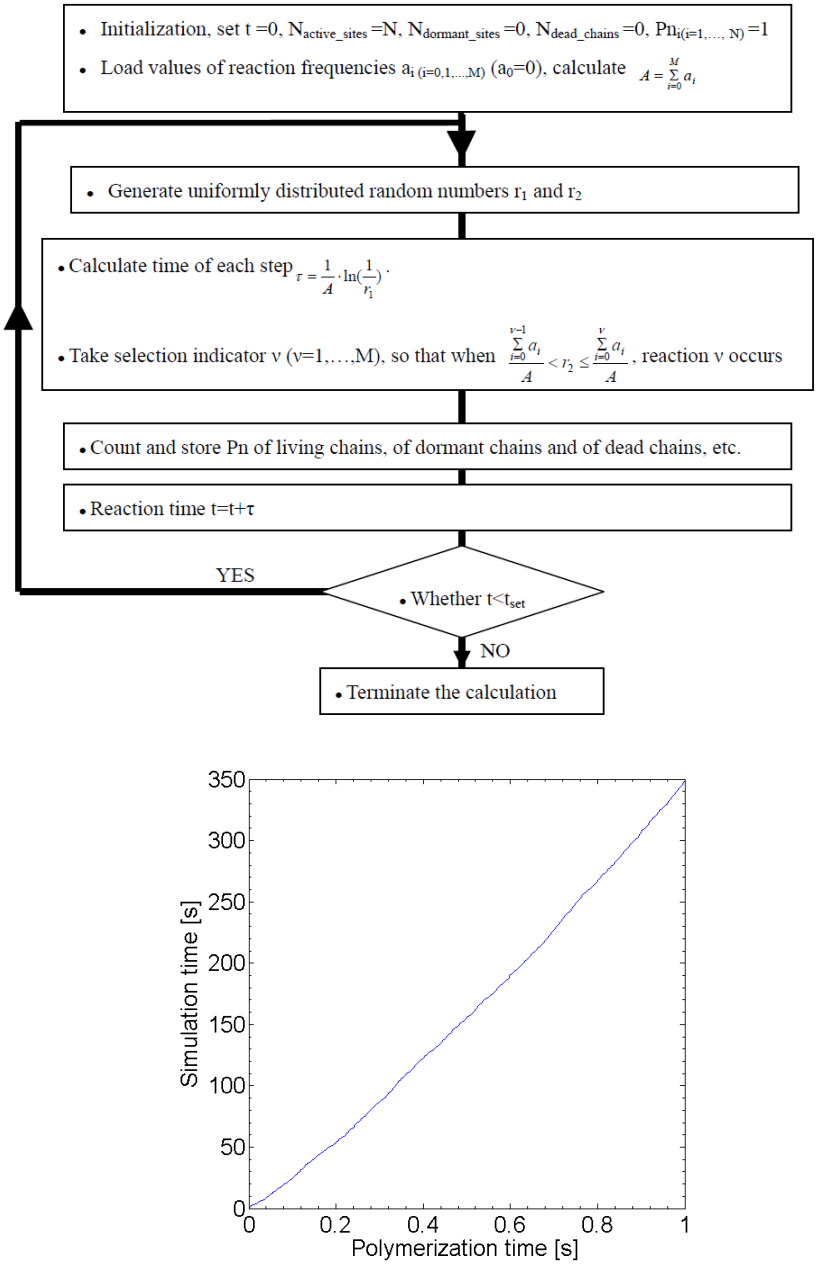


**Figure 2.** (Top) Scheme to describe the procedure of Monte Carlo simulation. (Bottom) Simulation performance, the time of simulation required for certain time of polymerization.

The detailed operations for each type of reaction are described as follows:

1) The polymerization degree (Pn) of the selected primary living chains is increased by 1;
2) The Pn of the selected primary living chains are copied to the Pn array of dead chains and then these living chains are re-started with a Pn = 1;
3) The Pn of selected primary chains is increased by 1 and then these chains are labeled as secondary chains;
4) The Pn of selected secondary chains is increased by 1 and then these chains are labeled as primary chains.

This program shows a quasi-linear scaling performance in terms of the time required for the simulation *versus* the real time of reaction (Figure 2).

## 4.4. Results and Discussion

### *4.4.1. Propene polymerization with ED*

*Apparent kinetics*

The kinetic profiles in Figure 3 show the precontact procedure has eliminated the induction period. The yield *versus* time profile appears to be a straight line in the first half second. However, after 1 s activity dropped to about 25% of its initial value. It is noticeable that this lower activity matches well with the overall activity of the 20 min slurry polymerization reaction. Figure 3b shows two activity regimes fitted by straight lines; a more reasonable smooth fit is shown in Figure 3d. This profile shows that activity declines during the first 2 s and then reaches a constant value. This behavior could be explained by dormancy as we will discuss later on.

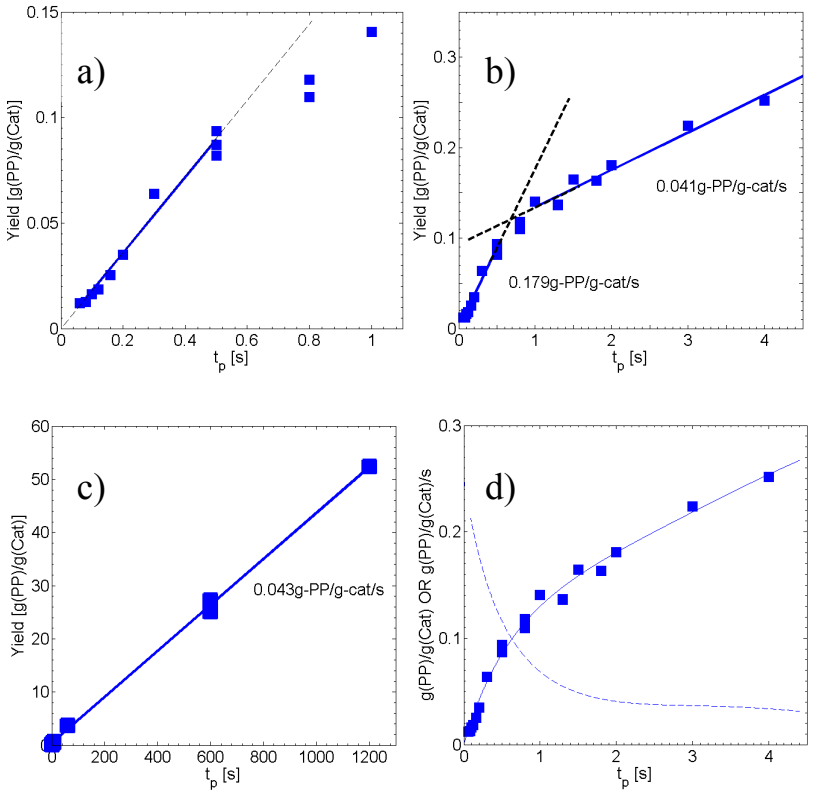


Figure 3. a), b) and c) Yield vs. time profiles showing straight-line fits; d) Fitting of the nascent part of yield-time profile with a smooth curve.

The quasi-living behavior of the polymerization is reflected by the variation of GPC profiles (Mn) with polymerization time as shown in Figure 4. If this were a single-site catalyst, one would expect to see PDI grow from 1 to 2 due to the gradual transition from quasi-living (Poisson distribution) to non-living (Schulz-Flory distribution) behavior. But since Ziegler-Natta catalysts intrinsically present multiple active sites, what is observed is an envelope produced by the overlapping GPC profiles corresponding to different kinetic parameters.

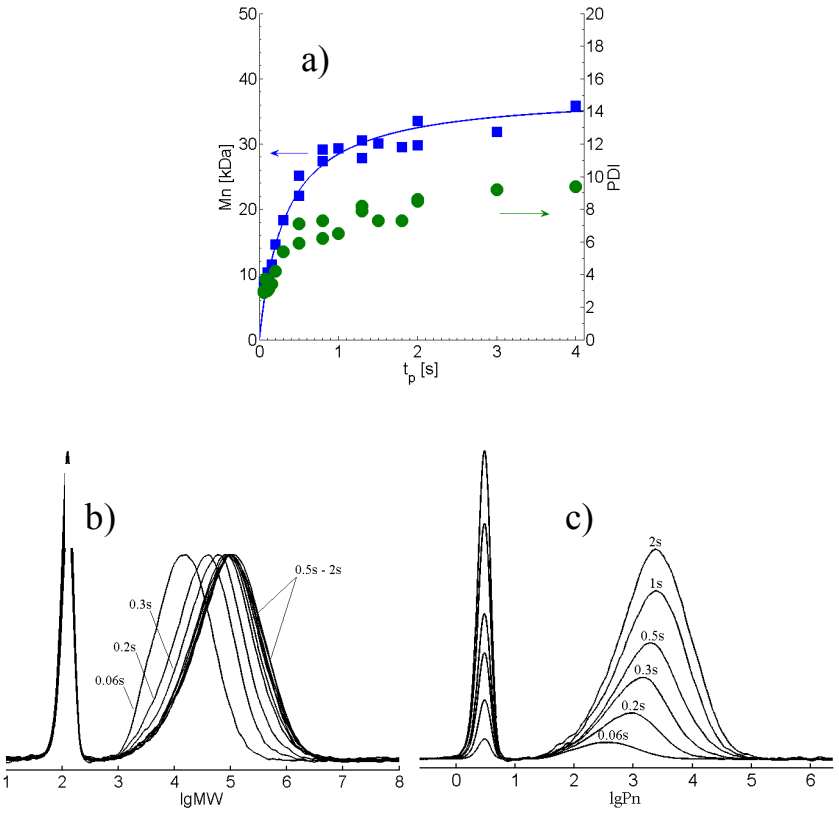


**Figure 4.** PP molecular weight distribution. a) Number-averge molecular weight (Mn) and polydispersity index (PDI) versus polymerization time; b) GPC profiles of PP prepared with different polymerization time, normalized to the same height; c) GPC profiles (lg Pn), the areas under the curves were normalized to PP yield.

*Average kinetic parameters*

For this system without an induction period, average kinetic parameters can be derived from a simple Natta plot ($1/P_n$ vs $1/t$):

$$\frac{1}{P_n} = \frac{1}{< f_p >} \cdot \frac{1}{t} + \frac{< f_{tr} >}{< f_p >} \qquad (1)$$

where $P_n$ is the average degree of polymerization; $<f_{tr}>$ is the average frequency of chain transfer; $<f_p> \equiv <k_p> \cdot [C_nH_{2n}]$ is the

average frequency of insertion; $<k_p>$ is the average insertion rate coefficient and [*M*] is the monomer concentration. From the linear least-squares fit (Figure 5), $<f_p>$ is obtained as the reciprocal of the slope, and $<f_{tr}>$ as the ratio of intercept to slope.

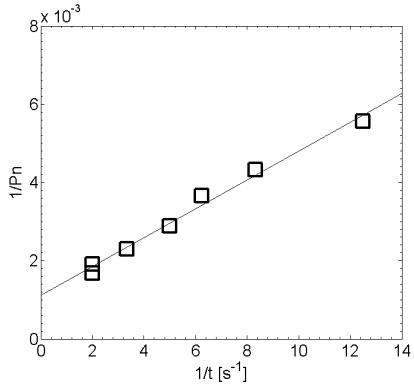


**Figure 5.** Natta's plot for PP prepared in the presence of ED. $R^2$=0.9878.

If we assume the system has a constant active-site content in the quasi-living first 0.5 s period (Figure 3a), the polymer yield as a function of time should follow a simple expression:

$$Y = < f_p > \cdot [C^*] \cdot t \qquad (2)$$

where *Y* is yield of polymer and [*C**] is active site content. Combination with the results from eq 1 yields a value for [*C**]. Table 1 gives the list of kinetic parameters.

**Table 1.** Kinetic parameters for propene polymerization prepared in the presense of ED. Errors were estimated with 95% confidence bound.

| $<f_p>$ / ($10^3$ $s^{-1}$) | $<k_p>$ / ($10^3$ $L \cdot mol^{-1} \cdot s^{-1}$) | $<f_{tr}>$ / ($s^{-1}$) | [*C**] / [$mmol \cdot mol(Ti)^{-1}$] |
|---|---|---|---|
| 2.71 ± 0.35 | 6.52 ± 0.83 | 3.01 ± 0.46 | 3.4 ± 0.4 |

Apparently the rate coefficient of insertion for phthalate system is slightly higher than EB-based system that was described in the

previous chapter. However the chain transfer frequency is similar. The major difference comes with the active sites content. The EB-based system has a value 4 times greater than the phthalate system.

According to a preliminary study of Terano et. al,[41, 44] the precontact does not greatly reduce the active sites content of DBP-type system, in line with the robustness of the system over alkyl aluminum. And it shows a similar value of active sites content. However in this study it gives a much higher $k_p$. For instance, Terano's reports gave $[C^*]$ = 3.8–6.1 mmol·mol(Ti)$^{-1}$ and $k_p$ = 1500–4000 L·mol$^{-1}$·s$^{-1}$ depending on the time of precontact.

*Chain ends analysis of polypropylene*

The microstructure of the PP samples is fairly as simple as shown in Figure 6. Only four types of chain ends are found: *iso*-butyl (*i*Bu), *n*-butyl (*n*Bu), *n*-propyl (*n*Pr) and 1-propen-2-yl (vinylidene or *vin*). *i*Bu chain ends can be formed in two ways: 1) the Ti-*i*Bu chain start groups produced during catalyst activation when *i*Bu is transferred from Al(*i*Bu)$_3$ to Ti-Cl species and 2) the last 1,2-insertion that generates the usual chain ends. *n*Bu should derive from 2,1 last-inserted unit and is interpreted as direct evidence of dormant species. *n*Pr and *vin* are due to the chain transfer with monomer (CTM). These mechanisms are summarized in Figure 7.

The content of chain ends is low; and the spectra present a significant level of noise when evaluating the signals of chain ends. Directly employing $^{13}$C-NMR integration for quantitative purposes might be risky when the signal-to-noise ratio is not high enough. In order to evaluate the errors that were brought by integration, as shown in Figure 8, a stepwise integration was performed between 10 ppm and 50 ppm with interval 0.04 ppm which is the typical width of a weak signal peak. The absolute values of the integrals are considered to reflect the integration errors which are below 3 when the integral of total carbon is set to 3× 10$^4$, meaning the error is

below $1 \times 10^{-4}$ per unit amount of carbon.

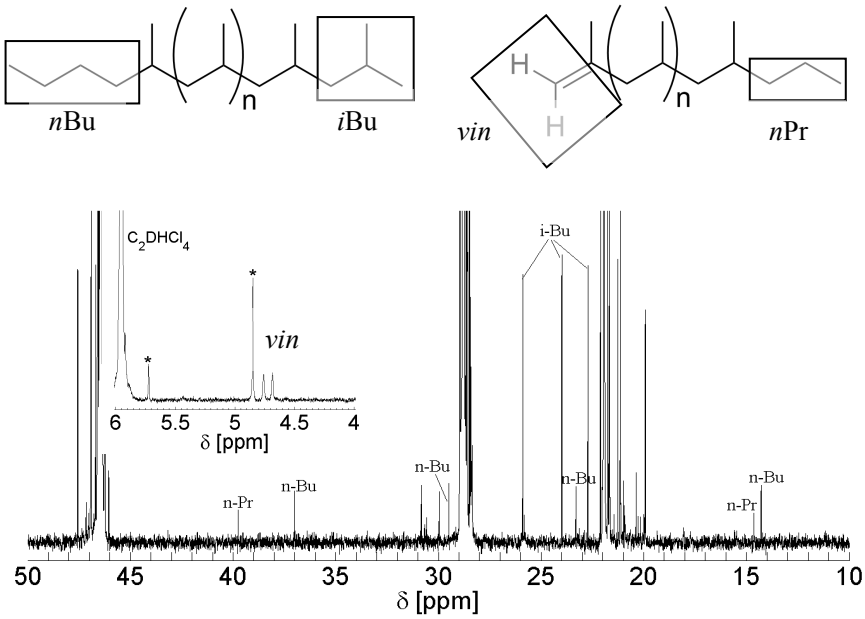


**Figure 6.** NMR signals assignment for the PP. (Larger) the alkyl region of a typical $^{13}$C-NMR spectrum; (insert) the olefinic region of the $^{1}$H-NMR spectrum. * denotes impurities.

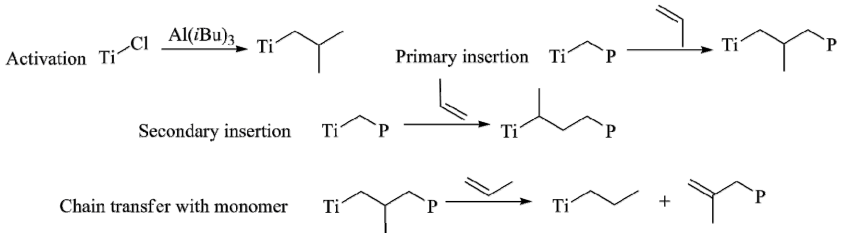


**Figure 7.** The mechanisms of chain ends being produced.

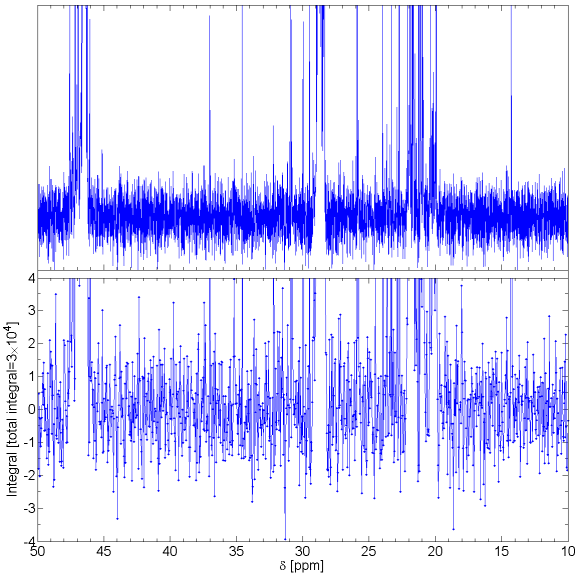


**Figure 8.** Error evaluation for NMR interation. The error=1× $10^{-4}$ per unit amount of carbon.

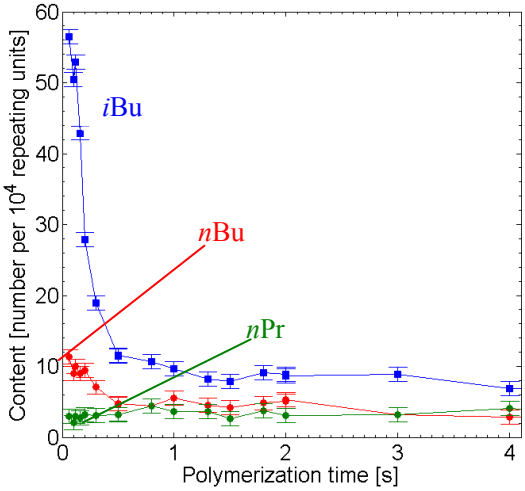


**Figure 9.** PP chain ends content vs polymerization time.

Figure 9 shows all chain ends excluding *vin* as a function of polymerization time. The unsaturated *vin* chain ends are easily modified or lost through chemical reactions induced by oxygen, heat or acid, making their quantification rather tricky. Therefore, we assume that the original *vin* content equals the content of *n*Pr groups, and in most samples this appears to be true (see Figure 12b).

When polymerization starts, most chain ends are *i*Bu since each polymer chain start with an *i*Bu group and other events are relatively rare. It should be noted here that *i*Bu is also produced by protonation following 1,2-insertion. The trend of declining *n*Bu content in the beginning reflects the change of overall regio-selectivity. Active sites with low regio-selectivity quickly become dormant while highly regio-selective sites keep on producing PP quickly. The *n*Pr content basically stays constant after the first second or so, indicating that the probability of chain transfer to monomer remains constant during the observation time.

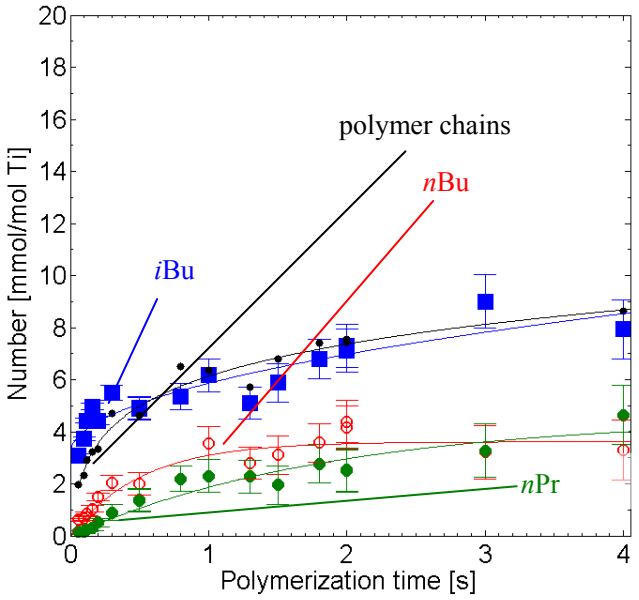


**Figure 10.** Absolute amount of chain ends in polypropylene versus polymerization time.

Multiplication of the chain end content with the number of polymer chains produces the absolute amount of chain ends (Figure 10). Extrapolation of the *i*Bu amount to $t = 0$ yields a value of about 4 mmol/mol(Ti), indicating that *i*Bu groups are already present at the beginning of the polymerization, as expected for activation with $Al(iBu)_3$. However, the *n*Bu and *n*Pr amounts both extrapolate to zero, implying they are produced *during* polymerization. The amount of polymer chains was obtained as one half of the sum of all chain ends including *vin* (assumed equal to *n*Pr).

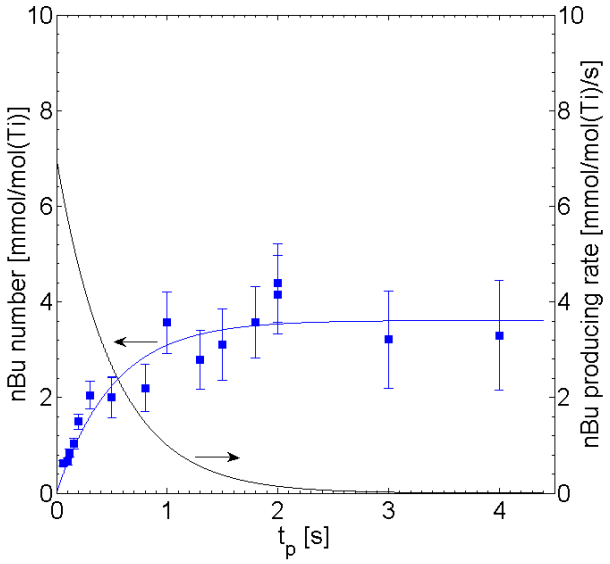


**Figure 11.** Development of *n*Bu groups with time. For the fitting $R^2$=0.88.

If one assumes the consumption of secondary sites Ti-$(CH_3)CHCH_2$-P (P denotes polymeryl) is negligible, the generation rate of *n*Bu could be expected to obey a first-order decay model. Least-squares fitting of the *n*Bu amount versus time gives a plateau value 3.6 mmol/mol(Ti) that nicely matches the active site content of 3.4 mmol/mol(Ti) (Table 1); the rate of formation of the *n*Bu end groups is approximately frequency 1.9 $s^{-1}$ per active site. And the overall initial producing rate of *n*Bu is about 7 $mmol \cdot mol(Ti)^{-1} \cdot s^{-1}$.

Chain end analysis can also provide some information on chain transfer to alkylaluminum and to monomer (BHT). For the moment we will discuss the latter reaction, which leads to formation of *n*Pr groups (Figure 12). The initial rate of formation of 3.7 $mmol \cdot mol(Ti)^{-1} \cdot s^{-1}$ corresponds to a reaction frequency of about 1 $s^{-1}$ per active site, assuming an active sites content of 3.4 $mmol \cdot mol(Ti)^{-1}$. It shows a plateau behaviour similar to that of *n*Bu, suggesting that both are formed from a pool of active sites which shrinks with time, through e.g. dormancy or deactivation.

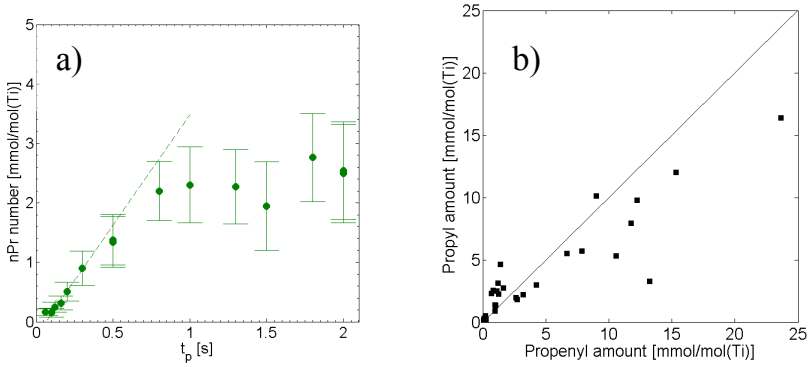


**Figure 12.** (a) Development of *n*Pr groups with time (initial slope=3.7 mmol/mol(Ti)/s); b) correlation between *n*Pr and *vin* amounts.

For an analysis of the chain end distribution, it is convenient to label all combinations of ends:

| End-Start | *n*Bu-*iBu* | *i*Bu-*i*Bu | *n*Bu-*n*Pr | *i*Bu-*n*Pr | *vin*-*i*Bu | *vin*-*n*Pr |
|---|---|---|---|---|---|---|
| Label | I | II | III | IV | V | VI |
| Start event | Al | Al | CTM | CTM | Al | CTM |
| End event | 2,1 | None/Al | 2,1 | None/Al | CTM | CTM |
| Amount | x | y | z | a | b | c |

1) Chains type I start with alkylation by Al($i$Bu)$_3$ and end with 2,1-insertion (or secondary insertion) of monomer.
2) Type II start with alkylation but are either terminated by transalkylation of Al($i$Bu)$_3$ (chain transfer to aluminum) or kept intact; of course, all the metal-polymeryl bonds (MPB) would be cleaved by protonation when polymerization is terminated by acidified methanol.
3) Type III start with the monomer insertion either during β-hydrogen transfer to monomer (BHT) or after β-hydrogen elimination (BHE); for clearance, both pathways are notated as chain transfer with monomer (CTM); and they end with 2,1-insertion.
4) Type IV start with CTM and either end with transalkylation or stay intact.
5) Type V start with alkylation and end with CTM.
6) Type VI start with $n$Pr produced by CTM and end with CTM.

If we assume the amount of I, II, III, IV, V, VI are x, y, z, a, b, c, we have

$$x+2y+a+b=i\mathrm{Bu} \quad (3)$$

$$x+z=n\mathrm{Bu} \quad (4)$$

$$b+c=vin=n\mathrm{Pr} \quad (5)$$

$$z+a+c=n\mathrm{Pr} \quad (6)$$

If we assume how chains start is independent from how they end, we have

$$x/y=z/a \quad (7)$$

$$y/b=a/c \quad (8)$$

Solving the equations, we have

$$x=(n\mathrm{Bu}^2 + i\mathrm{Bu}\cdot n\mathrm{Bu})/(i\mathrm{Bu} + n\mathrm{Bu} + 2n\mathrm{Pr}) \quad (9)$$

$$y=(i\mathrm{Bu}^2 - n\mathrm{Bu}^2)/(2i\mathrm{Bu} + 2n\mathrm{Bu} + 4n\mathrm{Pr}) \quad (10)$$

$$z=(2n\mathrm{Bu}\cdot n\mathrm{Pr})/(i\mathrm{Bu} + n\mathrm{Bu} + 2n\mathrm{Pr}) \quad (11)$$

$$a=(i\mathrm{Bu}\cdot n\mathrm{Pr} - n\mathrm{Bu}\cdot n\mathrm{Pr})/(i\mathrm{Bu} + n\mathrm{Bu} + 2n\mathrm{Pr}) \quad (12)$$

$$b =(i\mathrm{Bu}\cdot n\mathrm{Pr} + n\mathrm{Bu}\cdot n\mathrm{Pr})/(i\mathrm{Bu} + n\mathrm{Bu} + 2n\mathrm{Pr}) \quad (13)$$

$$c=(2n\mathrm{Pr}^2)/(i\mathrm{Bu} + n\mathrm{Bu} + 2n\mathrm{Pr}) \quad (14)$$

Therefore the amounts of all types of chains are obtained. In Figure 13 it shows the absolute amount of all types of chains. The plot clearly shows chains III, IV, V and IV are not present at the beginning. The significant amount of chains I at the beginning implies a high frequency of secondary insertion, corresponding to the higher content of secondary chain ends as shown in Figure 9. The increase of the amount of chains II can be explained by the mass transfer limit that was mentioned previously. It decreases because of the consumption by secondary insertion and by CTM. Clearly at the point of 2 s, most of the chains that are attached to metals end with secondary units. It is noticed, unlike II is surpassed by I after ~0.25s, III is higher than IV from the beginning; it seemingly implies the chains produced after CTM have lower regioselectivity than the chains starting with *i*Bu.

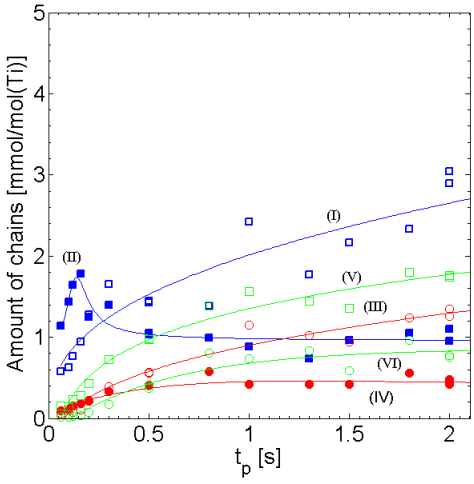


**Figure 13.** Temporal evolution of the absolute amount of chains type I, II, III, IV, V and VI. See text.

The primary chains (ending with 1,2-insertion) equals II+IV; and the secondary chains (ending with 2,1-insertion) equals I+III. Figure 14 gives the plot of the amount over time. Of course the dead chains equals to *vin*=*n*Pr and has already been discussed before (Figure 12).

The temporal evolution of the amount of primary chains, secondary chains and the metal-polymeryl bonds is shown in Figure 14. One can see a significant amount of secondary chains already at very short reaction times, and a decrease of primary chains accompanying the accumulation of secondary chains. The MPB amount increases slowly over time. Since it is unlikely that the Ti amount would increase in such short time after 13 min precontact, it should be reasonable to assume the whole increase of chains amount (>0.1 s) results from the transalkylation with $Al(iBu)_3$ (chain transfer). Over larger time scales, the rate of chain transfer to alkylaluminum is estimated.

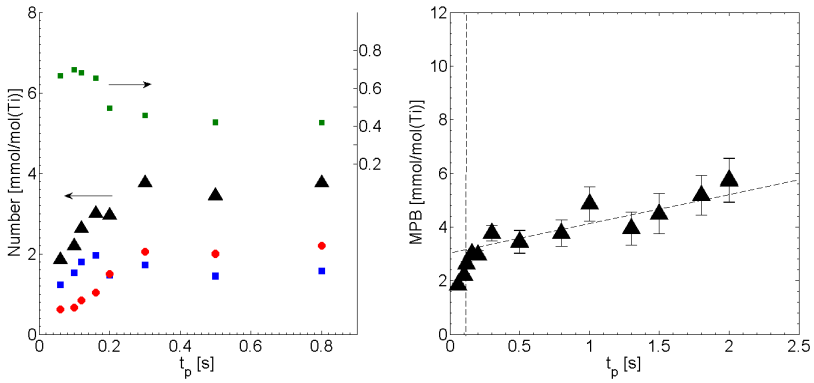


**Figure 14.** Temporal evolution of number of primary chains ■; secondary chains ●; metal-polymeryl bond (MPB) ▲ and the ratio of primary chains to secondary chains ■. For clarification, the error bar is omitted in the left figure.

The right figure shows the slope is about 1.1 $mmol \cdot mol(Ti)^{-1} \cdot s^{-1}$, slower than the chain transfer with monomer. A close inspection of the initial amount of MPB shows a surge in the first 0.1 s, in accordance with the trend of II in Figure 13. This might be a sign of initial mass transfer limitation, when the monomer has to diffuse into the whole catalyst particles on mixing of catalyst slurry and monomer solution.

*The effects of dormancy on Natta's plot*

The Natta plot analysis is based on the validity of equation (15) relating 1/*Pn* to 1/*t*. Its derivation assumes a constant active site content and constant kinetic parameters, neither of which applies to ZN catalysts:

1) dormancy changes the number of active sites
2) the presence of multiple active sites, and changes over time in their contributions to the product, make characterization with a single set of kinetic parameters dangerous

$$\frac{1}{P_n} = \frac{N_{chains}}{N_{monomer}} = \frac{f_{tr}\cdot[C^*]\cdot t + [C^*]}{f_p\cdot[C^*]\cdot t} \Rightarrow \frac{\sum\int f_{tr}\cdot[C^*]dt + [C^*]_0}{\sum\int f_p\cdot[C^*]dt} \Rightarrow ? \frac{1}{< f_p >}\cdot\frac{1}{t} + \frac{< f_{tr} >}{< f_p >} \quad (15)$$

Nevertheless, the Natta plot shown in Figure 5 looks reasonable, so it might be that the sensitivity of the Natta analysis to both of the above factors is limited. To understand this sensitivity issue, Monte Carlo simulations were carried out. Including first the onset of dormancy, and then, as a further refinement, an evolving probability of 2,1-insertion. In total four cases were simulated (for details see Table 2):

**Table 2.** Input conditions and the output of Monte Carlo simulation.

| run | Input conditions | | | | Output results | | |
|---|---|---|---|---|---|---|---|
| | $f_p$/ $s^{-1}$ | $f_{tr}$/ $s^{-1}$ | $f_{sec}/s^{-1}$ | $f_{sec\_p}/s^{-1}$ | $f_p$/ $s^{-1}$ | $f_{tr}$/ $s^{-1}$ | $Pn_\infty$* |
| a | 2713 | 3 | - | - | 2651 | 2.9 | 914 |
| b | 2713 | 3 | 2 | - | 2681 | 4.1 | 654 |
| c | 2713 | 3 | evolving | - | 2974 | 4.4 | 676 |
| d | 2713 | 3 | evolving | 1 | 2515 | 3.4 | 740 |

* $Pn_\infty$ denotes the final average polymerization degree, $Pn_\infty = f_p/f_{tr}$.

a) constant monomer incorporation frequency and constant chain transfer frequency

b) constant monomer incorporation frequency, constant chain transfer frequency, and 2,1-insertion with constant probability
c) constant monomer incorporation frequency, constant chain transfer frequency, and 2,1-insertion with evolving 2,1-insertion probability, as shown in Figure 15.
d) constant monomer incorporation frequency, constant chain transfer frequency, 2,1-insertion with evolving probability and constant consumption frequency of 2,1-active sites.

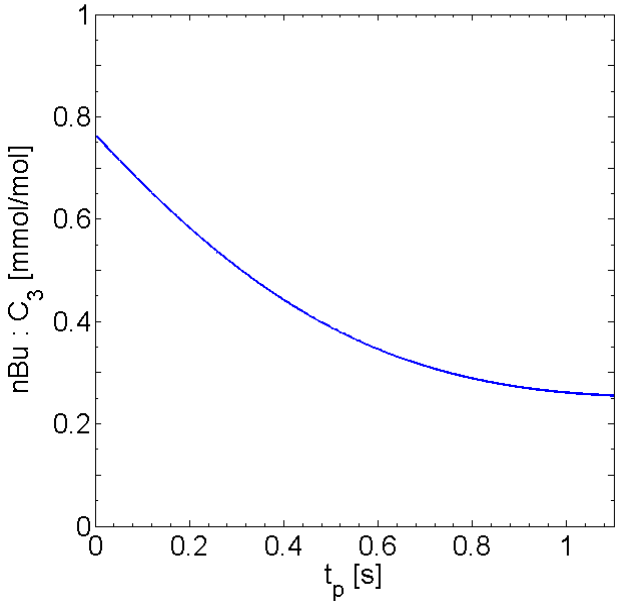


**Figure 15.** Experimental probability of 2,1-insertion.expressed in the ratio of generation frequency of *n*Bu to the incorporation frequency of monomer,

The results are as follows:.

a) This ideal situation without secondary insertion serves as a benchmark to verify the validity of the algorithm. The simulated Natta plot (Figure 16) perfectly reproduces the input numbers (insertion frequency and chain transfer

frequency), listed in Table 2.

b) When secondary insertion is present with a significant frequency $f_{sec}$, the chain transfer frequency is overestimated implying the formation of dormant species mimics the effect of chain transfer. Accordingly, the final number-average polymerization degree ($Pn_\infty$) was reduced, but the insertion frequency was not affected.

c) A changing $f_{sec}$ was adopted for this case did not show significant difference from constant-$f_{sec}$ case b except for the resulting apparent primary insertion frequency $f_p$.

d) If the secondary sites are allowed to reactivate, the Natta plot produces $f_{tr}$ and $Pn_\infty$ values intermediate between those of cases a and c.

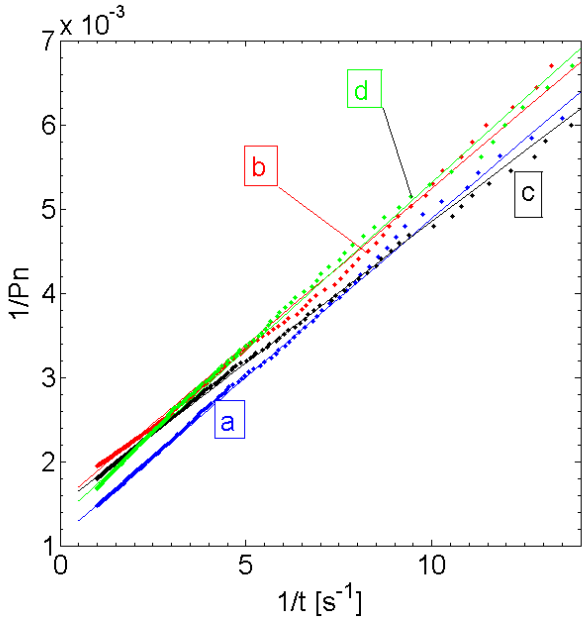


**Figure 16.** Simulated Natta's plots. For parameters, see Table 2.

From the results, it is clear that the Natta plot analysis is only moderately sensitive to the onset of dormancy and changing kinetic parameters. The same are Mn and PDI over time (Figure 17). But the influence of dormancy on t-yield plots is far more pronounced

(Figure 18).

It is undeniable that this is just the test for single-site model. However this verification with single-site model proved each group of active sites in a multiple sites catalyst can be described with Natta's plot satisfactorily even if they were significantly dormant. Overall the whole multiple sites system can also be described with Natta's plot since the equation is additive.

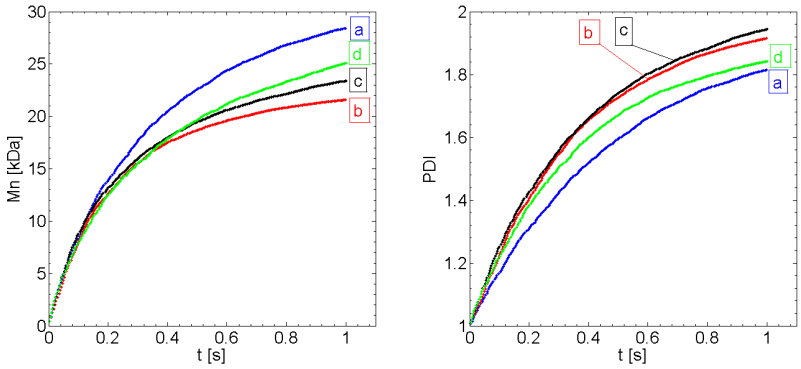


**Figure 17.** Simulated molecular weight distribution. For parameters, see Table 2.

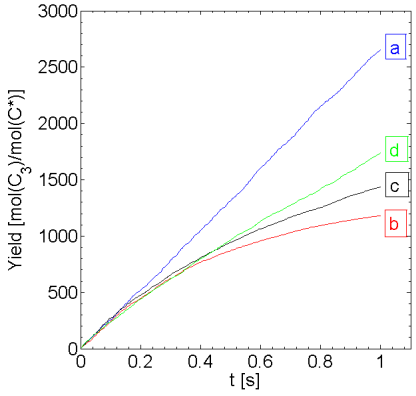


**Figure 18.** t-yield plots. For parameters, see Table 2.

*The temporal evolution of stereoerrors*

The three-site-model[45] on the genesis of stereoerrors includes 1) highly isotactic (enantiomorphic-site-controlled), 2) syndiotactic (chain-end-controlled) and 3) isotactoid blocks that are produced by interconverting sites.

Interestingly, the polypropylene produced in the beginning of polymerization is highly stereoregular. The detectable stereoerrors mostly belong to the *mrrm* segments that are produced by highly isotactic sites as the byproduct under enantiomorphic-site control because [*mmmr*]:[*mmrr*]:[*mrrm*]≈ 2:2:1. The stereoregularity deteriorates over time. The temporal evolution of [*mmmm*] shows a semi-logarithmic decay in the beginning but then deviates from the trend. In the following part, comparison with the data obtained in the absence of external donor will demonstrate this deviation results from the influences imposed by the external donor.

The absence of consecutive stereoerror (20.5 ppm-20.8 ppm) indicates there is not observable amount of atactic sites. The syndiotactic segments emerge over time, Figure 21, implying an evolving coordination environment of active sites. However with 13 min of precontact, this instant change of coordination environment is unlikely caused by the rearrangement of electron donors which are usually regarded as the key factors for chirality of active sites. If one considers the chain-end-control mechanism, living chains might render part of the active sites syndioregularity so that syndiotactic segments are produced.

Despite of the possibility of multiple sites evolving, the dormancy could probably complicate this process. It is likely that part of the active sites that are highly stereoselective become dormant over time and contribute less to isotacticity. This is evidenced by the well-known isotacticity enhancement upon hydrogen addition[46] (also see the following part on hydrogen addition).

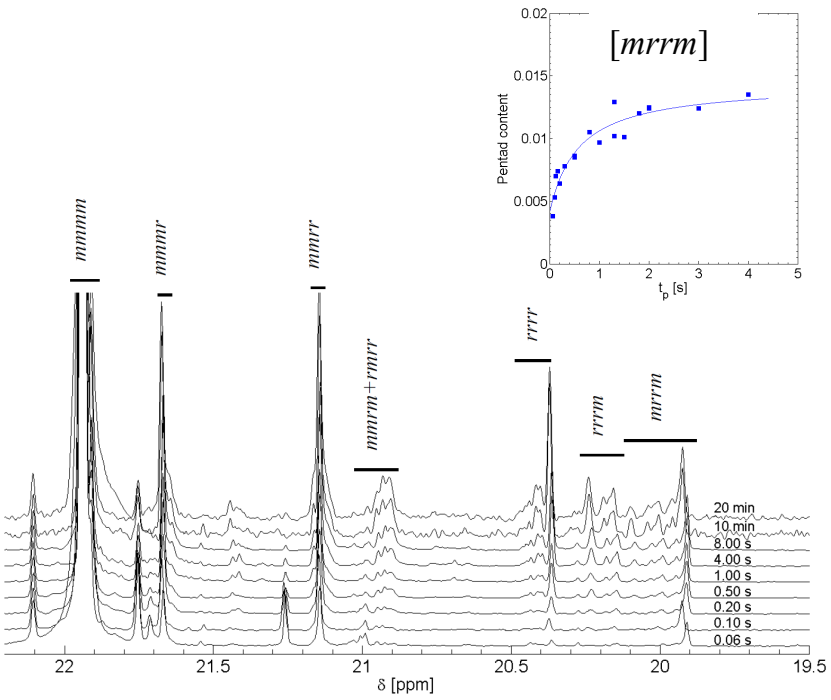


**Figure 19.** Methyl region of PP prepared with different polymerization time, showing the evolving stereoregularity. Insert is the temporal evolution of [*mrrm*].

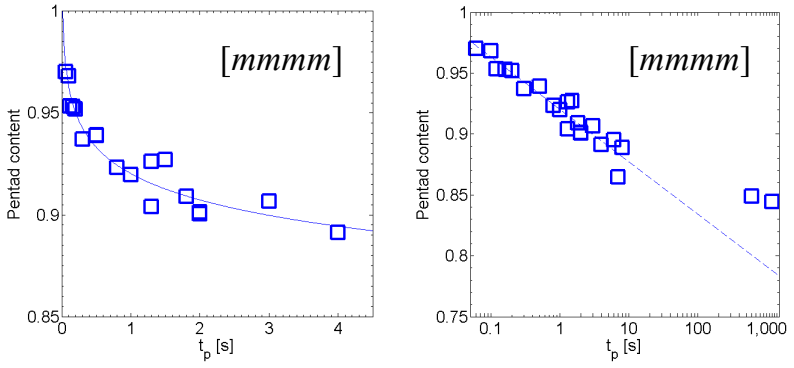


**Figure 20.** Meso pentad content evolving with time.

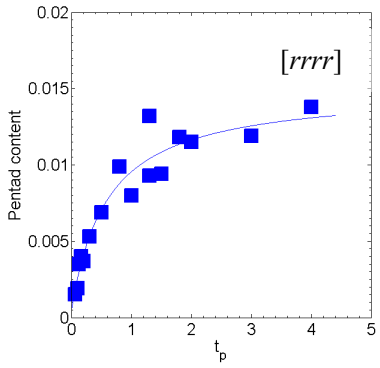


**Figure 21.** Racemo pentad content evolving with time.

The higher stereoselectivity but lower regioselectivity in the beginning suggest there is a clear difference for controlling factors of these two types of selectivities. This will be discussed again in the following part on the effects of external donor.

### *4.4.2. The effects of adding hydrogen or ethene on propene polymerization*

*Hydrogen addition*

Hydrogen is commonly used to control molecular weight in propene polymerization. It also increases overall activity and - importantly - enhances the isotacticity of the PP produced. All these facts are believed to be connected to its role as an efficient chain transfer agent. We have attempted to find direct evidence for this role in the nascent stage of polymerization.

Apparently the addition of hydrogen in the nascent stage even after precontact does not affect the activity of the catalyst within up to 3 s, see Figure 22.

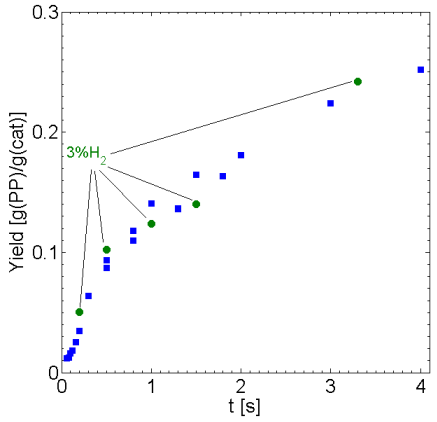


**Figure 22.** Effects of hydrogen addition on the t-yield plot of propene polymerization.

However Figure 23 shows the Mn (>1 s) is significantly reduced in the presence of hydrogen. This is compatible with studies by Terano et al.[47-48] on monoester (EB)-based catalyst where hydrogen response develops with precontacting. The EB-based catalyst is a highly regioselective catalyst in the nascent stage, so the lack of activity boosting with hydrogen is not surprising. For phthalate-based catalysts which are significantly dormant, we studied polymer microstructures to understand the low hydrogen response.

For samples prepared with 0.5 s and 1.5 s of polymerization, $^{13}$C-NMR (Figure 24 and Table 3) shows the content of *n*Pr and *i*Bu was increased. These are the expected trends for hydrogenolysis of Ti-polymeryl bonds. Based on the facts, it can be concluded hydrogen reacts with the active sites. However the zero effect of hydrogen on activity can only be explained via that the secondary sites are not highly reactive to hydrogen. The *vin* was slightly decreased only at longer time (1.5 s), suggesting even for primary sites $H_2$ is not that active compared to the propene monomer.

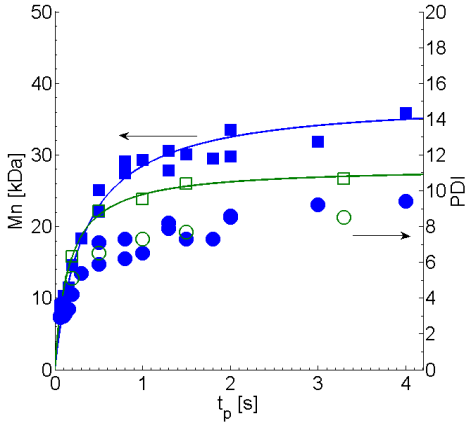


**Figure 23.** Effects of hydrogen addition on molecular weight distribution of PP. Solid squares, Mn of PP without $H_2$; solid circles, PDI of PP without $H_2$. Hollow squares, PP with $H_2$; hollow circles, PDI of PP with $H_2$.

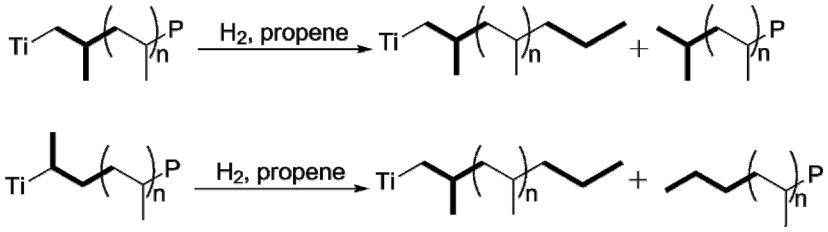


**Figure 24.** Possible mechanisms of reaction between hydrogen and primary and secondary sites.

**Table 3.** Comparison between chain ends content of PP without $H_2$ and that of PP with $H_2$.

| Sample code | $t_p$/s | Chain ends number, per 10000 repeating units | | | |
|---|---|---|---|---|---|
| | | *vin* | *i*Bu | *n*Bu | *n*Pr |
| QFCD51 (no $H_2$) | 0.5 | 2.28 | 11.47 | 4.69 | 3.24 |
| QFCD32 (with $H_2$) | 0.5 | 2.22 | 17.44 | 4.85 | 4.86 |
| QFCD57(no $H_2$) | 1.5 | 3.54 | 7.85 | 4.15 | 2.60 |
| QFCD117(with $H_2$) | 1.5 | 1.16 | 10.24 | 5.55 | 4.40 |

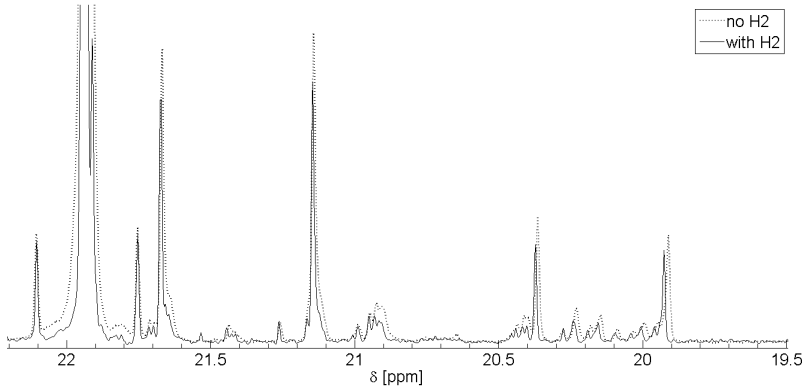


**Figure 25.** Comparison between the $^{13}C$ NMR spectra (methyl region) of PP prepared without and with $H_2$ (both 1.5 s), showing slight differences of the stereoregularity ([*mmmm*]=0.927 for PP without $H_2$ and 0.935 for PP with $H_2$). Methyl peaks (*mmmm*) are normalized to the same height.

Comparison of the methyl region (Figure 25) suggests a slight enhancement of isotacticity of polypropylene with a polymerization time of 1.5 s. It is in agreement with the well known isotacticity-enhancement upon $H_2$ addition in industry.[46]

*Ethene addition*

Ethene is an important comonomer for propene polymerization. EPR (ethylene propylene rubber) is a typical product of copolymerization of ethene and propene. Usually the addition of ethene results in a boost of activity. This is believed to result from the waking up of dormant species through ethene insertion, since ethene is supposed to more easily insert in dormant species, converting them into active ones.

However, according to the results (Figure 26) ethene does not show a significant enhancement of activity in the first 1 s, whereas indeed a significant activity boost was observed in a polymerization of 2 s. Use of higher ethene concentration (18.3%) does not change the scenario at < 1 s polymerization times.

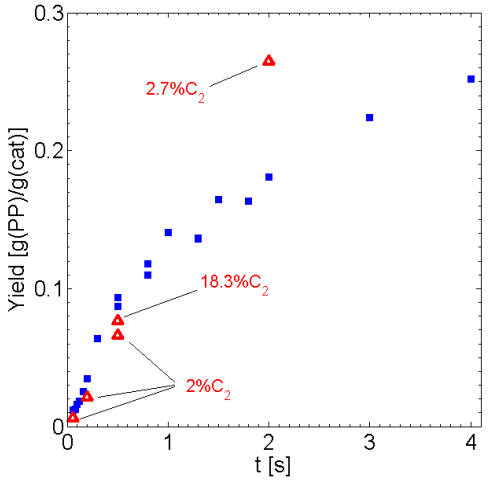


**Figure 26.** Effect of ethene addition on the t-yield plot of propene polymerization.

The reduction of the number of dormant secondary sites by ethene is reflected by a lowering of nearly 50% of the *n*Bu content of the product (Figures 27-28 and Table 4), even for the shortest polymerization run (0.06 s).

These facts can be accounted for by the time required to show the accumulative effects like time *vs*. yield. As one can see in Figure 18, the most dormant case even shows a quasi-linear t-yield plot in the very beginning like a non-dormant one does.

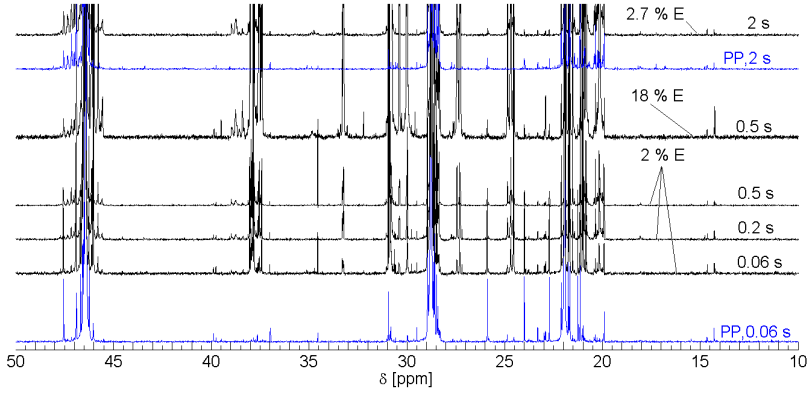


**Figure 27.** Effect of ethene incorpration on the structures of polypropylene backbone. Methyl peaks (*mmmm*) are normalized to the same height.

**Table 4.** Comparison between content of chain ends of polypropylene prepared without ethene addition and that with ethene addition.

| Sample code | $t_p$/s | Chain ends number, per 10000 repeating units | | |
|---|---|---|---|---|
| | | *i*Bu | *n*Bu | *n*Pr |
| QFCD54 (0% E) | 0.06 | 56.51 | 11.36 | 2.94 |
| QFCD23 (2% E) | 0.06 | 46.90 | 5.77 | 6.99 |
| QFCD61 (0% E) | 0.2 | 27.83 | 9.40 | 3.19 |
| QFCD24 (2% E) | 0.2 | 23.81 | 5.33 | 3.20 |
| QFCD51 (0% E) | 0.5 | 11.47 | 4.69 | 3.24 |
| QFCD25 (2% E) | 0.5 | 10.36 | 2.68 | 2.66 |
| QFCD63 (0% E) | 2.0 | 8.66 | 5.34 | 3.09 |
| QFCD66 (2.7% E) | 2.0 | 3.88 | 2.52 | 2.79 |

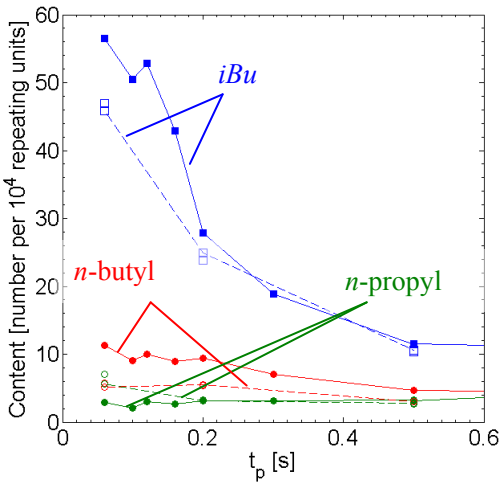


**Figure 28.** Effect of ethene incorpration on the chain ends content of polypropylene. Solid marks denote $C_3$ polymerization; and hollows marks denote $C_2$-$C_3$ polymerization.

According to previous study[49-51], for Ziegler-Natta catalyst system, there is $k_{pE}/k_{sE} = (Q_{pE}/Q_{sE})_0/(k_{sp}/k_{ps}) = (Q_{pE}/Q_{sE})_0/[(x_d^*)^{-1} -1]$, where $k_{pE}$ is the rate coefficient of ethene insertion after primary propene units, $k_{sE}$ is the rate coefficient of ethene insertion after secondary propene units, $Q_{pE}$ is the amount of ethene units inserted after a primary propene unit, $Q_{sE}$ is the amount of ethene units inserted after a primary propene unit, $k_{sp}$ is the rate coefficient of primary insertion of propene after secondary propene units, $k_{ps}$ is the rate coefficient of secondary insertion of propene after primary propene units, $x_d^*$ is the dormant species content. With $(Q_{pE}/Q_{sE})_0$ =30 (from the Ref. [51]) and $x_d^*$ =0.6 (for < 1 s, estimated with Figure 14 of this chapter) substitued, $k_{pE}/k_{sE}$ = 45. It means even if there has been 60% secondary sites among total sites, the ethene insertion after secondary propene units would be about 2% of total ethene units. If we recall the content of secondary sites actually has increased from 0 at the beginning to 0.6 at 1 s, the content of ethene units after secondary propene units would be expected to be even lower than 2%. Hence it is very difficult to observe the ethene insertion after secondary propene units in the nascent stage. It explains why only

the sample prepared with 18.3% ethene shows an ambiguous and weak signal of $S_{\alpha\beta}$ at about 35 ppm (Figure 27).

### *4.4.3. Effect of the external donor on propene polymerization*

In order to achieve a better understanding of the role of the external donor (ED) used so far (diisobutyldimethoxysilane), we also carried out polymerizations where this donor was not used. In the absence of the ED, propene polymerization with the phthalate-based catalyst shows a lower initial activity (Figure 29). While the system with ED shows a bending at about 0.5 s, in the absence of ED we observe a more nearly linear t-yield plot for up to 1 s. One might expect the system without ED to exhibit a slower accumulation of dormant species. However, this does not seem to be supported by chain end analysis as discussed later on. It is noticeable that despite of the lower activity in the nascent stage of polymerization, the system without ED actually displays a higher average activity for a 20 min polymerization experiment than does the system with ED.

The molecular weight distribution of PP prepared without ED does not show significant difference from PP prepared with ED, Figure 30. The PDI after 2 s is slightly lower compared to the system with ED, suggesting the presence of ED increases the diversity of active sites. This is supported by the active site content obtained from a Natta plot (Table 5). The calculated kinetic parameters suggest that the ED not only converts a fraction of the inactive sites into active ones, but also enhances the reactivity of already active sites. The presence of ED also suppresses the chain transfer probability as evidenced by the lower $f_{tr}$. As discussed earlier, the Natta plot analysis is somewhat sensitive to dormancy and changes in the distribution of active sites, to the extent that the plot may remain nearly linear but may still yield somewhat skewed results. Therefore, the differences in kinetic parameters in the Table should be considered tentative at best.

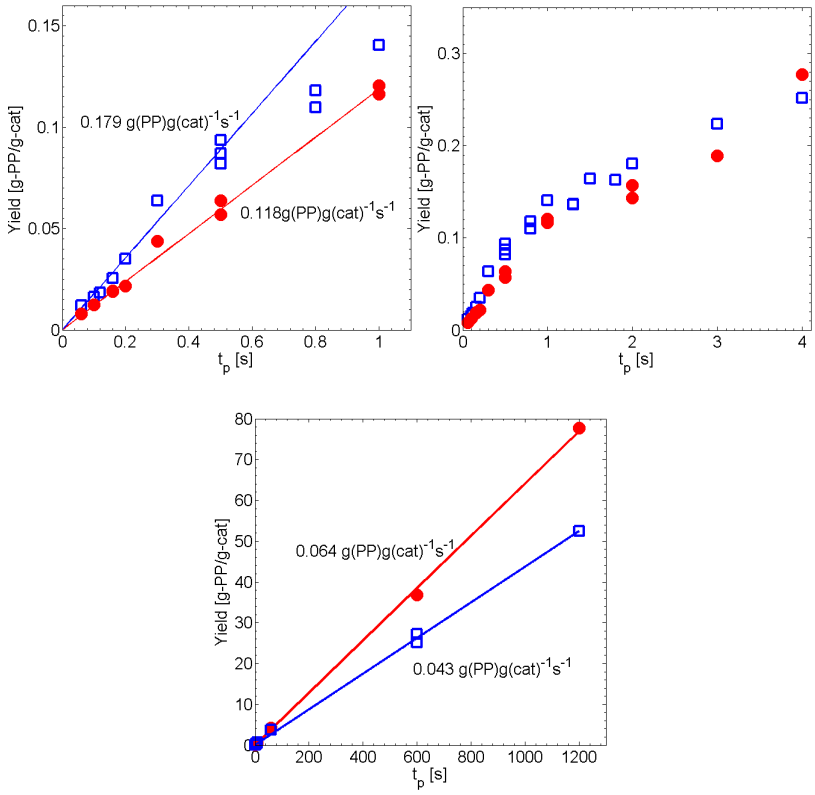


**Figure 29.** Comparison of t-yield plot of propene polymerization in the absence (●), and presence (□) of ED at different time scales.

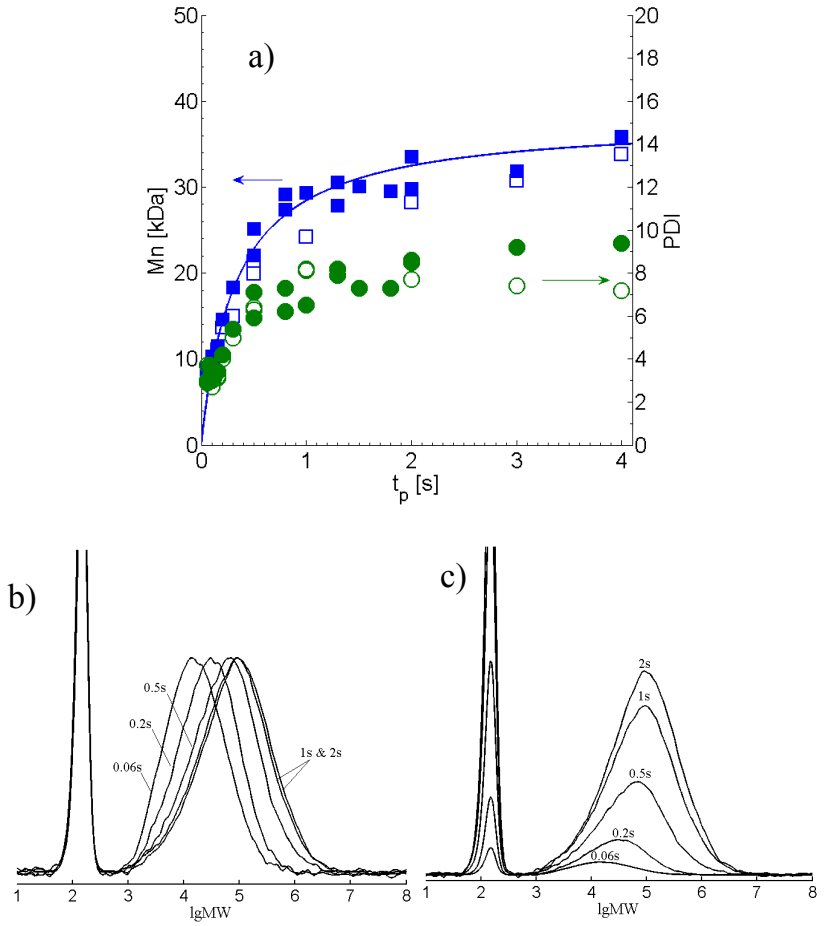


**Figure 30.** Molecular weight distribution profiles of PP prepared without ED. a) Number-average molecular weight (Mn) and polydispersity index (PDI) versus polymerization time; b) GPC profiles, normalized to the same height; c) GPC profiles, normalized to the yield of PP.

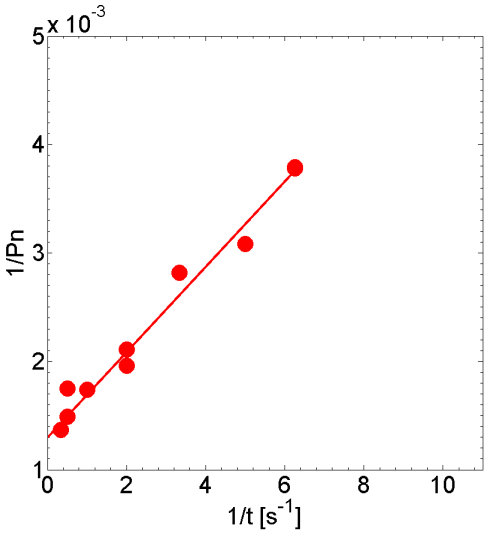


**Figure 31.** Natta plot for PP prepared without ED.

**Table 5.** Kinetic parameters for propene polymerization with and without

| Exp. cond. | $\langle k_p \rangle$ / ($10^3$ L·mol$^{-1}$·s$^{-1}$) | $\langle f_{tr} \rangle$ / (s$^{-1}$) | [$C$*] / [mmol·mol(Ti)$^{-1}$] |
|---|---|---|---|
| With ED | 6.52 ± 0.83 | 3.01 ± 0.46 | 3.4 ± 0.4 |
| No ED | 6.37 ± 0.75 | 3.64 ± 0.42 | 2.0 ± 0.2 |

Chain ends analysis clearly shows a higher content of *n*Pr for PP prepared without ED. There are also more polymer chains per Ti (Figure 33) although the Natta analysis indicates a lower content of active sites. Apparently the difference in number of polymer chains is mostly caused by chain transfer to monomer as deduced from the amount of *n*Pr (Figure 34); the *vin* content is less informative because of the stability issue mentioned earlier for these chain ends.

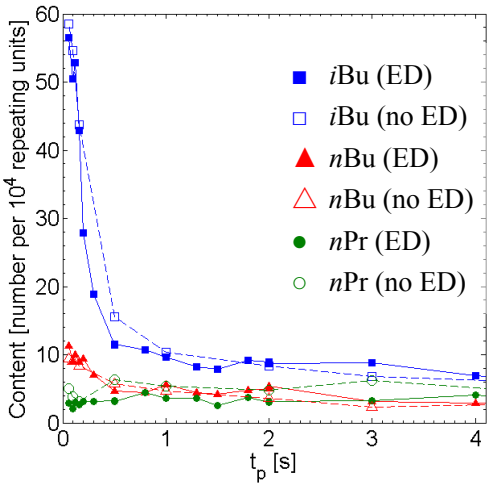


**Figure 32. C**hain ends content for PP prepared with and without ED.

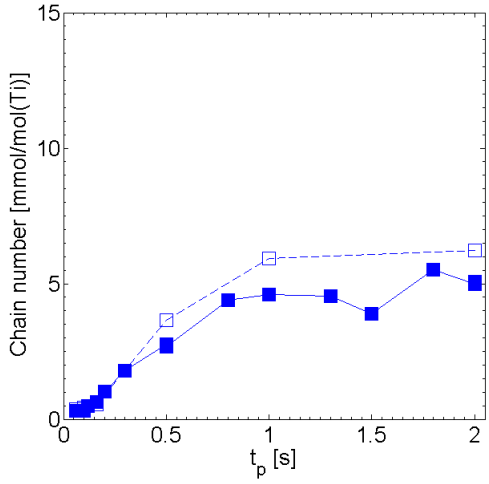


**Figure 33. C**hain amount for PP prepared with (■) and without (□) ED.

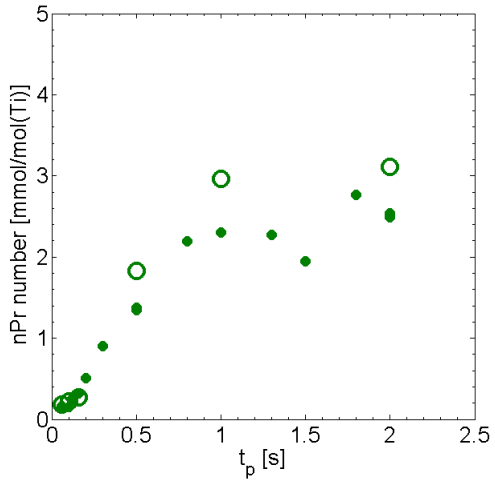


**Figure 34.** *n*Pr amount for PP prepared with (●) and without (○) ED.

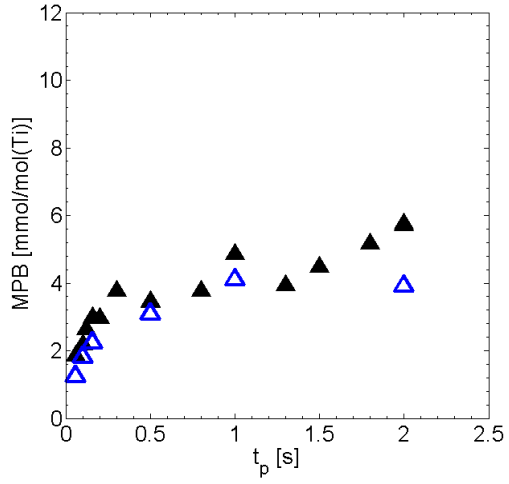


**Figure 35.** Metal-polymeryl bond (MPB) amount for PP prepared with (▲) and without (△) ED.

Indeed, the amount of polymer chains bonded to metals (MPB) is slightly lower for the system without ED. If chain transfer to cocatalyst is at all relevant here, the almost parallel t-MPB plots for systems with and without ED (Figure 34) suggest that the rate of

chain transfer to TIBA is not significantly affected by the ED.

The *n*Bu content is also very similar for systems with and without ED, implying that the ED (diisobutyldimethoxysilane) in this case, does not affect the regioselectivity of diisobutyl phthalate-based catalyst much. This is also reflected by the analysis of the composition of MPB (Figure 36). With slightly lower absolute amount of both primary chains and secondary chains, the ratio of primary chains to secondary chains is hardly affected by the presence of the ED.

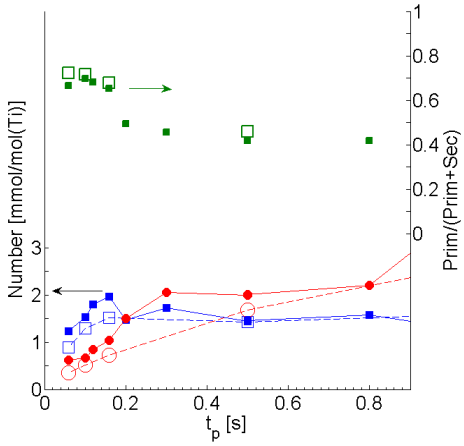


**Figure 36.** Temporal evolution of 1) number of primary PP chains with (■) and without (□) ED; 2) number of secondary PP chains with (●) and without (○) ED; 3) ratio of primary to secondary chains for PP with (■) and PP without (□) ED.

The stereoregularity of PP is significantly affected by the presence of the ED. The *meso* pentad content [*mmmm*] (Figure 37) keeps deteriorating in a semilogarithmic way over time when the ED is absent. The addition of ED substantially stabilizes the stereoselectivity of active sites. Based on the three-site-model for the genesis of stereoerrors in $MgCl_2$-supported Ziegler-Natta catalysis, two types of pentads were examined as indicators for chain-end-control and enantiomorphic-site-control mechanisms,

respectively. The presence of ED suppresses the production of *rrrr* more profoundly than it does to *mrrm* (Figure 38). It is noticeable [*mrrm*] reaches the plateau faster than [*rrrr*] over time in the absence of an ED. This may be taken as an indication that the active sites responsible for enantiomorphic-site-control reach a steady-state concentration faster than that for chain-end-control.

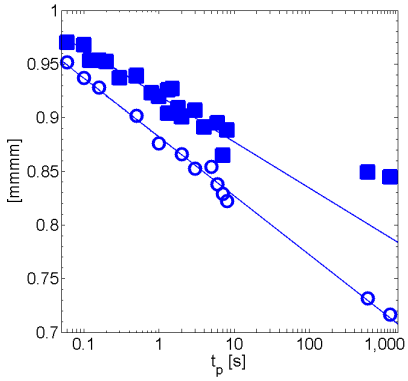


**Figure 37.** Evolution of meso pentad content with time, with (■) and without (○) ED.

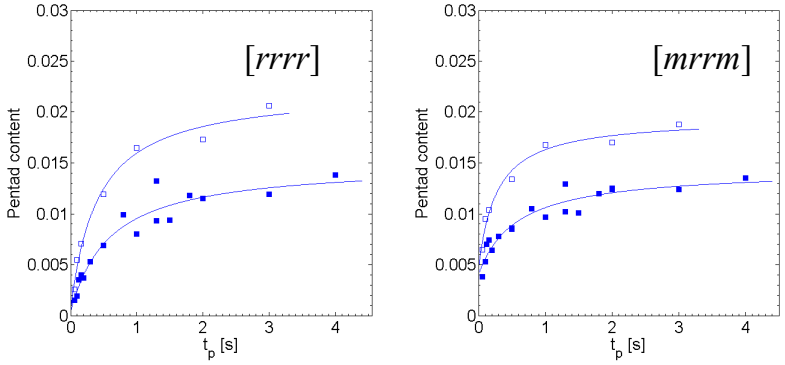


**Figure 38.** Evolution of stereoerrors with time: a) [*rrrr*] related to chain-end control. b) [*mrrm*] related to enantiomorphic-site-control; (■ ) with, (□) without ED.

### *4.4.4. Propene polymerization at different temperatures*

*Apparent Kinetics*

One might expect that higher temperature gives higher activity. However the results show declining apparent initial activities with increasing temperature, Figure 40a. The apparent activity results from the combined effects of monomer concentration, propagation rate coefficient and active sites content. By normalizing to constant monomer concentration, Figure 40b, the initial activity peaks at about 30 ℃, suggesting a balance between the rate coefficient and active sites content: the active sites content should decrease with increasing temperature.

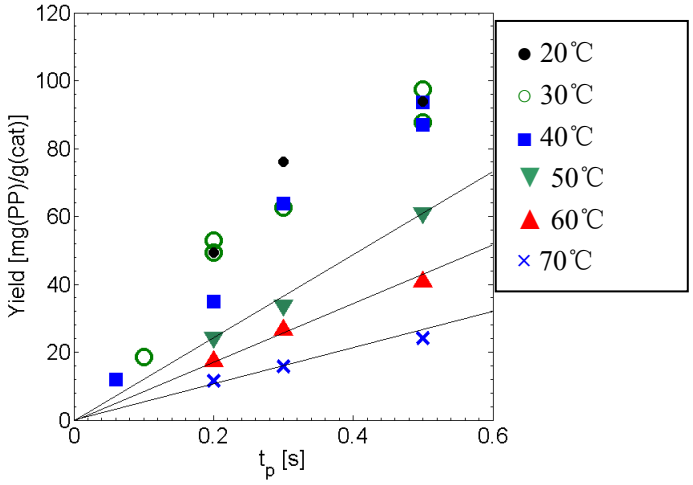


**Figure 39.** Initial part of t-yield profiles of propene polymerization at different temperatures.

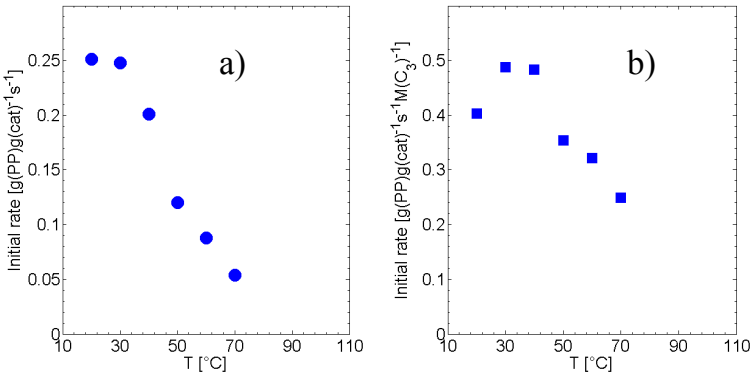


**Figure 40.** Initial activities of propene polymerization: a) apparent values; b) values normalized to constant monomer concentrations.

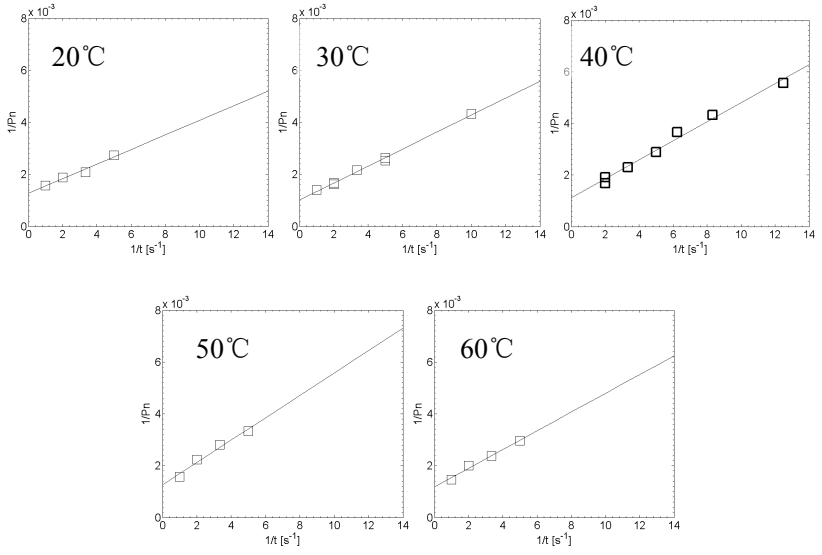


**Figure 41.** Natta plots at different temperatures (20-60 ℃). The data of 70℃ were not adopted for this purpose because of the instability reason.

**Table 6.** Kinetic parameters obtained with Natta's for different

| Temp. | $\langle f_p \rangle$ / ($10^3$ $s^{-1}$) | $\langle k_p \rangle$ / ($10^3$ $L \cdot mol^{-1} \cdot s^{-1}$) | $\langle f_{tr} \rangle$ / ($s^{-1}$) | $[C^*]$ /[$mmol \cdot mol(Ti)^{-1}$] |
|---|---|---|---|---|
| 20°C | 3.56 ± 1.25 | 5.71 ± 2.00 | 4.51 ± 1.17 | 3.2 ± 1.1 |
| 30°C | 3.06 ± 0.22 | 6.02 ± 0.44 | 3.10 ± 0.36 | 3.7 ± 0.3 |
| 40°C | 2.71 ± 0.35 | 6.52 ± 0.83 | 3.01 ± 0.46 | 3.4 ± 0.4 |
| 50°C | 2.31 ± 1.19 | 6.83 ± 3.52 | 2.91 ± 1.65 | 2.4 ± 1.2 |
| 60°C | 2.76 ± 1.07 | 10.10 ± 3.91 | 3.25 ± 1.24 | 1.4 ± 0.6 |

Natta plots were used to extract turnover frequencies and chain transfer frequencies. Combination of these with monomer concentrations and initial activities produced rate coefficients and active sites contents, listed in Table 6. The rate coefficient of polymerization clearly increases with temperature as expected, whereas active sites content decreases. The chain transfer frequency seems to be only slightly affected by temperature.

*Arrhenius plot*

The apparent activation energy is obtained from an Arrhenius plot of ln $k_p$ vs $1/T$ (Figure 42):

$$\ln(k_p) = -\frac{E_a}{R} \cdot \frac{1}{T} + \ln(A) \tag{16}$$

where $k_p$ is the rate coefficient, $L \cdot mol^{-1} \cdot s^{-1}$; $E_a$ is activation energy, $J \cdot mol^{-1}$; $R$ is the gas constant, 8.3145 $J \cdot K^{-1} \cdot mol^{-1}$; $T$ is the reaction temperature, K, and $A$ is the pre-exponential factor.

Although the complex and multi-site nature of ZN catalysts needs to be kept in mind, the plot appears to show a fairly linear correlation of [ln ($k_p$) vs $1/T$]. A low value of apparent activation energy is obtained.

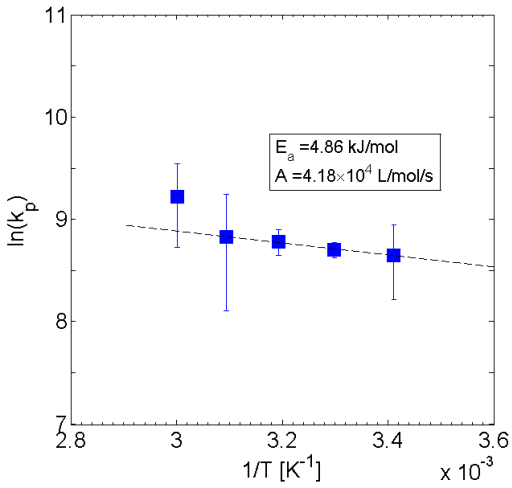


**Figure 42.** Arrhenius plot for propene polymerization at temperatures from 20 ℃ to 60 ℃. The point of 60 ℃ is not involved into fitting.

*Eyring plot*

The precise shape of the calculated potential energy surface for olefin polymerization at ZN sites depends strongly on the choice of basis set, functional and active site model.[52] Most methods agree that, like for homogeneous systems, the olefin capture barrier is small and mainly entropic. Depending on the method used, the insertion step may or may not have a barrier. In any case, we have also analyzed the temperature dependence using an Eyring plot [ln ($k_p/T$) vs $1/T$]:

$$\ln\frac{k_p}{T} = -\frac{\Delta H^{\ddagger o}}{R}\cdot\frac{1}{T} + \frac{\Delta S^{\ddagger o}}{R} + \ln\frac{k_B}{h} \qquad (17)$$

where $k_p$ is rate coefficient, $L\cdot mol^{-1}\cdot s^{-1}$; $T$ is reaction temperature, K; $\Delta^{\ddagger}H^{o}$ is the enthalpy of activation, $J\cdot mol^{-1}$; $R$ is the gas constant, 8.3145 $J\cdot K^{-1}\cdot mol^{-1}$; $\Delta^{\ddagger}S^{o}$ is the entropy of activation, $J\cdot mol^{-1}\cdot K^{-1}$; $k_B$ is Boltzmann constant, $1.3806\times10^{-23}$ $J\cdot K^{-1}$; $h$ is the Planck constant, $6.6261\times10^{-34}$ J·s. The results suggest a near-zero but rather low enthalpic barrier (2.3 kJ/mol) and a large entropy of activation (-165 J/mol/K)) corresponding to a bimolecular process. Recalling the

numbers of homogeneous systems discussed in Chapter 2, the enthalpy of ZNC is even lower than C1/MAO/BHT (11 kJ/mol), but the entropy is similar (-134 J/mol/K).

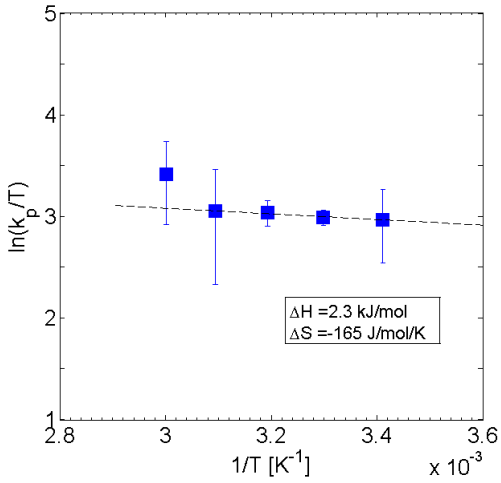


**Figure 43.** Eyring plot for propene polymerization at temperatures from 20 ℃ to 60 ℃. The point of 60 ℃ is not involved into fitting.

### *4.4.5. Ethene polymerization*

Comparison of the results described above with ethene polymerization reveals some interesting pieces of information. It should however be kept in mind that these types of phthalate-based catalysts are not commonly used in commercial PE production.

*Apparent Kinetics*

Similar to propene polymerization, ethene polymerization also shows a non-linear t-yield plot, Figure 44. The activity of ethene polymerization apparently keeps declining over time, differing from propene polymerization which seems to reach an activity plateau very soon. Even in the first fraction of second, Figure 45, there is some bending for the PE t-yield plot. The steric factors

relevant to propene polymerization, in particular dormancy, do not apply here, and hence the levelling off of activity must have a different explanation. One possibility is mass transfer limitation caused by the accumulation of PE on the catalyst surface (note that the initial activity for PE is far higher than for PP

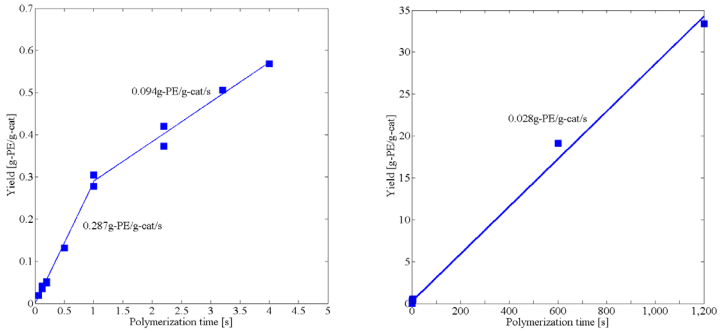


**Figure 44.** t-yield profiles for ethene polymerization with TIBA as cocatalyst.

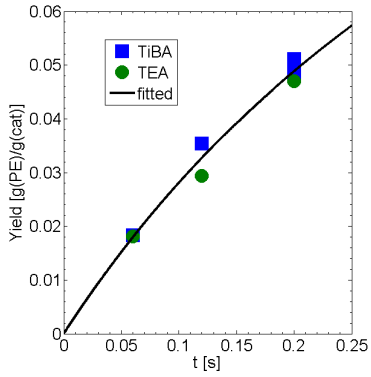


**Figure 45.** Effects of cocatalyst on t-yield profile.

It is noticeable that the activity is not affected in the nascent stage when the cocatalyst is changed from TIBA to TEA. However, the molecular weight distribution tells a rather different story, Figure 46 and Figure 47. The GPC data demonstrate that the TIBA system

produces a much higher molecular weight. This is due to the combination of a higher insertion turnover frequency and a significantly lower chain transfer frequency (Table 7). The results suggest:

1) TEA may bind more closely to the surrounding of active sites due to the smaller alkyl substituent, and this binding might hamper the monomer insertion
2) TEA also transfers the polymer chains more efficiently due to lower steric hindrance in approach to and chain exchange with active sites

Apparently the active sites content of the TIBA system is roughly similar to that of the TEA system. But considering the possibility of mass transfer limitation, the results of the Natta analysis should be treated with caution. However it is rather clear ethene polymerization reaction is much faster than propene polymerization, 4 folds of the latter one. And the chain transfer frequency of ethene polymerization is lower for the system with the same cocatalyst.

Based on detailed structural information from $^{13}$C-NMR, stoichiometric information regarding chain ends and backbone repeating units was extracted, Figure 48. The lack of evident signals of the tertiary long-chain branching carbon indicates this PE is highly linear.

**Table 7.** Comparison of kinetic parameters of propene polymerization with different cocatalysts (TIBA or TEA).

| Cocatalyst | $\langle k_p \rangle$ / [$10^3$ L·mol$^{-1}$·s$^{-1}$] | $\langle f_{tr} \rangle$ / [s$^{-1}$] | [$C^*$] / [mmol·mol(Ti)$^{-1}$] |
|---|---|---|---|
| TIBA | 22.12 ± 3.64 | 0.8± 0.7 | 10.1± 1.7 |
| TEA[1] | ~17 | ~8 | ~12 |

[1] Due to the limited number of data, the values are only as estimation.

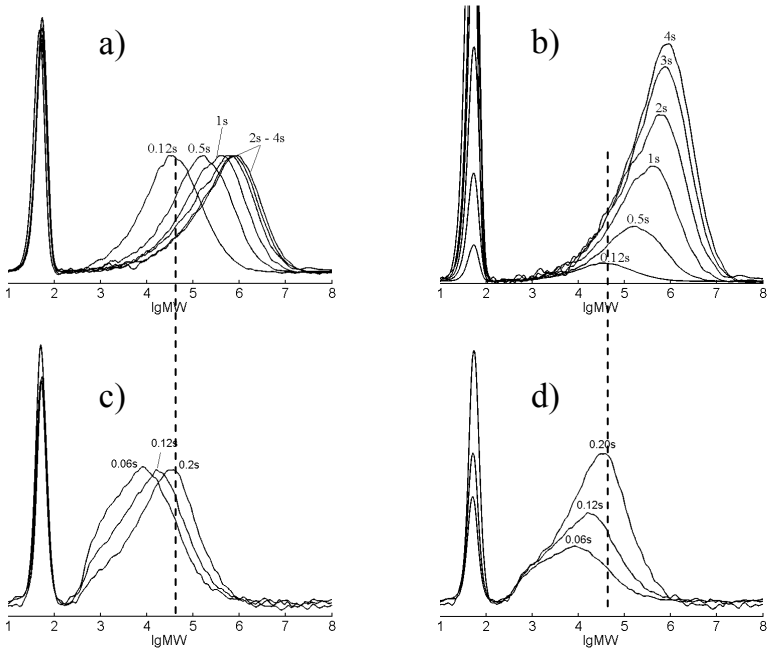


**Figure 46.** GPC profiles of PE prepared with TIBA (a, b) and TEA (c, d). a) and c) are profiles normalized to the same height; for b) and d), the areas under the curves are normalized with the yield.

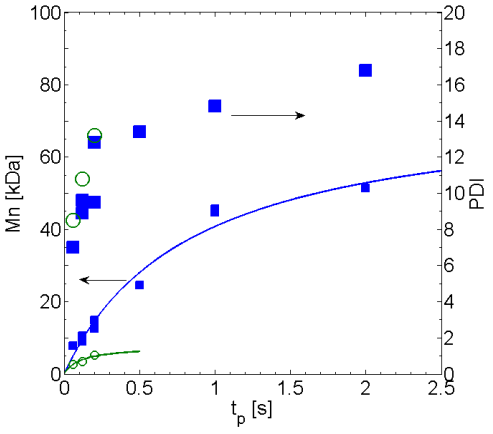


**Figure 47.** Molecular weight distribution of PE prepared with TIBA (■) and TEA (○).

*Chain Ends analysis*

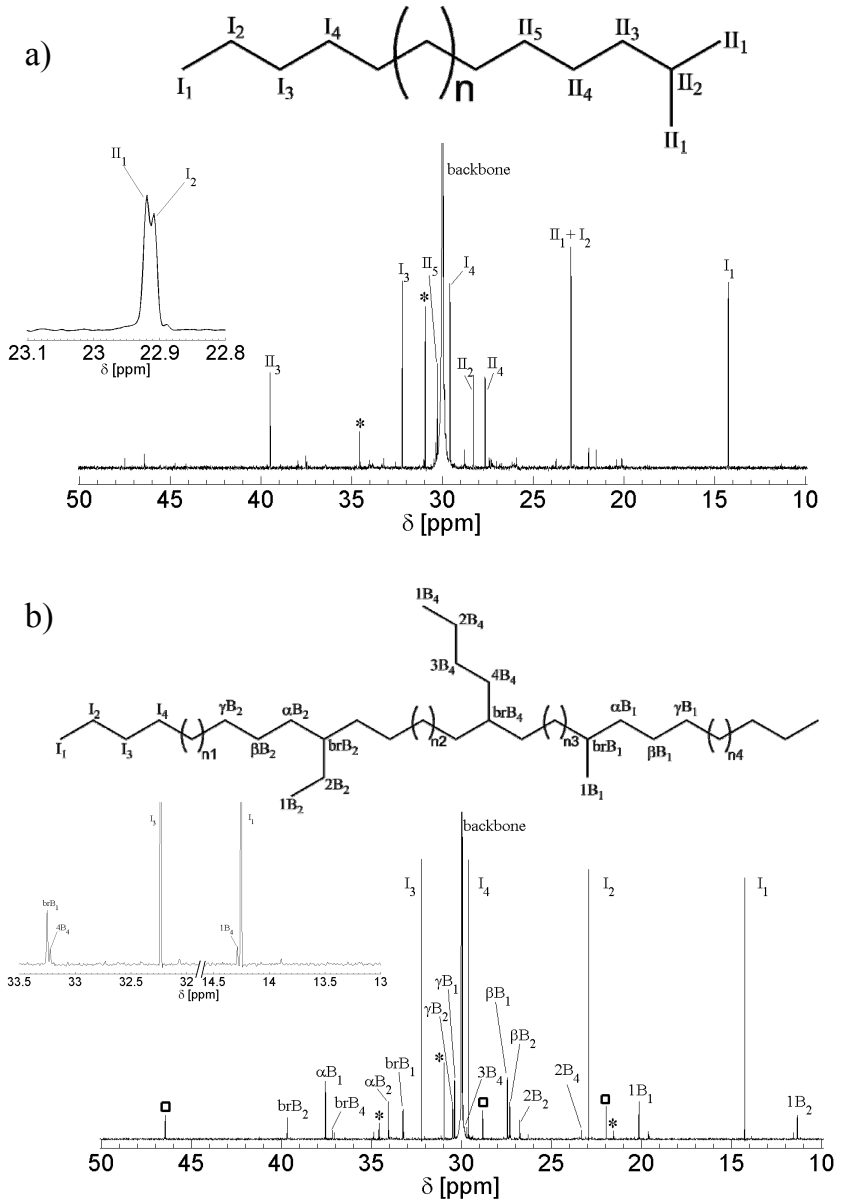


**Figure 48.** $^{13}$C-NMR spectra of a) PE prepared with TIBA and b) PE prepared with TEA. * denotes impurities; □ denotes the peaks belonging to PP that was probably brought by polymerization tubing.

For PE prepared with TIBA, it was found that there is a great excess of *n*Bu to *iso*-hexyl (*i*Hx), Figure 49a. If one assumes that every polymer chain is produced from an initial Ti-bound *i*Bu group, the amount of *n*Bu should equal to the amount of *i*Hx. Chain transfer to TIBA would produce equal amount of *n*Bu and *i*Hx. Chain transfer to monomer could produce excess *n*Bu but would also produces a corresponding amount of unsaturated groups which was not observed. So it is unlikely to obtain all of the excessive *n*Bu by chain transfer.

Furthermore, it was found the amount of *n*Bu has a linear correlation with the amount of *i*Hx ($A_{nBu}$=2.5 $A_{iHx}$), Figure 50a, except the sample with the shortest polymerization time (0.06 s). At this point no solid conclusions can be drawn on this fact.

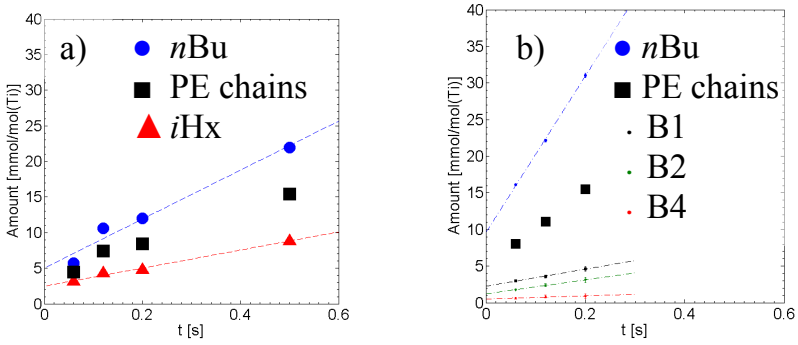


**Figure 49.** Temporal evolution of the amount of chain ends and branches. a) PE with TIBA, *n*Bu 34 mmol·mol(Ti)$^{-1}$·s$^{-1}$, *i*Hx 13mmol·mol(Ti)$^{-1}$·s$^{-1}$; b) PE with TEA, *n*Bu 107 mmol·mol(Ti)$^{-1}$·s$^{-1}$, B1, 12 mmol·mol(Ti)$^{-1}$·s$^{-1}$, B2, 10 mmol·mol(Ti)$^{-1}$·s$^{-1}$, B4, 2 mmol·mol(Ti)$^{-1}$·s$^{-1}$.

For propene polymerization, as we discussed previously, there was no polymer chains produced by Ti-H that was present before polymerization. This difference might imply a significant mechanistic difference between ethene and propene polymerization.

For PE with TEA, it was surprising to find significant content of short branches, Figure 49b. One might consider ethyl and butyl branches are produced by oligomerization during precontact since TEA system is known to produce ethene. However it cannot explain the appearance of methyl units which are even more abundant than ethyl and butyl. And the temporal evolution of the amount of branches, Figure 49b, illustrates the amount of branches evidently increases over time, suggesting there is significant amount of branches produced during polymerization. The lack of propyl branch suggests they are not all produced via a chain-walking mechanism.

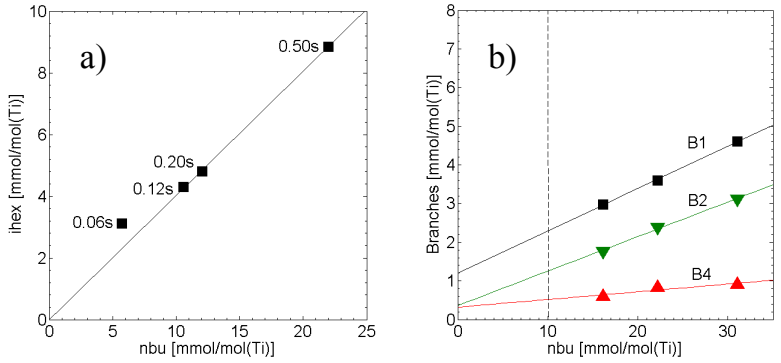


**Figure 50.** Correlation between the amount of *n*Bu and that of other chain ends or branches. a) PE prepared with TIBA; b) PE prepared with TEA.

Budzelaar[53] reviewed a series of possible genesis mechanisms of branches in PE however focused on homogeneous systems. If similar mechanisms are considered, the system in this study likely produces methyl via one-carbon chain-walking mechanism since methyl cannot be brought in by the cocatalyst. An ethyl branch can be produced via H-transfer to monomer followed by chain reinsertion, or through insertion of 1-butene; a butyl branch might be produced via ε C-H metathesis[54] or through insertion of 1-hexene. Given the preparation procedure (via $MgCl_2$-ethanol adducts) there might be residual traces of titanium alkoxides in the

catalyst that have not been completely removed by washing; and these are known to form ethene oligomerization catalysts when combined with TEA, particularly producing 1-butene and 1-hexene.[55-57] We consider it unlikely that TIBA would suppress the H-transfer/reinsertion mechanism for Et branching or the ε C-H metathesis for *n*Bu branching mentioned above, but it is entirely possible that TIBA would be less efficient in generating oligomerization catalysts from Ti alkoxides. Thus, the lower Et and *n*Bu branch contents for TIBA systems support the oligomer incorporation model for TEA systems. In any case, these observations illustrate the impact of different cocatalysts.

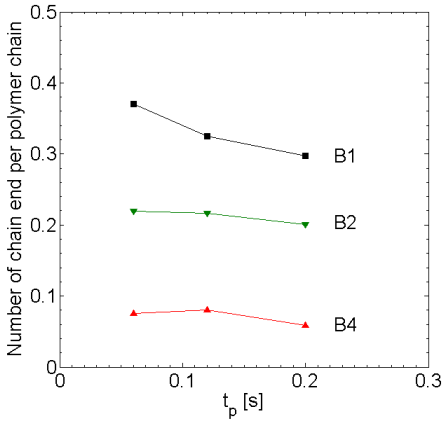


**Figure 51.** Number of chain ends per polymer chain versus time.

### *4.4.6. Calibrating GPC data with NMR*

Gel permeation chromatography (GPC) is a routine approach for characterizing the molecular weight distribution of polymer. The common universal calibration method is based on the relationship

$$[\eta]M = \Phi\alpha^3 < h^2 >^{1.5} \quad (18)$$

where $[\eta]$ is the intrinsic viscosity of the solution of the polymer of molecular weight $M$, $\Phi$ is the Flory constant, $\alpha$ is the expansion factor of the polymer molecule and $<h^2>$ is the mean-square radius

of gyration. Due to the correlation between $\langle h^2 \rangle$ and elution volume ($V_e$), it was found

$$[\eta]M = f(V_e) \tag{19}$$

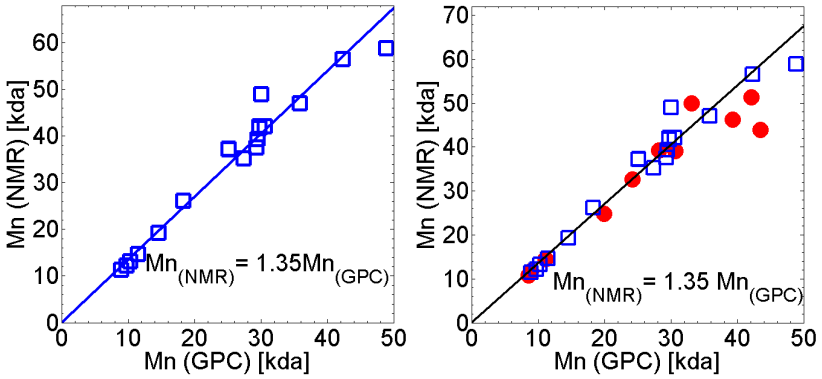


**Figure 52.** Correlation between the number average molecular weight (Mn) measured with NMR and the Mn measured with GPC. Polypropylene prepared in the presence (□) and absence (●) of ED.

And $f(V_e)$ is a linear function within a certain range of $V_e$. By applying the Mark–Houwink equation

$$[\eta]M = KM^{\alpha+1} \tag{20}$$

a correlation between $V_e$ and $M$ can be established. However different polymer chains might present different $f(V_e)$ due to the effects of segments distribution and/or the expansion extent. Thus the standard samples, polystyrene (PS) usually adopted, do not necessarily give an accurate calibration curve for $f(V_e)$.

To investigate how accurate the results given by PS standards are, an absolute calibration based on NMR data was carried out for PP and PE. It was found:

1) PP samples prepared with various catalyst systems follow the same linear calibration curve
2) the calibration curve of PP is different from that of PE

which is in an exponential form.

Figure 52 illustrates the correlation for PP prepared with phthalate-based Ziegler-Natta catalyst (ZNC) in the presence and absence of external donor. Clearly the correlation is not affected by the significant difference in stereoregularity of PP that was discussed earlier.

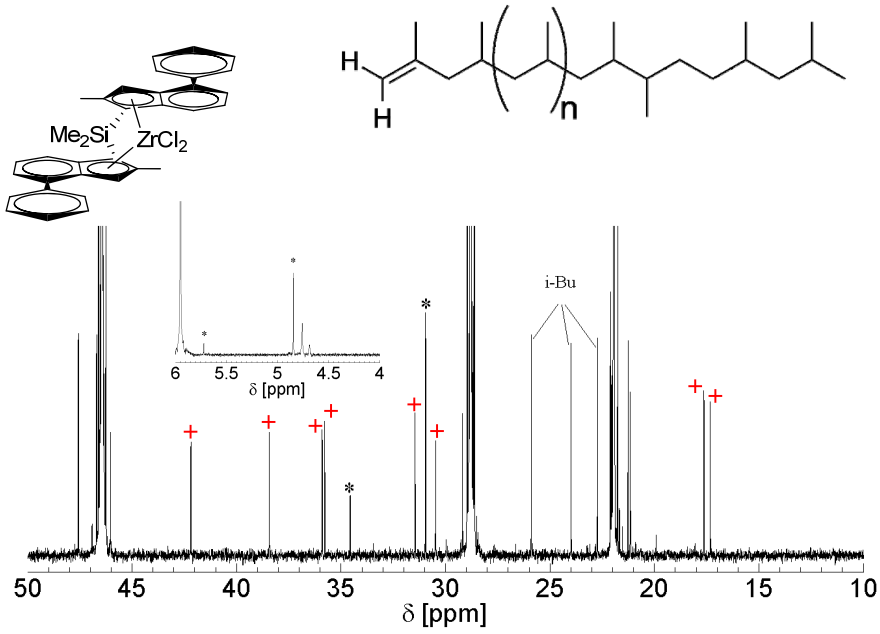


**Figure 53.** NMR spectra of polypropylene prepared with metallocene catalyst. (Out layer) $^{13}$C-NMR spectrum; (insert) $^{1}$H-NMR spectrum. + signs denote the signals of carbons of head-to-head segment produced by primary insertion following the secondary insertion.

One could image that PP produced with metallocene catalysts might behave differently from PP that was prepared with ZNCs. For instance, the same isotacticity does not necessarily result in the same melting point,[58] which can be explained by the distributions of stereo- and/or regio-errors that affect the folding of polymer chains and thus influence the product morphology. Since stereo-

and/or regio-errors could possibly affect the gyration of polymer coil in solution, one could expect PP with a significant amount of head-to-head segments might present a different calibration curve. However as illustrated in Figure 54, even PP prepared with a metallocene (shown in Figure 53) follows the same curve, proving that the calibration curve is not sensitive to the distribution of stereo- and regio-errors. Of course, this calibration curve has not been tested fore extreme situations, such as atactic PP or highly regioirregular PP.

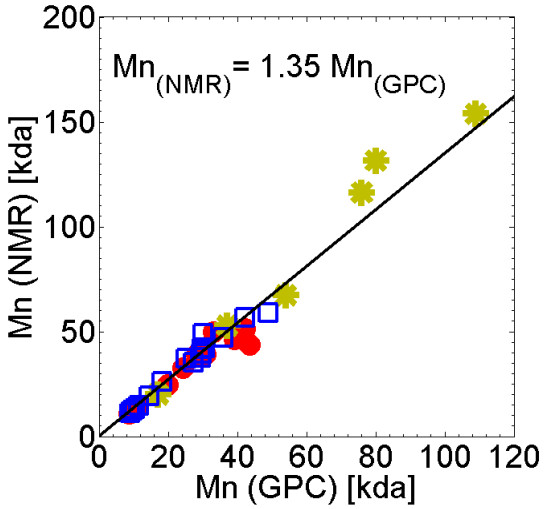


**Figure 54.** Correlation between the number average molecular weight (Mn) measured with NMR and the Mn measured with GPC. (□) Polypropylene prepared with phthalate catalyst in the presence of ED; (●) polypropylene prepared with phthalate catalyst in the absence of ED; (*) polypropylene prepared with metallocene catalyst in Figure 52.

Surprisingly, the Mn of PE calculated from NMR does not correlate linearly with the Mn obtained from GPC, Figure 55. One might imagine that $^{13}C$ NMR integration errors due to incomplete relaxation could contribute.[59] However, we checked that $^{1}H$ NMR data, where relaxation is much less of an issue, show the same trend (Figure 56) and support the $^{13}C$ data. It turned out the Mn

correlation for PE is better described with a logarithmic function as shown in Figure 57.

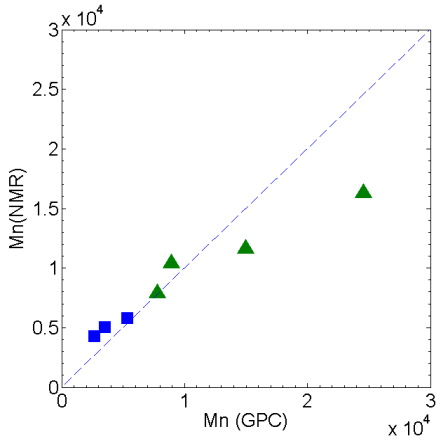


**Figure 55.** Correlation of PE Mn values from GPC and NMR, for PE prepared using a phthalate catalyst and either TIBA (▲) or TEA (■) as cocatalyst.

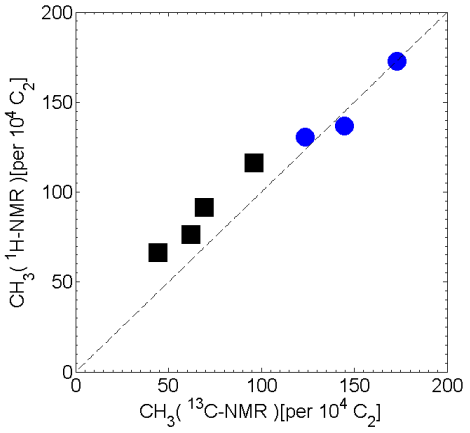


**Figure 56.** Correlation between methyl content measured with $^{1}H$ NMR and $^{13}C$ NMR, for PE prepared with phthalate catalyst and (■) TIBA or (●) TEA cocatalyst.

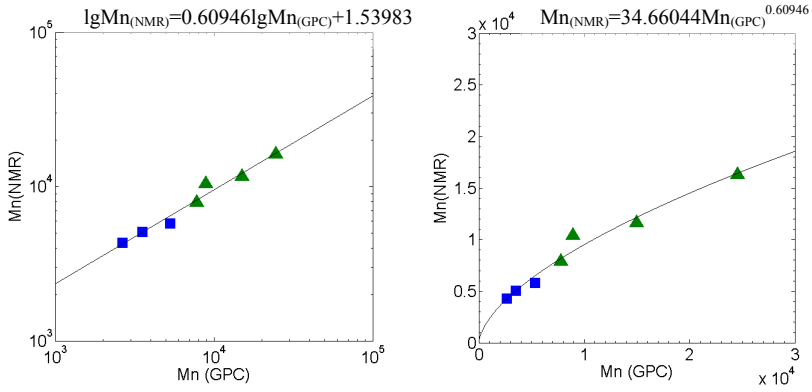


**Figure 57.** Correlation between the number average molecular weight (Mn) measured with NMR and the Mn measured with GPC for polyethylene prepared with phthalate catalyst and TIBA (▲) or TEA (■) cocatalyst.

Recalling the correlation functions of GPC Equation (19) and (20) giving

$$f(V_e) = KM_{GPC}^{\alpha+1} \tag{21}$$

and substituting the correlation of $Mn_{(GPC)}$ and $Mn_{(NMR)}$ there is

$$f(V_e) = K(\frac{M_{NMR}}{1.35})^{\alpha+1} = \frac{K}{1.35^{\alpha+1}} M_{NMR}^{\alpha+1} = K'M_{NMR}^{\alpha+1} \tag{22}$$

for PP, where K' is the calibrated value of K. This means only K needs to be modified to obtain accurate results of molecular weight for PP.

For PE, there is

$$f(V_e) = K(\sqrt[0.60946]{\frac{M_{NMR}}{34.66044}})^{\alpha+1} = \frac{K}{336.1668} M_{NMR}^{1.64080(\alpha+0.39054)+1} = K'M_{NMR}^{\alpha'+1} \tag{23}$$

where K' and α' are the calibrated values of K and α, respectively. This suggests the values of both K and α need to be adjusted to obtain an accurate molecular weight for PE.

## 4.5. Conclusions and comments

A combined approach of quenched-flow polymerization and cryoprobe NMR was adopted to study phthalate-based ZNCs. The results unambiguously demonstrate dormant behavior. The presence of *n*Bu groups has long been taken as direct evidence of dormant species: it is produced when the last inserted monomer inserts in secondary (2,1) mode. The presence of such *n*Bu, and their development over time was proven in this study. It was found:

1) the production rate of *n*Bu follows the first-order-decay-like rule
2) accumulation of *n*Bu starts immediately, and head-to-head segments (from primary insertion following the secondary insertion) were not observed

Overall, the evidence indicates this system is highly dormant.

Monte Carlo simulations were used to show that dormancy does not invalidate the Natta analysis, explaining why a linear 1/t-1/Pn relationship is still obtained even with the onset of dormancy. The *in silico* experiments support the use of Natta plots for extracting kinetic parameters such as reaction frequencies and active sites content. The latter one was also confirmed with NMR results.

The use of an external donor was shown not to affect the regio-specificity of active sites much, but to significantly affect stereo-specificity. Benzoate-based catalysts have been found to present high regio-selectivity as described in the previous chapter. The comparison of benzoate and phthalate systems suggests the internal donor might play a critical role in determining the regio-selectivity of the catalyst. The exact roles of donors are still an open question. X-ray spectroscopies, e.g. XPS or XAFS are powerful tools to obtain the overall information about the catalyst, such as atomic distances, oxidation states and coordination numbers[60]. However, the relevance of such information remains questionable due to the extremely low content of active sites.

This study also includes a few examples of long time polymerization,. Apparently the data obtained under quenched-flow conditions are representative, meaning there is no distinct features found for long time polymerization from the later stage of quenched-flow conditions. The system has shown a smooth transition over time. Some features, e.g. activity, even reach the constant value in the first seconds. One may consider this low pressure polymerization is similar to the prepolymerization step during the industrial production which is crucial for maintaining a satisfactory morphology of polymer particles. This study might be valuable for understanding the corresponding process.

2,3-substituted succinate has a similar spacing between the ester groups as phthalate. However, succinate-based catalysts produce polypropylene with a distinctly broader molecular weight distribution and higher average molecular weight.[61] This suggests that a detailed comparison of phthalate and succinate catalysts might provide more insight in the nature of the active sites and their deactivation, even more than 60 years after the invention of Ziegler-Natta catalysis.

## References

1. Luciani, L.; Kashiwa, N.; Barbe, P.; Toyota, A. α-olefin polymerization catalyst. JPS52151691 (A) 1977.

2. Parodi, S.; Nocci, R.; Giannini, U.; Barbe, P.; Scata, U. Components and catalysts for the polymerization of olefins. EP0045977 (A2), 1982.

3. Giannini, U.; Cassata, A.; Longi, P.; Mazzocchi, R. Procede pour la polymerisation stereoreguliere des α-olefines. BE785332 (A1), 1972.

4. Polyolefins: 50 years after Ziegler and Natta. I. Polyethylene and polypropylene. In *Adv Polym Sci*, Kaminsky, W., Ed. Springer-Verlag Berlin: Berlin, 2013; Vol. 257, pp 1-257.

5. Yang, C. B.; Hsu, C. C., Propene polymerization with $MgCl_2$-supported $TiCl_4$/dioctylphthalate catalyst .1. Catalyst behavior. *J Appl Polym Sci* **1995,** *58* (8), 1229-1235.

6. Chadwick, J. C.; Miedema, A.; Ruisch, B. J.; Sudmeijer, O., Effects of

procatalyst composition on the stereospecificity of a Ziegler-Natta catalyst system. *Makromol Chem* **1992,** *193* (6), 1463-1468.

7. Choi, J. H.; Chung, J. S.; Shin, H. W.; Song, I. K.; Lee, W. Y., The effect of alcohol treatment in the preparation of MgCl2 support by a recrystallization method on the catalytic activity and isotactic index for propylene polymerization. *Eur Polym J* **1996,** *32* (4), 405-410.

8. Kim, J. H.; Lee, Y. S. Preparation method of catalyst for polymerization of olefin and preparation method of polyolefin using the catalyst. KR2003035413-A; KR451085-B, KR2003035413-A 09 May 2003 C08F-004/654 200365 KR451085-B 02 Oct 2004 C08F-004/654 200511.

9. Yang, Y.; Dang, X. F.; Yao, J. Y.; Li, H. Y.; Hu, Y. L., Ziegler-Natta catalysts with internal electron donors. *Acta Polym Sin* **2013,** (4), 511-517.

10. Garoff, T.; Leinonen, T.; Liskola, E.; Iiskola, E. Polymerisation catalyst preparation, used for olefin(s) - Contains ester(s) of carboxylic acid which are transesterified with an alcohol also connected in the catalyst. EP491566-A; EP491566-A2; NO9105000-A; CA2056531-A; JP4296305-A; US5234879-A; EP491566-A3; NO178731-B; EP491566-B1; DE69122483-E; JP2559084-B2; ES2094798-T3; CA2056531-C; EP491566-B2, EP491566-A EP491566-A2 24 Jun 1992 199226.

11. Gupta, V.; Patil, D. G.; Gupta, V. K.; Naik, D. G.; Patil, H. R.; Patil, H.; Naik, D. Making Ziegler Natta procatalyst used in α-olefin polymerization involves multistage treatment of magnesium alkoxide with recovered titanium tetrachloride and chlorobenzene mixture and successive washing of product with recovered hexane. KR2011009110-Y1; WO2009116057-A2; IN200800541-I3; WO2009116057-A8; WO2009116057-A3; EP2257576-A2; US2011015355-A1; KR2011009110-A; IN253292-B; US8283424-B2; EP2257576-B1, KR2011009110-Y1 WO2009116057-A2 24 Sep 2009 C08F-004/654 200968.

12. Singh, G.; Kaur, S.; Makwana, U.; Patankar, R. B.; Gupta, V. K., Influence of internal donors on the performance and structure of $MgCl_2$ supported titanium catalysts for propylene polymerization. *Macromol Chem Physic* **2009,** *210* (1), 69-76.

13. Makwana, U.; Naik, D. G.; Singh, G.; Patel, V.; Patil, H. R.; Gupta, V. K., Nature of phthalates as internal donors in high performance $MgCl_2$ supported titanium catalysts. *Catal Lett* **2009,** *131* (3-4), 624-631.

14. Potapov, A. G.; Bukatov, G. D.; Zakharov, V. A., DRIFTS study of the

interaction of the internal donor in $TiCl_4$/di-n-butyl phthalate/$MgCl_2$ catalysts with $AlEt_3$ cocatalyst. *J Mol Catal A-Chem* **2010,** *316* (1-2), 95-99.

15. Bailly, J. C.; Sandis, S.; Blaya, A.; Crouzet, P.; Bailly, J.; Havas, L. Catalyst support for α-olefin polymerisation. Comprising magnesium chloride spherical particles of controllable size distribution. EP99774-A1; EP98196-A1; FR2529206-A1; EP98196-A; FR2529206-A; AU8316134-A; AU8316136-A; JP59022907-A; NO8302264-A; JP59030806-A; FI8302317-A; PT76920-A; ES8403933-A; US4490475-A; US4497904-A; CA1189053-A; EP98196-B; DE3361776-G; EP98196-B2; CS9104017-A2; JP95080928-B2; JP95116252-B2, EP99774-A1 EP98196-A 11 Jan 1984 198403.

16. Makino, K.; Tsuda, K.; Takaki, M., Preparation of soluble $TiCl_3$ catalysts by reduction of $TiCl_4$ with Grignard reagents and their use for copolymerization of ethylene with propylene. *Polym Bull* **1991,** *26* (4), 371-376.

17. Muñoz-Escalona, A.; García , H.; Albornoz, A., Homopolymerization and copolymerization of ethylene with highly-active catalysts based on $TiCl_4$ and Grignard compounds. *J Appl Polym Sci* **1987,** *34* (3), 977-988.

18. Barbe, P. C.; Noristi, L.; Baruzzi, G., Effect of the internal external donor pair in high-yield catalysts for propylene polymerization .2. Polymerization results. *Makromol Chem* **1992,** *193* (1), 229-241.

19. Xu, J. T.; Feng, L. X.; Xie, T.; Yang, S. L., The roles of Grignard reagent in the Ziegler-Natta catalyst for propylene polymerization. *J Appl Polym Sci* **1997,** *65* (5), 925-930.

20. Soga, K.; Shiono, T.; Doi, Y., Influence of internal and external donors on activity and stereospecificity of Ziegler-Natta catalysts. *Makromol Chem* **1988,** *189* (7), 1531-1541.

21. Yang, C. B.; Hsu, C. C., Effect of catalyst aging on catalyst activity and stereospecificity for $MgCl_2$/ethyl benzoate or dioctyl phthalate/$TiCl_4$-triethylaluminum for propene polymerization. *Macromol Rapid Commun* **1995,** *16* (4), 311-316.

22. Chien, J. C. W.; Hu, Y. L.; Vizzini, J. C., Superactive and stereospecific catalysts .4. Influence of structure of esters on $MgCl_2$ supported olefin polymerization catalysts. *J Polym Sci A- Polym Chem* **1990,** *28* (2), 273-284.

23. Kakkonen, H. J.; Pursiainen, J.; Pakkanen, T. A.; Ahlgren, M.; Iiskola, E., $TiCl_4$ diester complexes - relationships between the crystal structures and properties of Ziegler-Natta catalysts. *J Organomet Chem* **1993,** *453* (2),

175-184.

24. Cavallo, L.; Del Piero, S.; Ducere, J. M.; Fedele, R.; Melchior, A.; Morini, G.; Piemontesi, F.; Tolazzi, M., Key interactions in heterogeneous Ziegler-Natta catalytic systems. Structure and energetics of $TiCl_4$-Lewis base complexes. *J Phys Chem C* **2007,** *111* (11), 4412-4419.

25. Yang, C. B.; Hsu, C. C.; Park, Y. S.; Shurvell, H. F., Infrared characterization of $MgCl_2$ supported Ziegler-Natta catalysts with monoester and diester as a modifier. *Eur Polym J* **1994,** *30* (2), 205-214.

26. Ribour, D.; Monteil, V.; Spitz, R., Detitanation of $MgCl_2$-supported Ziegler-Natta catalysts for the study of active sites organization. *J Polym Sci A-Polym Chem* **2008,** *46* (16), 5461-5470.

27. Arzoumanidis, G. G.; Karayannis, N. M., Infrared spectral characterization of supported propene polymerization catalysts. A link to catalyst performance. *Appl Catal* **1991,** *76* (2), 221-231.

28. Boero, M.; Parrinello, M.; Weiss, H.; Huffer, S., A first principles exploration of a variety of active surfaces and catalytic sites in Ziegler-Natta heterogeneous catalysis. *J Phys Chem A* **2001,** *105* (21), 5096-5105.

29. Correa, A.; Piemontesi, F.; Morini, G.; Cavallo, L., Key elements in the structure and function relationship of the $MgCl_2/TiCl_4$/Lewis base Ziegler-Natta catalytic system. *Macromolecules* **2007,** *40* (25), 9181-9189.

30. Credendino, R.; Liguori, D.; Morini, G.; Cavallo, L., Investigating phthalate and 1,3-diether coverage and dynamics on the (104) and (110) surfaces of $MgCl_2$-supported Ziegler-Natta catalysts. *J Phys Chem C* **2014,** *118* (15), 8050-8058.

31. Andoni, A.; Chadwick, J. C.; Niemantsverdriet, H. J. W.; Thune, P. C., The role of electron donors on lateral surfaces of $MgCl_2$-supported Ziegler-Natta catalysts. Observation by AFM and SEM. *J Catal* **2008,** *257* (1), 81-86.

32. Cheruvathur, A. V.; Langner, E. H. G.; Niemantsverdriet, J. W.; Thune, P. C., In situ ATR-FTIR studies on $MgCl_2$-diisobutyl phthalate interactions in thin film Ziegler-Natta catalysts. *Langmuir* **2012,** *28* (5), 2643-2651.

33. Sacchi, M. C.; Tritto, I.; Shan, C. J.; Mendichi, R.; Noristi, L., Role of the pair of internal and external donors in $MgCl_2$-supported Ziegler-Natta catalysts. *Macromolecules* **1991,** *24* (26), 6823-6826.

34. Sacchi, M. C.; Forlini, F.; Tritto, I.; Mendichi, R.; Zannoni, G.; Noristi, L., Activation effect of alkoxysilanes as external donors in $MgCl_2$-supported

Ziegler-Natta catalysts. *Macromolecules* **1992,** *25* (22), 5914-5918.

35. Harkonen, M.; Seppala, J. V.; Vaananen, T., External alkoxysilane donors in Ziegler-Natta catalysis. Effects on poly(propylene) microstructure. *Makromol Chem* **1991,** *192* (3), 721-734.

36. Poonpong, S.; Dwivedi, S.; Taniike, T.; Terano, M., Structure-performance relationship for dialkyldimethoxysilane as an external donor in stopped-flow propylene polymerization using a Ziegler-Natta catalyst. *Macromol Chem Physic* **2014,** *215* (18), 1721-1727.

37. Panchenko, V. N.; Goryachev, A. N.; Vorontsova, L. V.; Paukshtis, E. A.; Zakharov, V. A., Basicity of stereoregulating electron donor compounds in Ziegler-Natta catalysts: A study by infrared spectroscopy and chemical exchange reactions. *J Phys Chem C* **2014,** *118* (49), 28572-28579.

38. Busico, V.; Causa, M.; Cipullo, R.; Credendino, R.; Cutillo, F.; Friederichs, N.; Lamanna, R.; Segre, A.; Castellit, V. V., Periodic DFT and high-resolution magic-angle-spinning (HR-MAS) $^{1}$H NMR investigation of the active surfaces of $MgCl_2$-supported Ziegler-Natta catalysts. The $MgCl_2$ matrix. *J Phys Chem C* **2008,** *112* (4), 1081-1089.

39. Mori, H.; Saito, H.; Yamahiro, M.; Kono, H.; Terano, M., Stopped-flow study of the interaction of $MgCl_2$-supported Ziegler catalyst with $Me_nSi(OEt)_{4-n}$. A tool for understanding the active sites precursors and the correlation to stereospecificity. *Macromol Chem Physic* **1998,** *199* (4), 613-618.

40. Ohnishi, R.; Konakazawa, T., Role of tert-butyl methyl ether (TBME) as an external donor in propene polymerization with dibutyl phthalate (DBP)-containing $MgCl_2$-supported Ti catalysts activated with $Al(i\text{-}C_4H_9)_3$. *Macromol Chem Physic* **2004,** *205* (14), 1938-1947.

41. Nitta, T.; Liu, B. P.; Nakatani, H.; Terano, M., Formation, deactivation and transformation of stereospecific active sites on $TiCl_4$/dibutylphthalate/$Mg(OEt)_2$ catalyst induced by short time reaction with Al-alkyl cocatalyst. *J Mol Catal A-Chem* **2002,** *180* (1-2), 25-34.

42. Gillespie, D. T., Exact stochastic simulation of coupled chemical reactions. *J Phys Chem* **1977,** *81* (25), 2340-2361.

43. Platkowski, K.; Reichert, K. H., Application of Monte Carlo methods for modelling of polymerization reactions. *Polymer* **1999,** *40* (4), 1057-1066.

44. Liu, B. P.; Matsuoka, H.; Terano, M., Stopped-flow techniques in Ziegler catalysis. *Macromol Rapid Commun* **2001,** *22* (1), 1-24.

45. Busico, V.; Cipullo, R.; Monaco, G.; Talarico, G.; Vacatello, M.; Chadwick,

J. C.; Segre, A. L.; Sudmeijer, O., High-resolution $^{13}C$ NMR configurational analysis of polypropylene made with $MgCl_2$-supported Ziegler-Natta catalysts. 1. The "model" system $MgCl_2/TiCl_4$-2,6-dimethylpyridine/$Al(C_2H_5)_3$. *Macromolecules* **1999,** *32* (13), 4173-4182.

46. Alshaiban, A., Propylene polymerization using 4th generation Ziegler-Natta catalysts. Polymerization kinetics and polymer microstructural investigation. *University of Waterloo Dissertation* **2011**.

47. Mori, H.; Tashino, K.; Terano, M., Study of the chain transfer reaction by hydrogen in the initial stage of propene polymerization. *Macromol Rapid Commun* **1995,** *16* (9), 651-657.

48. Liu, B. P.; Murayama, N.; Terano, M., Transformation of polymerization sites into hydrogen dissociation sites propylene polymerization catalyst induced by the reaction with Al-alkyl cocatalyst. *Ind Eng Chem Res* **2005,** *44* (8), 2382-2388.

49. Busico, V.; Cipullo, R.; Ronca, S., Propene/ethene-[1-C-13] copolymerization as a tool for investigating catalyst regioselectivity. 1. Theory and calibration. *Macromolecules* **2002,** *35* (5), 1537-1542.

50. Busico, V.; Cipullo, R.; Polzone, C.; Talarico, G.; Chadwick, J. C., Propene/ethene-[1-C-13] copolymerization as a tool for investigating catalyst regioselectivity. 2. The $MgCl_2/TiCl_4$-$AlR_3$ system. *Macromolecules* **2003,** *36* (8), 2616-2622.

51. Busico, V.; Chadwick, J. C.; Cipullo, R.; Ronca, S.; Talarico, G., Propene/ethene-[1-C-13] copolymerization as a tool for investigating catalyst regioselectivity. $MgCl_2$/internal donor/$TiCl_4$-external donor/$AlR_3$ systems. *Macromolecules* **2004,** *37* (20), 7437-7443.

52. Boero, M.; Parrinello, M.; Huffer, S.; Weiss, H., First principles study of propene polymerization in Ziegler-Natta heterogeneous catalysis. *J Am Chem Soc* **2000,** *122* (3), 501-509.

53. Budzelaar, P. H. M., Mechanisms of branch formation in metal-catalyzed ethene polymerization. *WIREs Comput Mol Sci* **2012,** *2* (2), 221-241.

54. Sauriol, F.; Sonnenberg, J. F.; Chadder, S. J.; Dunlop-Brière, A. F.; Baird, M. C.; Budzelaar, P. H. M., Remarkable reactions and intermediates in titanocene(IV) chemistry: Migratory insertion reactions of 2,2-disubstituted-1-alkenes, intramolecular 1,5-σ bond metathesis via ε-agostic interactions, and a rare example of a β-agostic alkyltitanocene complex. *J Am Chem Soc* **2010,** *132* (38), 13357–13370.

55. Pillai, S. M.; Tembe, G. L.; Ravindranathan, M.; Sivaram, S., Dimerization of ethylene to 1-butene catalyzed by the titanium alkoxide trialkylaluminum system. *Ind Eng Chem Res* **1988,** *27* (11), 1971-1977.

56. Alsadoun, A. W., Dimerization of ethylene to butene-1 catalyzed by $Ti(OR')_4$-$AlR_3$. *Appl Catal a-Gen* **1993,** *105* (1), 1-40.

57. McGuinness, D. S., Olefin oligomerization via metallacycles. Dimerization, trimerization, tetramerization, and beyond. *Chem Rev* **2011,** *111* (3), 2321-2341.

58. Busico, V.; Cipullo, R., Microstructure of polypropylene. *Prog Polym Sci* **2001,** *26* (3), 443-533.

59. Freed, D. E., Dependence on chain length of NMR relaxation times in mixtures of alkanes. *J Chem Phys* **2007,** *126* (17).

60. da Silva, A. A.; Alves, M. D. M.; dos Santos, J. H. Z., XPS and EXAFS characterization of Ziegler-Natta catalyst systems. *J Appl Polym Sci* **2008,** *109* (3), 1675-1683.

61. Potapov, A. G.; Zakharov, V. A.; Bukatov, G. D., State of various stereoregulating electron-donating compounds in titanium-magnesium catalysts for propylene polymerization. A diffuse reflectance IR spectroscopic study. *Kinet Catal* **2007,** *48* (3), 403-408.

# Chapter 5. Conclusions and Outlook

This work represents a contribution to a better mechanistic understanding of catalytic olefin polymerizations by means of a combination of Quenched-Flow (QF) kinetic studies and NMR polymer analyses. To the best of our knowledge, it is the first time that the two approaches have been integrated, and applied to molecular (homogeneous) as well as heterogeneous catalyst systems.

Previous studies by Keii and Terano had demonstrated that some important kinetic parameters of Ziegler-Natta propene polymerizations (namely, the specific rate of chain propagation ($k_p$) and the fraction of active metal) can be determined from the build-up of polymer yield and molecular weight in the initial transient of controlled kinetics, accessible with QF methods. In the present work, we extended the scope of the approach to evaluations of activation parameters (at least in single-center molecular catalysis), and also to the determination of the elusive 'dormant' sites in Ziegler-Natta systems for polypropylene production.

In a first part (Chapter 2), we validated our QF setup and methods in ethene polymerization mediated by a bis(phenoxyimine)Ti(IV) catalyst known for a long-lasting controlled kinetics up to relatively high temperatures. From variable-temperature QF measurements of $k_p$ (in nice agreement with the previous literature) we determined the values of $\Delta^{\ddagger}H^{o}$ (~3 kcal·mol$^{-1}$) and $\Delta^{\ddagger}S^{o}$ (-32 cal·K$^{-1}$·mol$^{-1}$); along with a fraction of active Ti close to 100%; these results highlighted a kinetic behavior in line with the simple catalytic cycle shown in Figure 1. This, however, is not necessarily the case with other molecular systems.

As a matter of fact, a similar study in the presence of a well-known *ansa*-zirconocene, namely *rac*-$Me_2Si$(2-Me-4-Ph-1-Ind)$_2ZrCl_2$, ended up with non-trivial results, indicating a strong dependence of chain propagation kinetics on the nature of the co-catalyst (namely, methylaluminoxane (MAO) with or without the addition of

butylhydroxytoluene (BHT) as an $AlMe_3$ trap). In particular, we found that *entropy* of activation is an extremely important variable in this catalysis, and that catalysts featuring a rather high *enthalpy* of activation can be much faster than less activated ones provided that the entropic penalty typical of a bimolecular process ($-T\Delta^{\ddagger}S^{o}$ ~10 kcal·mol$^{-1}$ at R.T.) is removed. This can be the case, e.g. when the chain propagation mechanism involves a catalyst resting state with a 'donor' molecule (e.g. $AlMe_3$) temporarily hindering monomer access to the transition metal center; donor displacement upon monomer capture can be the reason for entropy compensation. It should be added that for the aforementioned zirconocene the fraction of active transition metal was estimated to be fairly low (10 %), likely due to interactions of the active cations with the variety of Lewis bases inherently present in the reaction pool.

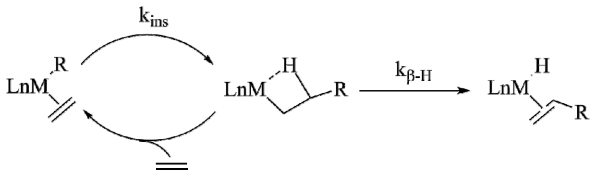


**Figure 1**. Catalytic cycle of olefin polymerization.

Overall, Chapter 2 demonstrates that the QF approach is robust and reliable, but also that one cannot assume *tout-court* a trivial Cossee-Arlman mechanism for catalytic olefin polymerization, even in case of supposedly simple single-center molecular catalysts.

Not surprisingly, heterogeneous Ziegler-Natta catalysts (ZNCs) turned out to be even more complex than homogeneous ones. The ill-defined nature of the active species and their (very) low concentration are not the only complicating factors; as a matter of fact, issues related with the accumulation of 'dormant' sites are also important in the polymerization of propene (and other substituted olefins).

In Chapter 3, we benchmarked our system and protocols by investigating propene polymerization in the presence of a 3rd-generation ZNC with ethyl benzoate (EB) as the Internal Donors (ID). This system had been thoroughly studied before by Terano et al. Our results are substantially in line with the previous literature, which is of course reassuring. On the other hand, the integration with NMR polymer analysis shed some additional light on catalyst behavior, which turned out to be rather insensitive to the possible occurrence of regioirregular (2,1) monomer insertions. It is worthy to note that pre-contacting the precatalyst with the Al(*i*Bu)$_3$ (TIBA) co-catalyst was not necessary to observe activity under QF conditions; as a matter of fact, only a very short (less than 0.1 s) induction period was observed at 30°C. Based on that, one can probably rule out the hypothesis that precatalyst activation involves extensive processes of surface reconstruction, or even the formation of a separate crystalline $TiCl_3$ phase. Rather, the observed picture is better compatible with 'molecular'-like catalytic species consisting of $TiCl_x$ adducts on the $MgCl_2$ support.

The 'heart' of the present work was the kinetic investigation of a 4th-generation ZNC with a diisobutyl phthalate (DIBP) ID, reported and discussed in Chapter 4. We confirmed previous literature indications that pre-contacting the precatalyst with TIBA is necessary here to observe activity under QF conditions; while we cannot propose a univocal explanation for this fact, we suggest that this bidentate ID hinders most Ti centers in the precatalyst, and needs to be removed (in this work by reacting with TIBA) for catalytic activity to develop. This is a first major difference with respect to the catalyst system of Chapter 3 (ID = EB).

Another was the major impact of regioirregular 2,1 insertions on the kinetics of propene polymerization, clearly pointed out by $^{13}C$ NMR analyses of the produced polymers. Indeed, we demonstrated conclusively that the most stereoselective catalytic species in this system rapidly develop into 'dormant' sites due to the accumulation of α-Me-branched Ti-Polymeryls. Less stereoselective catalytic

species, in turn, seem to feature a less dormant character, and keep on propagating despite the slowing down effect of the regiodefects. As a result, a peculiar time dependence of polymer stereoregularity was observed, the degree of isotacticity declining in the first few seconds of polymerization and ultimately attaining a steady-state level. *This finding is key to understand the dramatic impact of $H_2$ added to the system as a chain transfer agent;* in fact, the boost of productivity and the strong enhancement of stereoselectivity in the presence of $H_2$ can now be explained in terms of its waking-up action on the most stereoselective catalytic species.

We are aware that this thesis is only the start of a systematic kinetic investigation, and that much more work for both molecular and heterogeneous catalysts will be necessary to completely work out the mechanism of catalytic olefin polymerization. On the other hand, we are convinced that our approach, integrating QF methods with NMR analyses of the polymerization products, is a most powerful tool, and will lead to major advances in fundamental understanding in the near future.